Universidade de São Paulo
FFCLRP - Departamento de Física

VINICIUS LIMA CORDEIRO

Models of neural networks with stochastic neurons and different topologies: construction and analysis

Ribeirão Preto - SP
2019

VINICIUS LIMA CORDEIRO

Models of neural networks with stochastic neurons and different topologies: construction and analysis

Dissertação apresentada à Faculdade de Filosofia, Ciências e Letras de Ribeirão Preto da Universidade de São Paulo, como parte das exigências para a obtenção do título de Mestre em Ciências.

Área de Concentração:
Física aplicada à Medicina e Biologia.

Orientador:
Prof. Dr. Antônio Carlos Roque da Silva Filho.

Versão corrigida
Versão original disponível na FFCLRP-

Ribeirão Preto - SP
2019

FICHA CATALOGRÁFICA

Lima Cordeiro, Vinicius

Models of neural networks with stochastic neurons and different topologies: construction and analysis / Vinicius Lima Cordeiro; orientador Prof. Dr. Antônio Carlos Roque da Silva Filho. Ribeirão Preto - SP, 2019.

104 f.:il.

Dissertação (Mestrado - Programa de Pós-graduação em Física aplicada à Medicina e Biologia) - Faculdade de Filosofia, Ciências e Letras de Ribeirão Preto da Universidade de São Paulo, 2019.

1. Modelo estocástico. 2. Ruído de canal. 3. Ressonância estocástica. 4. Redes complexas. 5. Córtex cerebral.

Nome: Lima Cordeiro, Vinicius

Título: Models of neural networks with stochastic neurons and different topologies: construction and analysis

Dissertação apresentada à Faculdade de Filosofia, Ciências e Letras de Ribeirão Preto da Universidade de São Paulo, como parte das exigências para a obtenção do título de Mestre em Ciências.

Aprovado em:____/____/____.

Banca Examinadora

Prof. Dr. : _____ Instituição: _____

Julgamento: _____ Assinatura: _____

Prof. Dr. : _____ Instituição: _____

Julgamento: _____ Assinatura: _____

Prof. Dr. : _____ Instituição: _____

Julgamento: _____ Assinatura: _____

Dedico esta dissertação ao meu avô Jairo, que muitas vezes com seu silêncio me ensinou mais coisas do que aqueles que se esgotam de palavras. Sabedoria essa que espero levar por toda vida.

Agradecimentos

Agradeço à minha família. Primeiramente à minha mãe Valéria cujo o amor incondicional e incentivo têm sido minha força motriz ao longo de minha vida. À minha irmã Mariana, e sobrinha Alice que mesmo com poucos meses de vida tem me proporcionado extrema alegria. Sou grato aos meus demais familiares pelo apoio que sempre recebi e que fora de grande importância;

Ao meu orientador, Prof. Dr. Antônio Roque, por ter me orientado desde o período da graduação como aluno de iniciação científica, e durante esse mestrado, período no qual obtive muito aprendizado sob sua supervisão;

Aos colégas de laboratório Rodrigo Pena, Renan Shimoura, César Ceballos, Nilton Kamiji, Fernanda Dellajustina, João Paulo, Mauricio Schappo pelo aprendizado e incentivo no ambiente de trabalho.

Aos meus amigos Luiz Obst, Letícia Rocha e Estevan Marquês que por se fazerem presentes me ajudaram de um modo ou de outro na conclusão deste trabalho.

To my supervisor abroad Dr. Demian Battaglia for his support, and for his guidance that allowed me to learn so much during my interniship abroad.

À FAPESP (Fundação de Amparo à Pesquisa do Estado de São Paulo) pelo financiamento de minha pesquisa de Mestrado (Bolsa de Mestrado, processo 2017/05874-0; Bolsa Estágio de Pesquisa no Exterior (BEPE), processo 2018/07673-4);

This thesis was produced as part of the activities of FAPESP Research, Innovation and Dissemination Center for Neuromathematics (grant #2013/ 07699-0, S.Paulo Research Foundation).

Ao Programa de Pós-graduação em Física Aplicada à Medicina e Biologia da USP Ribeirão Preto.

O presente trabalho foi realizado com apoio da Coordenação de

Aperfeiçoamento de Pessoal de Nível Superior - Brasil (CAPES) - Código de Financiamento 001.

"What I cannot create I do not understand."

Richard Feynman

Resumo

LIMA, Vinicius **Models of neural networks with stochastic neurons and different topologies: construction and analysis**. 2019. 104 f. Dissertação (Mestrado - Programa de Pós-graduação em Física aplicada à Medicina e Biologia) - Faculdade de Filosofia, Ciências e Letras de Ribeirão Preto, Universidade de São Paulo, Ribeirão Preto - SP, 2019.

O sistema nervoso é submetido a diversas fontes de ruído. Em geral essas fontes se classificam em endógenas e exógenas. O ruído sináptico e o ruído de canais iônicos são as principais fontes de ruído endógeno. O ruído exógeno pode ser atribuído à variabilidade advinda de estímulos externos. O sistema nervoso é munido de estratégias para lidar com a presença do ruído, contudo muito é discutido acerca do papel do ruído no processamento neuronal. Em modelos matemáticos de neurônios, há ao menos duas maneiras de introduzir as fontes de ruído endógenas: uma delas é considerar um modelo determinístico e adicionar termos estocásticos às entradas iônicas ou sinápticas recebidas pelo neurônio, a outra é assumir que o disparo de um neurônio é um evento intrinsecamente aleatório. É possível modelar o último caso por meio de um limiar de disparo que flutua aleatoriamente, onde a ocorrência de um potencial de ação é definido por uma função de probabilidade de disparo dependente da voltagem. Na presente dissertação, utilizamos um modelo intrinsecamente aleatório com o objetivo de determinar as influências que o seu ruído possui em fenômenos a nível celular e de rede. Para isso, primeiro propomos um método para estimar as curvas de probabilidade de disparo de neurônios a partir de registros eletrofisiológicos. Em seguida, utilizamos essas curvas no modelo estocástico para estudar o efeito do ruído intrínseco em fenômenos neurais de importância destacada como confiabilidade nos tempos de disparo e ressonância estocástica. Terminamos a dissertação com o estudo do efeito da topologia sobre a estocasticidade intrínseca dos neurônios individuais em redes complexas de maior porte. Estudamos as topologias com conectividade aleatória e com conectividade específica de uma microcircuitaria cortical. Utilizando uma série temporal do potencial de membrana de ratos, derivamos a curva de probabilidade de disparo utilizada no modelo estocástico, mostrando que para os dados utilizados ela possui uma forma exponencial como observado na literatura. Dentre os resultados obtidos pode-se observar a existência de ressonância estocástica devido ao ruído intrínseco do neurônio e a reprodutibilidade do fenômeno de aumento na confiabilidade nos tempos de disparo em função do ruído sináptico inserido no neurônio. Por fim, os estudos em redes mostraram que a influência causada pelo neurônio estocástico é dependente do estado dinâmico e topologia da rede, surtindo menos efeito em redes aleatórias assíncronas e regulares.

Palavras-chave: 1. Modelo estocástico. 2. Ruído de canal. 3. Ressonância estocástica. 4. Redes complexas. 5. Córtex cerebral.

Abstract

LIMA, Vinicius **Models of neural networks with stochastic neurons and different topologies: construction and analysis**. 2019. 104 f. Dissertation (M.Sc. - Postgraduate program in Physics applied to Medicine and Biology) - Faculty of Philosophy, Sciences and Literature, University of São Paulo, Ribeirão Preto - SP, 2019.

The nervous system is submitted to several sources of noise. In general, those sources can be classified as endogenous and exogenous. Synaptic noise and ionic channel noise are the main endogenous sources of noise. The exogenous noise can be assigned to the variability existent in external stimuli. The nervous system has strategies to deal with the presence of noise, however, it has been discussed the role of noise in neuronal processing. There are at least two ways of introducing endogenous noise sources in mathematical neuron models: the first is to consider a deterministic model and add stochastic terms to the ionic or synaptic inputs received by the neuron, the second is to assume that the emission of an action potential is an intrinsically stochastic event. It is possible to model the latter by introducing a random fluctuating spike threshold, where the occurrence of an action potential is defined by means of a voltage-dependent spike probability function. In this dissertation, we have used an intrinsically stochastic neuron model, aiming to determine the influences of its noise on cellular and network scales. To do so, first, we propose a method to estimate the spike probability curves from eletrophysiological data. Then, we use those curves in the stochastic model to study the effect of the intrinsic noise on relevant natural phenomena as the spiking time reliability and stochastic resonance. We finish the dissertation studying the effect of different network topologies on the intrinsic stochasticity of individual neurons. We study topologies with random connectivity and specific connectivity of a cortical microcircuit. Using a time series of membrane potential we have estimated the spiking probability curve used in the stochastic model, showing that it has an exponential shape as observed in the literature. Among the results obtained, it can be observed the existence of stochastic resonance caused by the neuron's intrinsic noise, and the reproducibility of the increasing spiking time reliability due to input synaptic noise into the neuron. Finally, studies of the network show that the influence caused by the stochastic neuron is dependent on the network's dynamical state and topology, with weaker effects on asynchronous and regular random networks.

Key-words: 1. Stochastic model. 2. Channel noise. 3. Stochastic resonance. 4. Complex networks. 5. Cerebral cortex.

List of abbreviations

LFP	Local field potential
PLV	Phase locking value
LIF	Leaky integrate-and-fire model
IT	Information theory
MI	Mutual information
AP	Action potential
CNS	Central nervous system
FLOP	Float point operation

Contents

Chapter 1

Introduction

1.1 General Introduction

Neuroscience is a relatively new field of research, which started by what is known today as the neuronal doctrine, born when Cajal proposed the role of neurons as the fundamental component of the nervous system, in his 1888 book entitled *Estructura de los centros nerviosos de las aves* (y Cajal, 1888; Yuste, 2015). In 1897 Sherrington introduced the concept of synapse, the fundamental principle of how neurons communicate with each other (Shepherd & Erulkar, 1997). Those early works started not only a journey to unveil brain phenomena, but an inner journey in which the ultimate goal would reveal the basic principles of what makes us humans.

The first mathematical description of neuronal membrane's potential came with the seminal work by Hodgkin and Huxley (Hodgkin & Huxley, 1952) where not only the mechanisms involved in the generation of action potentials in neurons were described, but also a computational simulation using the mathematical equations derived from this work was performed, being the first reproduction *is silico* of the neuronal membrane's potential. Since then many mathematical models were developed to describe the dynamics of single neurons (Izhikevich, 2003a; Gerstner & Brette, 2009; Galves & Löcherbach, 2013) most of them pursue to simplify the formalism proposed by Hodgkin and Huxley allowing easy mathematical handling and low computational cost of simulations.

The field of neuronal simulations was structured years later in 1985 when Eric L. Schwartz coined the term "computational neuroscience". The key concepts

of this field, that before was referred to as different names such as theoretical neuroscience, brain theory, neural modelling, and neural networks, was published in 1990 by Schwartz in a book called *Computational Neuroscience* (Schwartz, 1993). A recent definition for this research field, by the organization for computational neuroscience (OCNS), state as follows: *"Computational neuroscience (CNS) is an interdisciplinary field for development, simulation, and analysis of multi-scale models and theories of neural function from the level of molecules, through cells and networks, up to cognition and behavior."*

Within the past few years the development in neuroscience techniques produced an enormous amount of data, from electrophysiological recordings, anatomical information as the one provided by the Allen atlas (Dong, 2008), to functional imaging data (Poldrack & Gorgolewski, 2014). This steep increase in technology and data acquisition required changes in how neuroscience is approached, several projects as the Human Brain Project were funded around the world and bigger research groups started interacting (Kandel, Markram, Matthews, Yuste, & Koch, 2013; Landhuis, 2017). At the same time, the development of mathematical and computational tools in neuroscience were required to study the data available (Bzdok & Yeo, 2017; Vogt, 2018). In this context, computational simulations showed themselves as a valuable tool to model the data available. Particularly, computational models allowed experimentalist to manipulate relevant parameters involved in a given phenomenon for further understand its influence in the system dynamics. Then, the outcome of those simulations can be tested experimentally and even be used to make predictions of phenomena not yet observed.

The development of large-scale models, using hundreds of thousands neurons, seeks to approach brain scale hoping that phenomena observed in *in vivo* recordings will emerge from the system's dynamics (Plesser, Eppler, Morrison, Diesmann, & Gewaltig, 2007; Potjans & Diesmann, 2014a; Kunkel et al., 2014; Schmidt et al., 2015). In some sense, the development of complex network models, and the improvement of computational tools to write, share, and collaboratively construct program scripts to simulate the brain (M. L. Hines & Carnevale, 1997; Brette et al., 2007; Goodman & Brette, 2009; M. Hines, Davison, & Muller, 2009; Eppler, Helias, Muller, Diesmann, & Gewaltig, 2009; Gleeson et al., 2019) follow the philosophy

that in order to understand the brain we might have to "build" one from scratch.

1.2 Goals

The main goal of this dissertation is to study effects of the intrinsic stochasticity present in the firing of single neurons on the collective behavior of neuronal networks. For that we will use a stochastic model inspired by the recently introduced Galves-Löcherbach neuron model (Galves & Löcherbach, 2013) and its continuous time version (De Masi & Presutti, 2015; Duarte & Ost, 2016). (see also the simplified version of Brochini et al. (Brochini et al., 2016)). This model consists of a differential equation (or map in its discrete form) for the membrane potential in which the emission of an action potential is given by a voltage-dependent probability of firing. Therefore, differently from traditional integrate-and-fire models where the spike is set every time the membrane potential crosses a threshold, the GL model is inherently stochastic. The specific goals of the dissertation are listed below:

- In its generic form the stochastic model can be modeled using any plausible probability function. The studies done so far with the model (Brochini et al., 2016; Costa, Brochini, & Kinouchi, 2017) used theoretical functions chosen due to their simplicity, which facilitates analytical treatment. Our first goal is to develop a method for estimating the probability function from experimental data, and apply it to obtain neuron models suitable to be used in network simulations;

- Our second goal is to describe the differences between well known network models composed of integrate-and-fire neurons and their counterparts composed of stochastic neurons. For that we will use the Brunel model (Brunel, 2000), and the model of the cortical microcircuit proposed by Potjans and Diesmann (Potjans & Diesmann, 2012).

Other goals are:

- To study possible phenomena at the single neuron level that might be reproducible by the stochastic model. More specifically, we are interested in studying phenomena such as spike time reliability and stochastic resonance;

- To study the computational performance of the stochastic model and networks made of it.

1.3 Organization of the dissertation

A summary of the internal structure of each chapter follows:

- In Chapter 2, we review the background and literature. We go through basic neuroscience concepts. Then we focus on discussing the sources, and the role of the noise present in the brain justifying the use of the stochastic neuron model adopted in this dissertation. We finish this chapter discussing the neuron and network models used in this dissertation.

- In Chapter 3 we present our general methods. There, we explain all the statistical measures used along the dissertation. However, specific methods are presented in their respective results chapter.

- In Chapter 4, the first chapter with results, we present the method to estimate the voltage-dependent spiking probability of a neuron. We finish this chapter by applying the method to the experimental data to estimate the spiking probability for the stochastic model used in this dissertation.

- In Chapter 5 we study single neuron phenomena with the stochastic model. In particular, we study the phenomenon of spike time reliability and stochastic resonance due intrinsic noise.

- In Chapter 6, the last results chapter, we present a study of the stochastic model in a random network. We compare the differences of the same network using deterministic and stochastic models by means of first- and second-order statistics.

- In Appendix A we briefly study the computational performance of the stochastic model used in this dissertation in terms of FLOPS, and CPU cycles per time step of simulation.

- In Appendix B we did a similar to the network analysis in Chapter 6 using the stochastic model, however using a complex topology of a cortical microcircuit model.

1.4 Scientific publications derived from this dissertation

During the studies of the author of this dissertation and MSc candidate, he has published articles in peer reviewed journals that are directly related to this dissertation, but also published articles that are not directly related to this dissertation. The latter ones are the product of the interaction with his colleagues on their respective projects, and without their incentive and collaboration this would not have been possible. The complete list of all articles that the MSc. candidate published during his studies (from 2017 to 2019) is shown below.

Peer reviewed journals:

- **Lima., V.**, Pena, R.F.O., Ceballos, C.C., Shimoura, R.O., Roque, A.C. (2018). Aplicações da teoria da informação à neurociência. *Revista Brasileira de Ensino de Física, 41*:e20180197.
  doi.org/10.1590/1806-9126-rbef-2018-0197

- Pena, R.F.O., Ceballos, C.C., **Lima., V.**, Roque, A.C. (2018). Interplay of activation kinetics and the derivative conductance determines resonance properties of neurons. *Physical Review E, 97*:042408.
  doi.org/10.1103/PhysRevE.97.042408 and preprint in arxiv.org/pdf/1712.00306.pdf

- Shimoura, R.O., Kamiji, N.L., Pena, R.F.O., **Cordeiro, V.**, Ceballos, C.C., Romaro, C., Roque, A.C. (2018). [Re] The cell-type specific cortical microcircuit: relating structure and activity in a full-scale spiking network model. *The ReScience Journal, 4* :785–806.
  doi.org/10.5281/zenodo.1243268

- Pena, Rodrigo Felipe de Oliveira; **Cordeiro, Vinicius Lima**; Ceballos, Cesar Augusto Celis; Shimoura, Renan Oliveira; Silva Filho, Ântonio Carlos Roque

da. A new measure to evaluate subthreshold resonance in neurons. In: Nayara Araújo Cardoso; Renan Rhonalty Rocha; Maria Vitória Laurindo. (Org.). A produção do conhecimento na Engenharia Biomédica. 1ed. Ponta Grossa: *Atena Editora*, 2019, p. 87–93
doi: 10.22533/at.ed.8281901069

Manuscripts submitted or in preparation:

- Pena, R.F.O., **Lima., V.**, Ceballos, C.C., Shimoura, R.O., Roque, A.C., Asymmetrical voltage response in resonant neurons shaped by nonlinearities. **in review.**
  Preprint available in arxiv.org/abs/1804.04748

- Pena, R.F.O., **Lima., V.**, Shimoura, R.O., Novato, J.P., Roque, A.C., Optimal interplay between synaptic strengths and network structure enhances activity fluctuations and information propagation in hierarchical modular networks. **in preparation.**
  Preprint available in arxiv.org/abs/1905.01181

Chapter 2

Background to the study and review of the literature

In this chapter, we will start by reviewing the basic concepts on neuronal signaling and communication, followed by discussing which are the main sources of noise present at different brain scales. How the brain manages the presence of noise, and how noise can potentially be essential for some neuronal and brain functions (Section 2.1). We are particularly interested in reviewing the potential benefits of noise to justify the goals of this dissertation (see Section 1.4). In the following, we discuss how to mathematically model neurons, and some approaches used when choosing which model to use. Then, we briefly discuss how to insert noise in a neuron model. We finish this chapter describing in more details neuron and network models used in this dissertation. (Section 2.2).

2.1 Noise in the brain

The nervous system is composed of billions of neurons interacting with each other by means of about a trillion of synapses (Lent, 2004; Herculano-Houzel, Catania, Manger, & Kaas, 2015) forming several interconnected regions (Hagmann et al., 2008; Cordes et al., 2000). In particular, cortical neurons that encode similar features of the external stimuli in the primary sensory cortices can be seen as segregated in what is known as cortical microcolumns (Mountcastle, 1997; Potjans & Diesmann, 2012; Shimoura et al., 2018). These local connectivities aggregate to give rise to different cortical regions, which, by their turn, communicate

among themselves by means of long range fiber projections, creating pathways by which information can be conveyed across the whole cortex. The structure of these pathways can be estimated using diffusion imaging techniques (DIT) (Wedeen et al., 2008; Basser, Pajevic, Pierpaoli, Duda, & Aldroubi, 2000). Other than anatomical projections, the functional structure of interacting regions during, for instance, a cognitive task can be mapped using functional magnetic resonance imaging (Gazzaley, Rissman, & D´ esposito, 2004; Roy et al., 2009). These connectivity studies, both anatomical and functional, reveal a modular and hierarchical connectivity structure (Meunier, Lambiotte, & Bullmore, 2010; Sporns, 2010). Such an intricate wiring is successful in processing every kind of task, from motor activities, to face recognition and cognition itself. However, this same complex structure makes the system susceptible to several sources of noise (Faisal, Selen, & Wolpert, 2008a), ranging from neuronal fluctuations (Pecher, 1939; Adrian, 1957; Verveen, 1960; Movshon, 2000) to network noise (Pena, Zaks, & Roque, 2018). But how can the brain successfully process the diversity of natural stimuli to which we are exposed even when constrained by noise? By which mechanisms the brain deals with noise? And, more importantly, how can the brain take advantage of the presence of noise?

Neurons are considered to be the main building blocks for information processing in the central nervous system. This is known as the *neuron doctrine* (y Cajal, 1888; Yuste, 2015). Glial cells, the other type of cells found in the brain, may also be equally important for information processing, but they will not be considered here[1]. Usually, the neuronal response to a given stimulus is observed by measuring the membrane potential over a time window (see Figure 2.1). In particular, when the stimulus (e.g. a step DC current) reaches a certain level (known as rheobase current) the neuron emits an action potential (AP), a phenomenon in which the voltage rises abruptly above a threshold[2] up to a maximum and then is reset to a

[1] The computational role of glial cells are discussed elsewhere (De Pittà et al., 2012; Zhang & Haydon, 2005).

[2] Although the concept of threshold voltage is useful for mathematical treatment and computational modeling (Lapicque, 1907; Gerstner & Brette, 2009; Izhikevich, 2000, 2007a), real neurons do not exhibit a clear threshold (Gerstner, Kistler, Naud, & Paninski, 2014). In fact, the threshold value will vary depending on the method used to estimate it (Sekerli, Del Negro, Lee, & Butera, 2004).

resting value (Gerstner et al., 2014; Lent, 2004; Bear, Connors, & Paradiso, 2007a). In Figure 2.1 we show the membrane potential of a mouse V1 cortical cell for four different DC step currents (onset at 100 ms). For currents with amplitude above 240 pA the neuron emitted APs regularly (the inset zooms in one AP). The voltage time series registered can be converted into a spike train[3] where if an AP occurred at time t a spike value will be set to one at this time, otherwise it will be set to zero (Dayan & Abbott, 2001). The spike trains are considered to be the means by which neurons encode stimuli and communicate among themselves. Spikes are said to be the elements that implement the neural code[4] (Rieke & Warland, 1999; Bialek, Rieke, Van Steveninck, & Warland, 1991).

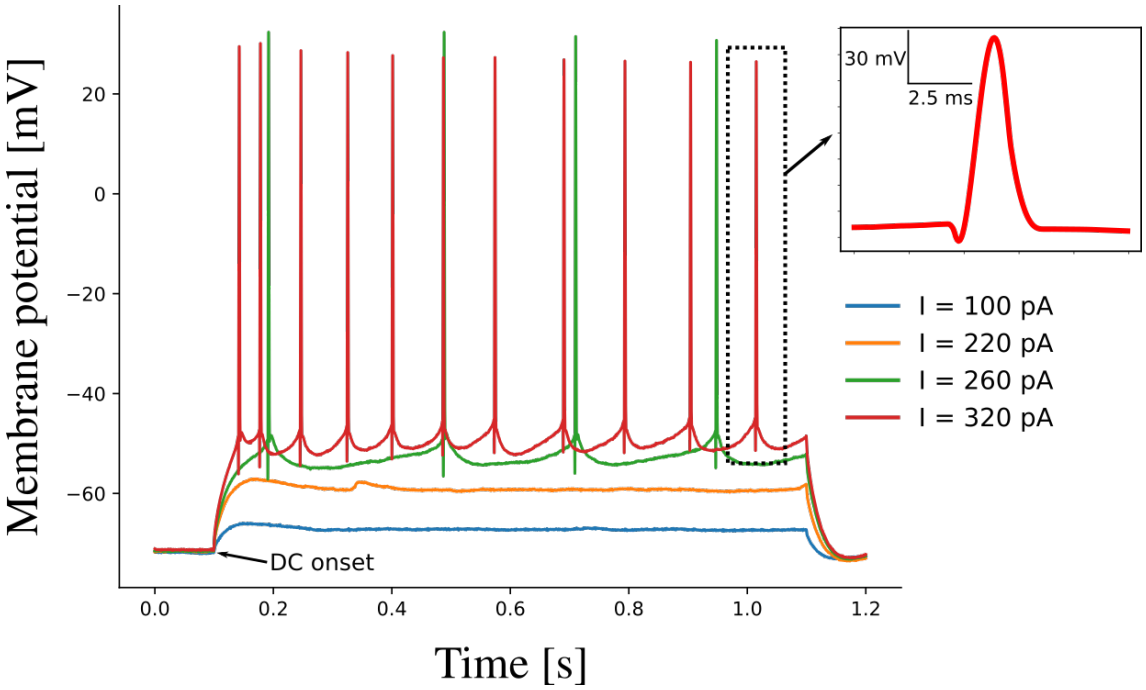

Figure 2.1: *Electrophysiological recordings of a mouse V1 cortical neuron in vitro, stimulated with a DC step current (onset at* 100 *ms) for four different amplitudes (i)* 100 *pA in blue (ii)* 220 *pA in orange (iii)* 260 *pA in green, and (iv)* 320 *pA in red. For this neuron the rheobase current was approximately* 240 *pA. The inset zooms in on an AP for the current amplitude of* 320 *pA.*

The information encoded by the spike trains is transmitted among neurons, mainly by chemical synapses[5] (chemical synapses will be referred to simply by

[3] Action potentials are constantly referred to as spikes by the neuroscience community.
[4] There is some criticism to the concept of neural coding. See, e.g. (Brette, 2019).
[5] Another form of neuronal communication is the electrical synapse (or gap junction), where the

synapses here, for short) (Lent, 2004; Bear, Connors, & Paradiso, 2007b). In a synaptic communication the neuron sending information (presynaptic neuron) stimulates the neuron receiving information (postsynaptic neuron) by releasing chemical agents known as neurotransmitters in the synaptic cleft (Figure 2.2 shows a representative illustration of a synapse). The neurotransmitters will diffuse and bind to receptors in the postsynaptic neuron membrane resulting in a stimulation in this neuron, that can be of an excitatory or inhibitory nature [6]. The effect of a synapse on the membrane voltage of the postsynaptic neuron can be to elevate the voltage (depolarize) above the resting level (excitatory synapse), generating an excitatory postsynaptic potential (EPSP), or to drop the voltage (hyperpolarize) below the resting level (inhibitory synapse), generating an inhibitory postsynaptic potential (IPSP) (Lent, 2004; Bear et al., 2007b; Purves et al., 2019). For a sufficiently strong depolarization (in general, caused by a sum of EPSPs), the voltage is raised above threshold generating an AP, which will be propagated from the neuron to neurons postsynaptic to it.

Electrophysiological recordings *in vitro*, where neurons are isolated from the influence of other cells, show that even in face of the same stimuli neuronal responses are not the same across trials, showing variability[7] in the spike times (Mainen & Sejnowski, 1995; Brette & Guigon, 2003; Ermentrout, Galán, & Urban, 2008; Movshon, 2000; van Steveninck, Lewen, Strong, Koberle, & Bialek, 1997). One of the sources of this variability is the intrinsic stochasticity in the behavior of ion channels present at the neuronal membrane (Faisal et al., 2008a; White, Rubinstein,

membranes of connected neurons are in contact through channel proteins called connexins (Evans & Martin, 2002) that allow electrical currents to flow bidirectionally between the two cells.

[6] There is a diversity of neurotransmitters, which cause different effects on the postsynaptic neuron membrane voltage (Krnjević, 1974). For example glutamate is the main excitatory neurotransmitter, while GABA is the main inhibitory neurotransmitter.

[7] One hypothesis states that stimulus is encoded by the rate of the neuron's spiking (Stein, 1967; Talbot, Darian-Smith, Kornhuber, & Mountcastle, 1968; Gao, Kostlan, Wang, & Wang, 2016); other hypothesis assumes that the precise timing of spikes is relevant for encoding information (Tovee, Rolls, Treves, & Bellis, 1993; Richmond & Optican, 1990; Carr, 2004), with the time of the first spike (Johansson & Birznieks, 2004; VanRullen, Guyonneau, & Thorpe, 2005) or the phase relation between the spike times and an ongoing brain oscillation being relevant for stimulus encoding and transmission (Siegel, Warden, & Miller, 2009; Kayser, Montemurro, Logothetis, & Panzeri, 2009; Montemurro, Rasch, Murayama, Logothetis, & Panzeri, 2008). Therefore, it is of great importance to understand the source of variability in neuronal spiking, since it can constrain the computational capabilities of neurons. For instance, if the spike time is relevant one should expect some degree of reliability if the same stimulus is applied to the neuron.

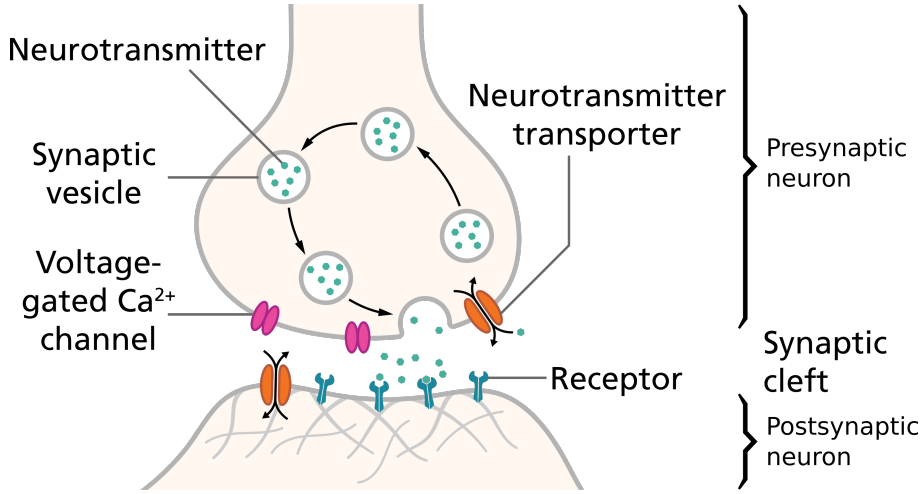

Figure 2.2: *Illustrative representation of a chemical synapse. Notice that in this type of communication the cellular membrane of pre and postsynaptic neurons do not have a physical contact, instead the presynaptic signal is transmitted by means of neurotransmitters, which diffuse through the synaptic cleft towards the postsynaptic neuron membrane. Reaching the postsynaptic neuron the neurotransmitters bind to receptors located in its membrane causing an EPSP or IPSP (see text). Image by Thomas Splettstoesser, en.wikipedia.org/wiki/Neurotransmitter#/media/File:SynapseSchematic_lines.svg.*

& Kay, 2000). These ion channels act as "gates" that open/close to allow/impede specific ions to come in or out of the cell [8] (Hille, 2001). In Figure 2.3(a) we schematically depict an ion channel and its intra and extracellular media. The switching between the open ("on") and closed ("off") states of the ion channel is stochastic (Figure 2.3(b)), reverberating on the membrane voltage dynamics (White et al., 2000). These effects can be observed as sub-threshold voltage fluctuations (Steinmetz, Manwani, Koch, London, & Segev, 2000) that might affect AP emission timing (Jacobson et al., 2005), threshold variability (Sigworth, 1980; Azouz & Gray, 1999), and the probability of spontaneous spikes (Chow & White, 1996). One way to quantify the stochasticity of neuronal response is by computing the probability of response as a function of the voltage pulse amplitude (Pecher, 1939; White et al., 2000). It is possible to reduce the neuronal variability (in this scenario the probability curve would tend to a step function with value one after a sufficiently

[8] The ion flux through the neuronal membrane causes the membrane potential to move towards of what is called the Nernst potential of the ion, for instance the flux of Na^+ to the inside of the cell tends to depolarize the membrane while the flux of K^+ to the outside tends to hyperpolarize it (Hodgkin & Huxley, 1952; Lent, 2004; Bear et al., 2007b).

strong input, see for example the green curve in Figure 2.3(c)) by increasing the number of ionic channels in the membrane (Figure 2.3(c)) (White et al., 2000), but there is always a trade-off between the number of ion channels, ion pumps and the metabolic cost (Laughlin, van Steveninck, & Anderson, 1998; Attwell & Laughlin, 2001).

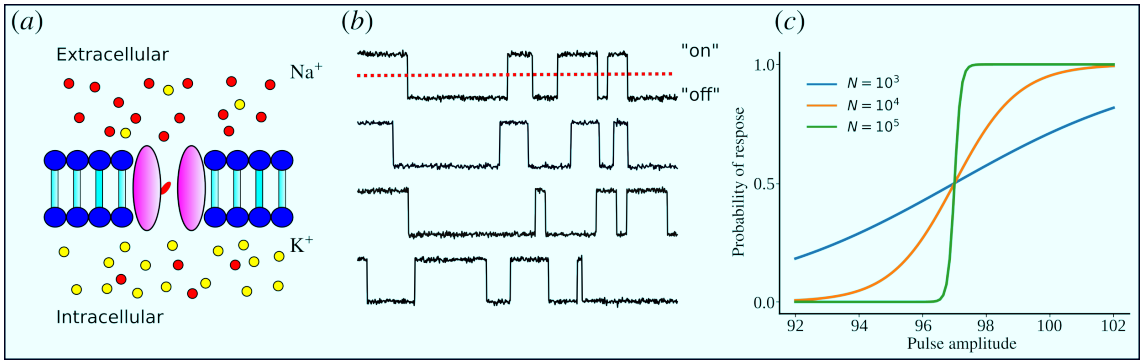

Figure 2.3: *(a) Schematic representation of an ion channel on the phospholipid bilayer neuronal membrane. The concentration of Na^+ ions is higher in the extracellular medium than in the intracellular medium, while the opposite happens to the concentration of K^+ ions. The opening (and closing) of an ion channel gate is voltage dependent. (b) The recording of current flowing through an ion channel shows that the duration of activation and inactivation sequences is highly variable across trials. (c) Probability of neuronal response as a function of input pulse amplitude for three different numbers of ion channels in the membrane. Increasing the number of channels increases the tendency that the neuron responds deterministically.*

Variability is observed in signals obtained *in vivo* (or brain slice preparations) for all brain scales[9] (McDonnell, Goldwyn, & Lindner, 2016), from single neurons to electrical activity registered from neuronal populations, such as local field potentials (LFP) recorded from neuronal ensembles using multiple unit activity (MUA) devices[10] (Barna, Arezzo, & Vaughan Jr, 1981; Herreras, 2016), and cortical electrical activity recorded with electroencephalography (EEG) using electrodes placed at the subject's scalp[11] (Kirschstein & Köhling, 2009; Lopes da Silva &

[9] The brain can be thought as a multilevel organ, i.e., as working at different levels of organization: from single neurons functioning as key components of the nervous system to entire brain regions interacting to give rise to behavior (van den Heuvel & Yeo, 2017).

[10] Recently developed devices allow the recording of a whole cortical hemisphere in non-human primates (Salazar, Dotson, Bressler, & Gray, 2012; Dotson, Hoffman, Goodell, & Gray, 2017).

[11] Here we are referring to techniques that measure electrical activity. Other techniques, such as functional magnetic resonance imaging (fMRI), allow the measurement of the activity from a neuronal population indirectly by using a technique called BOLD (initials for blood oxygenation

Niedermeyer, 1998). For single cell recordings this variability can be measured by the variance of the inter-spike intervals (ISI) distribution, in other words by the irregularity[12] in APs emission (Calvin & Stevens, 1968; Stevens & Zador, 1998). Besides that, postsynaptic neuronal response varies for each trial when receiving the same stimuli (Tomko & Crapper, 1974; Tolhurst, Movshon, & Dean, 1983; Faisal, Selen, & Wolpert, 2008b; Kleppe & Robinson, 2006).

This variability could be accounted by for noise present in the synaptic inputs (Gómez-Laberge, Smolyanskaya, Nassi, Kreiman, & Born, 2016; Faisal et al., 2008b; Calvin & Stevens, 1968), coming from the (on average) 10000 synapses received by neocortical neurons (DeFelipe & Fariñas, 1992; Abbott, Varela, Sen, & Nelson, 1997; Larkman, 1991), usually referred to as "synaptic background noise" [13] (Fellous, Rudolph, Destexhe, & Sejnowski, 2003; Faisal et al., 2008b). The sources of this noise comes from the intrinsic unreliability present in synaptic communication (Faure, Kaplan, & Korn, 2000). Neurotransmitters are released in the form of small packages or quanta (Purves et al., 2019), and the release has a probabilistic nature (Katz, 1969; Hessler, Shirke, & Malinow, 1993). The spontaneous release of quanta, could cause miniature postsynaptic currents (mPSCs) (Fatt & Katz, 1950; Faisal et al., 2008b), called *minis*, which can potentially generate miniature excitatory or inhibitory postsynaptic potentials (mEPSPs or mIPSPs) (Kavalali, 2015; Pulido & Marty, 2017; Faisal et al., 2008b) that contribute to membrane voltage fluctuations observed *in vivo* and irregularities in the AP emission (Destexhe, Rudolph, Fellous, & Sejnowski, 2001).

Other sources of variability in the response of postsynaptic neurons were pointed by Faisal et. al., (2008), namely (i) variations in the concentration of neurotransmitters inside vesicles (Wu et al., 2007); (ii) randomness due to the diffusion process of neurotransmitters; (iii) locations were the neurotransmitter is released in the synaptic cleft (Franks, Stevens, & Sejnowski, 2003); (iv) channel

level dependent) imaging, where the activity is measure by means of the blood diffusing into the region (Haacke, Brown, Thompson, Venkatesan, et al., 1999; Hare et al., 1998).

[12] The inter-spike interval, is the time elapsed between two consecutive spikes. Usually the variance (or the CV) of the ISIs are used as a measure of regularity in the emission of APs (Dayan & Abbott, 2001).

[13] It is discussed elsewhere (Faisal et al., 2008b; Kleppe & Robinson, 2006) that noise in the synaptic background could come from complex deterministic processes.

noise in the postsynaptic membrane receptors (Nimchinsky, Yasuda, Oertner, & Svoboda, 2004); and (v) the density of receptors in the postsynaptic membrane (Nusser, Cull-Candy, & Farrant, 1997; Lim, Alvarez, & Walmsley, 1999).

In summary, the main sources of noise are (i) channel noise, and (ii) synaptic noise. Other minor sources are, for instance, ephaptic interactions (Debanne, 2004), by which the local potential of an axon affects nearby neurons and exogenous noise due to the noisy nature of natural stimuli. But now, getting back to our first question: how the brain manages the presence of noise?

As already discussed, channel noise can be compensated by increasing the number of ion channels present in the cell membrane, but always taking the metabolic cost into account (White et al., 2000). The existence of synaptic noise could limit the capacity of information that can be conveyed via synaptic communication (Shannon, 1948), therefore it is expected that the brain has strategies to manage its presence. Next we discuss some of those strategies.

When subjected to a constant DC stimulation neurons fire irregularly, showing low reliability on their spiking times over trials (Faisal et al., 2008b), but maintaining their spike count distributions over stimulation time[14]. It was shown that adding a fluctuating signal[15] to the DC current increases the reliability of spiking times across trials (Mainen & Sejnowski, 1995; Stevens & Zador, 1998). This could be a way by which a given neuronal population would respond reliably to oscillatory inputs coming from other brain regions (Buracas, Zador, DeWeese, & Albright, 1998).

Another strategy to lower the influence of noise is via averaging over neuronal populations. In this scheme neurons would take advantage of the redundancy present in the input signal to represent it using a population coding that when averaged would reduce the influences of individual sources of noise (Georgopoulos, Schwartz, & Kettner, 1986; Lee, Rohrer, & Sparks, 1988; Faisal et al., 2008b). In a process called divergence, the signal is sent through many axons redundantly, reducing the risk of loss when it is reconstructed in its final destination (Faisal et

[14] This would support a rate coding scheme but not a temporal coding, where spiking time precision is necessary to encode stimuli.

[15] The experiment is done by fixating the fluctuating signal across trials, and, for this reason, it is called *frozen signal* (Ermentrout et al., 2008).

al., 2008b; Glowatzki & Fuchs, 2002). Lastly, neurons can use prior knowledge about a given stimulus to compensate the presence of noise (Adelman, Bialek, & Olberg, 2003; Faisal et al., 2008b). One of the hypothesis on how the brain deals with the variability in natural stimuli states that by using *a priori* knowledge about a given natural signal, a visual stimulus for instance, the brain will infer an *a posteriori* probability of what it is most probably seeing. This hypothesis in called "Bayesian coding hypothesis" or "Bayesian brain hypothesis" (Ma, Beck, Latham, & Pouget, 2006), in which information about sensory stimulus is represented in probability distributions (Knill & Pouget, 2004).

Even though the brain possess mechanisms to manage noise as discussed above, some benefits of its presence are known. In fact, much is argued about the functional role of noise in the brain (Traynelis & Jaramillo, 1998; McClintock, 2002; Stein, Gossen, & Jones, 2005; Faisal et al., 2008a; McDonnell & Ward, 2011). Next, we will approach our second question: how the brain can take advantage from the presence of noise?

Experiments show that channel noise may be crucial to: (i) determine reliability in spike times (Schneidman, Freedman, & Segev, 1998) (ii) influence the dynamics of entorhinal cortex neurons (White, Klink, Alonso, & Kay, 1998), (iii) cause changes in firing patterns in sensory neurons (Braun, Wissing, Schäfer, & Hirsch, 1994; Braun et al., 1997)[16], and (iv) perithreshold oscillations in entorhinal stellate neurons (Dorval & White, 2005). The presence of correlated noise[17] can cause neuronal populations to synchronize (Kurrer & Schulten, 1995; Galán, Fourcaud-Trocmé, Ermentrout, & Urban, 2006). This is particularly relevant because some hypotheses state that the encoding of similar stimuli in the brain is performed via activity synchronization among regions (Gray & McCormick, 1996; Ermentrout et al., 2008; Fries, 2015).

The fact that the brain seems to use noise to certain functions might be due to its evolution under noise influence (McDonnell & Abbott, 2009; Faisal et al., 2008b).

[16] In these papers the authors show that in sharks the presence of noise is crucial to make sensory cells detect perithreshold oscillations, and the detection of electric fields in receptors sensitive to them in the catfish.

[17] Theoretically is is known that the presence of weak correlated noise can induce oscillators to synchronize (Rosenblum, , Kurths, Schäfer, & Tass, 2001).

One interesting example towards this direction is the phenomenon of stochastic resonance (SR)[18], where non-linear systems can optimally enhance the detection of low-amplitude oscillatory inputs for a certain level of noise (McDonnell & Abbott, 2009; Dykman & McClintock, 1998; Gammaitoni, Hänggi, Jung, & Marchesoni, 1998). This phenomenon has been observed both experimentally (Stacey & Durand, 2001; Douglas & Martin, 2004; Mori & Kai, 2002; Ward, MacLean, & Kirschner, 2010), and in neuron models (Moss, Douglass, Wilkens, Pierson, & Pantazelou, 1993; Bezrukov & Vodyanoy, 1995; Stocks & Mannella, 2001; Schmerl & McDonnell, 2013)

2.2 Neuron models

A mathematical model is the description of a phenomenon (or system) using mathematical formalism (Kac, 1969; Frigg & Hartmann, 2006; Griffiths, 2010).

In neuroscience, mathematical models try to capture neuronal and network behavior. In this regard, computational neuroscience tries to model the different spatial-temporal scales of the brain. Particularly, two modeling approaches (Gerstner, Sprekeler, & Deco, 2012) can be used: (i) the bottom-up approach (Figure 2.4(a,b)) tries to model the functioning of brain structures based on details of their constituting components (microscopic scale). Taking these components as neurons, the bottom-up approach starts by modeling single neuron behavior through mathematical equations that describe how the membrane potential evolves given a time varying input (Lapicque, 1907; Hodgkin & Huxley, 1952; Izhikevich, 2003b; Izhikevich & FitzHugh, 2006; Izhikevich, 2007b; Brette & Gerstner, 2005; Gerstner & Brette, 2009; Gerstner et al., 2014); (ii) the top-down approach (Figure 2.4(c)) tries to model the function of a brain structure without relying on a detailed description of their components (macroscopic scale). For example, the dynamics of a whole neuronal population can be described by a single quantity describing its short-time average firing rate (*mean-field* approach), and the dynamics of the interaction between different populations can be modeled by coupled equations for their rates without reference to the individual neurons that constitute the populations (Pinto, Brumberg, Simons, Ermentrout, & Traub, 1996; Destexhe &

[18] The term stochastic resonance (or stochastic facilitation) was first coined in studies concerning the periodicity of ice ages (Wiesenfeld & Moss, 1995).

Sejnowski, 2009).

In this dissertation we will focus on the bottom-up approach, i.e., the behavior of the network models will be based on the behavior of their individual neurons. In Sections 2.2.1 and 2.2.2 we present the single neuron models used. To construct networks, the single neurons will be linked following specific connectivity rules (in Sections 2.3.1 and 2.3.2 we present the network models used).

When working with the bottom-up approach, the single neuron model has to be chosen. In this regard, how to choose which model to use? First it is important to establish which kind of problem one is trying to solve. For certain problems it is important to use a neuron model as detailed as possible, where the morphology of the cell and the biophysical properties of its membrane channels need to be taken into account. In such cases, the dendritic tree, the axon and cell body are constructed using compartmental approach, and the dynamics of the membrane potential is described by the Hodgkin-Huxley (HH) formalism where the time-varying conductances are explicitly modeled (Figure 2.4(a)). If the morphology is not relevant, one still can use the HH formalism to describe a single compartment (usually the soma). On the other hand, if one is interested on phenomenological aspects, such as spiking times, rather than on faithfully modeling the membrane potential one could choose the integrate-and-fire model (IF) and its variations and generalizations: leaky integrate-and-fire (LIF), resonate-and-fire, adaptive IF, quadratic IF, Izhikevich, and AdEx models (Figure 2.4(b)). Another important aspect to take into account is the computational cost of the model (Izhikevich, 2004; Girardi-Schappo, Bortolotto, Stenzinger, Gonsalves, & Tragtenberg, 2017). In Figure 2.5, we show some of the most used neuron models, comparing their number of biological features with their computational cost in FLOPS per time step.

The neuron models discussed so far are called deterministic because applying the same stimulation on them will always yield the same output. In this dissertation we are interested in studying the effects of intrinsic stochasticity (which can be thought as due to channel noise as discussed in the last section) in neuron models. In computational neuroscience noise is introduced in a neuron model basically in two different ways. The first one is to consider a deterministic model (LIF, Izhikevich, AdEx or any other) and add stochastic terms to the ionic or synaptic inputs received

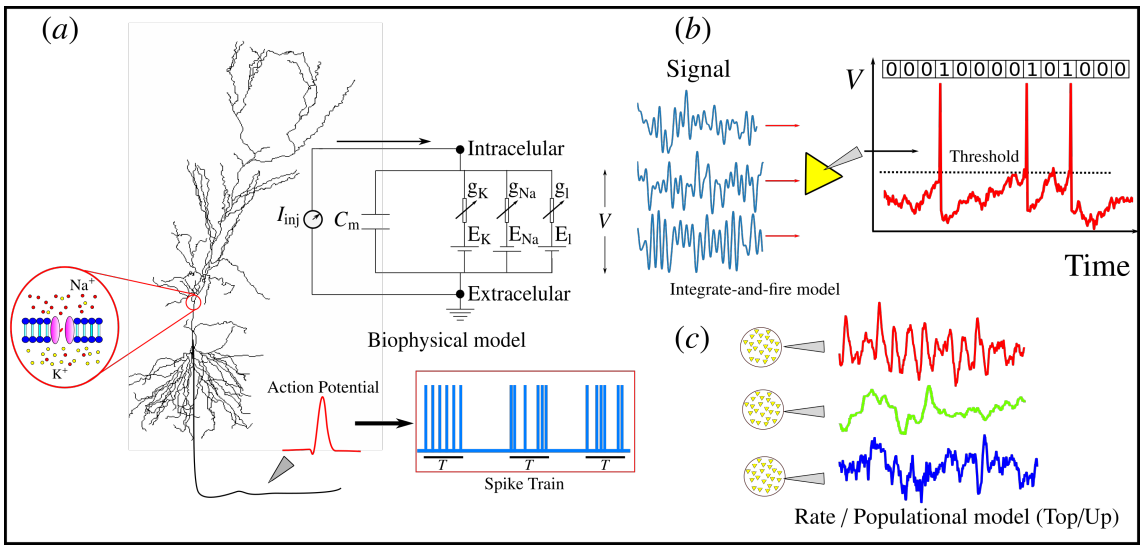

Figure 2.4: *Bottom-up, (a) and (b), and top-down (c) approaches. (a) Biophysically detailed neuron model, considering its morphology and channel dynamics. The biophysical model can be represented by an equivalent circuit with time-varying conductances (for each considered ion) and their respective reversal potentials. The output of the model is the membrane potential (V) at different points of its surface with the APs, which can be converted to a spike train once a threshold value is determined; (b) Integrate-and-fire models, where the membrane potential is modeled as an RC circuit. The output of the model is the membrane potential, and the APs are manually set every time V crosses a threshold; (c) Population models where the dynamics of a ensemble of neurons is modeled by the short-time average of their firing rates; the output of the model is a single variable giving the population rate.*

by the neuron (Tuckwell, 1988; Burkitt, 2006; Gerstner et al., 2014; Longtin, 2013). The second one is to assume that the spike itself is an inherently random event. The latter case can be modeled in different, but equivalent ways: (i) by modeling the ion channels states transitions (from "open" to "close", and vice-versa) via Markov models (Koch & Segev, 1998); (ii) via a threshold that floats randomly, as in the escape rate model (Gerstner et al., 2014; Plesser & Gerstner, 2000a); or (iii) by introducing a voltage dependent spike probability function $\phi(V)$. The stochastic model recently introduced by Galves and Löcherbach (Galves & Löcherbach, 2013) uses the third approach. The Galves and Löcherbach model, which will be referred to here as *GL model* for short, was an inspiration for the stochastic model used in this dissertation.

In Figure 2.5 we represent the neuron models in terms of two of their characteristics: number of biological features and computation cost to be

implemented. The stochastic model considered in this dissertation was included in the figure. We assumed that the stochastic model has one more biological feature than the IF model, and the computational cost was estimated by the lower-bound on the number of FLOPS per time step (FLOPS/ts) used to simulate the model (see Appendix A for a detailed performance analysis of the stochastic model). In the next sections we will discuss in more detail the neuron models (LIF and stochastic) and the network models used in this dissertation.

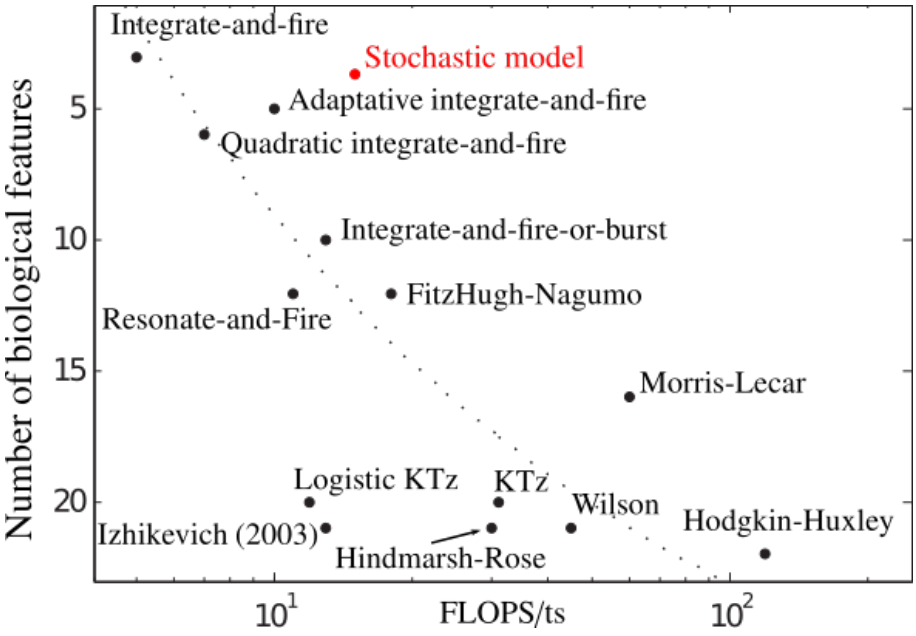

Figure 2.5: *Comparison of the number of biological features for some of the most used neuron models, and the computational cost required to simulate them in FLOPS per time step (FLOPS/ts). In red we show the stochastic model. Figure adapted from Girard et. al., (2017) (Girardi-Schappo et al., 2017).*

2.2.1 Deterministic leaky integrate and fire model (LIF)

The leaky integrate and fire model describes the sub-threshold dynamics (see Figure 2.7(a)) of the neuronal membrane potential by assuming that the membrane can be approximately described as an equivalent RC circuit as shown in Figure 2.6, where C_{m} and R_{m} are the membrane capacitance and resistance, respectively, V_{r} is the resting potential, I_{inj} an external current injected into the neuron, and V the membrane potential. The model is described by Equation 2.1, named membrane equation.

$$\frac{dV(t)}{dt} = -\frac{V(t) - V_{\mathrm{r}}}{\tau_{\mathrm{m}}} + \frac{I_{\mathrm{inj}}(t)}{C_{\mathrm{m}}}, \tag{2.1}$$

where τ_{m} is the membrane time constant, given by the product $\tau_{\mathrm{m}} = R_{\mathrm{m}}C_{\mathrm{m}}$.

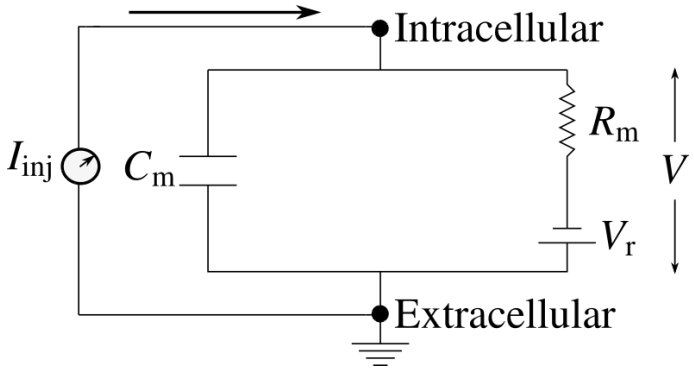

Figure 2.6: *Equivalent RC circuit used to model the difference of potential between the intra- and extracellular medium (V), given an input current I_{inj}, the membrane capacitance C_{m}, resistance R_m, and a reversal potential V_{r}.*

Equation 2.1 only describes the sub-threshold dynamics of the membrane potential and does not have a mechanism to generate an action potential. To implement an action potential, the LIF model defines a threshold voltage V_{th} and sets a reset rule so that every time V crosses V_{th} it is considered that the neuron fired. This fire-and-reset mechanism is described in Equation 2.2.

$$V(t) \geq V_{\mathrm{th}} \Rightarrow \begin{cases} \text{Spike at time } t \\ V(t + \tau_{\mathrm{ref}}) = V_{\mathrm{reset}}, \end{cases} \tag{2.2}$$

where τ_{ref} is the absolute refractory time, during which the membrane potential is maintained at its reset value V_{reset}. Figure 2.7(b), illustrates the numerical integration of Equations 2.1 and 2.2. Note that because there is a fixed threshold the neuron will always behave equally given the same constant input, i.e. the LIF model is a deterministic model.

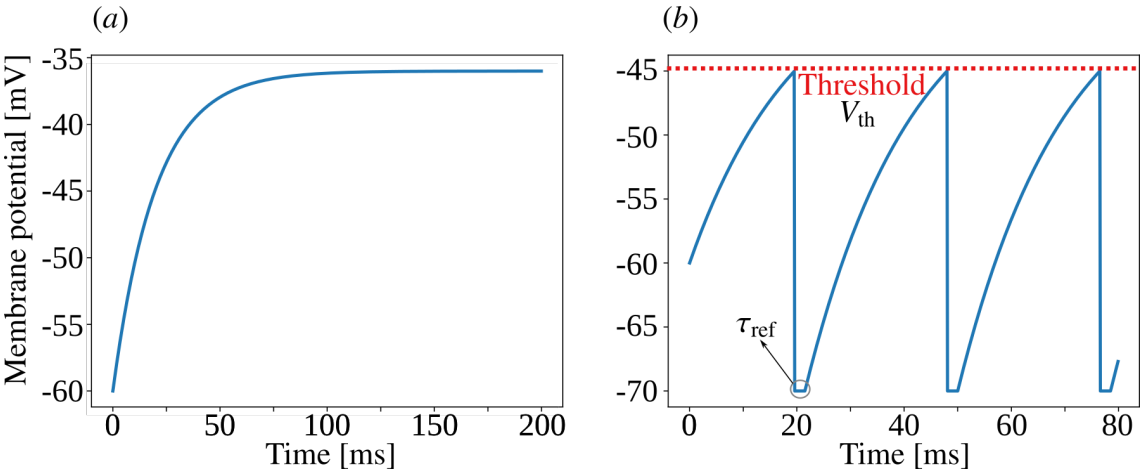

Figure 2.7: *Integration of the Equation 2.1 (a) if the input is not strong enough to make the neuron spike, it will only drive the membrane potential to a saturation value until the moment in which the external current is turned off; (b) if the input is greater than the rheobase current the neuron will fire regularly (threshold indicated by red dashed line). After each spike (not shown), the membrane potential remains in its rest value for a period equal to* τ_{ref}*. The parameters to generate those curves are* $\tau_m = 20\ ms$*,* $I_inj = 30\ mV$*,* $V_r = -60\ mV$*,* $V_{\text{th}} = -45\ mV$*, and* $\tau_{\text{ref}} = 2\ ms$*.*

In this dissertation, the LIF model is used to implement the nodes' dynamics of the followinfg networks: (i) the random network (Brunel, 2000), and (ii) the cortical microcircuit model (Potjans & Diesmann, 2014b). See Sections 2.3.1, and 2.3.2, respectively.

2.2.2 Stochastic model

The stochastic neuron model considered in this dissertation is inspired by the GL model (Galves & Löcherbach, 2013), and its continuous time version (De Masi & Presutti, 2015; Duarte & Ost, 2016). For a time interval in which the neuron does not fire, its membrane potential is described by the same equation used to describe the time evolution of the LIF model (Equation 2.1). However, at any moment in time the neuron can fire with a probability $\phi(V(t))$, where $\phi(V)$ is a non

decreasing function of the neuron's instantaneous membrane potential that tends to zero (one) for hyperpolarized (depolarized) membrane potentials. Following Galves and Löcherbach (Galves & Löcherbach, 2013) (see also (Brochini et al., 2016)), we will use a variable $X(t)$ to denote whether or not the neuron has emitted a spike at time t. If $X(t) = 1$, the neuron has fired at time t, and if $X(t) = 0$, the neuron has not fired. The refractory period τ_{ref} is defined such that, $t^\star < X(t) = 0 < t^\star + \tau_{\text{ref}}$ if $X(t^\star) = 1$.

The difference between the stochastic and the LIF model is the firing function $\phi(V)$. The existence of $\phi(V)$ allows the stochastic model to display a variable output for different trials where the same DC step current is injected to the neuron as shown in Figure 2.8.

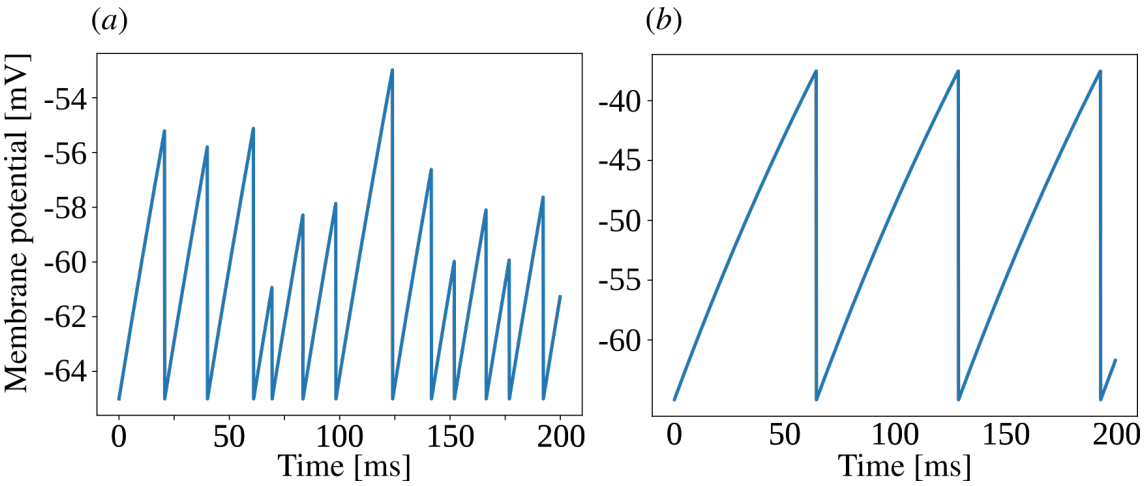

Figure 2.8: *Comparison between the stochastic and LIF models. The graphs show the membrane potential under the same input conditions for (a) the stochastic model and (b) the LIF model. It is possible to see that for the stochastic model the firing threshold and inter-spike intervals are variable in comparison to the regular LIF model. The parameters to generate those membrane potentials are the same as in Figure 2.7.*

2.3 Network Models

2.3.1 The random network

The random network implemented in this dissertation is the same as described by Brunel (2000) (Brunel, 2000). The original network consists of N LIF neurons. The parameters used for the neuron model are given in Table 2.1 (for

more details on the parameter see Section 2.2.1).

V_{th}	V_{r}	V_{reset}	τ_{m}	τ_{ref}
20 mV	0 mV	10 mV	20 ms	2 ms

Table 2.1: *Parameters of the LIF model used in the random network.*

The network is divided into two populations: one with $N_{\text{e}} = 0.8N$ excitatory neurons and the other with $N_i = 0.2N$ inhibitory neurons. Each neuron receives $C = \epsilon N$ connections chosen randomly, of which $C_{\text{e}} = 0.8C$ are excitatory and $C_{\text{i}} = 0.2C$ are inhibitory.

Apart from the network internal connectivity, each neuron receives $C_{\text{e}}^{\text{ext}} = C_{\text{e}}$ synaptic inputs from a external, not explicitly modeled, population, with the same synaptic weight (equal to the internal connection weight J, see below). These entries are modeled as independent Poisson processes with rate ν_{ext}. This rate is determined as a function of the minimum frequency necessary (ν_{thr}) to make the neuron reach its threshold in the absence of feedback input, and is given by Eq. 2.3.

$$\nu_{\text{thr}} = \frac{V_{\text{th}}}{JC_{\text{e}}\tau_{\text{m}}}. \tag{2.3}$$

If the ratio $\nu_{\text{ext}}/\nu_{\text{thr}}$ is known, one can use Eq. 2.3 to determine ν_{ext}.

In this model the synaptic input from the pre-synaptic neuron j to the post-synaptic neuron i is given by Eq. 2.4.

$$RI_{\text{i, sin}} = \tau_{\text{m}} \sum_j J_{ij} \sum_k \delta(t - t_j^{f,k} - d), \tag{2.4}$$

where τ_{m} is the membrane time constant, J_{ij} is the synaptic weight of the $j \to i$ connection, $t_j^{f,k}$ is the time of the k^{th} spike form neuron j, and d the transmission delay. All excitatory connections have the same weight J. For the inhibitory connections the weight is multiplied by the factor $-g$, called the relative strength of inhibitory connections.

Table 2.2 shows the values of the parameters of the network.

Despite its simplicity, this model allows the reproduction of several activity regimes found in the cerebral cortex by only varying the parameters g and $\nu_{\text{ext}}/\nu_{\text{thr}}$. These regimes are listed below as defined by Brunel (Brunel, 2000):

N_e	N_i	C_e	C_i	J	d
10000	2500	1000	250	0.1 mV	2 ms

Table 2.2: *Parameter values for the random network.*

- **Synchronous and regular state** (SR), in which neurons are almost totally synchronized and behave like oscillators; in this regime, the excitation dominates inhibition and the distribution of synaptic times possess a dominant peak;

- **Asynchronous and regular state** (AR), with steady global activity and neurons with almost regular individual firing; in this regime, the excitation dominates inhibition and the distribution of synaptic times possess several peaks;

- **Asynchronous and irregular state** (AI), with steady global activity and strong irregularity in neuronal firing, maintaining low frequency; in this regime, inhibition dominates excitation for an intermediate interval of external frequencies;

- **Synchronous and irregular state** (SI), with oscillatory global activity and strong irregularity in neuronal firing with low frequency (with respect to the global oscillation); in this regime, inhibition dominates the excitation both for low (slow oscillations) and high frequencies (fast oscillations) of the external inputs. When the mean value of the time constant is sufficiently high, these two regions merge.

The parameters g and ν_{ext} that reproduce the four activity regimes mentioned above are displayed in Table 2.3.

State	g	ν_{ext} [Hz]	D [ms]
SR	3.0	20	1.5
AI	5.0	20	1.5
SI (slow)	4.5	9	1.5
SI (fast)	6.0	40	1.5

Table 2.3: *Parameter values that lead the random network to display the four activity states (SR, AI, SI slow, and SI fast) described by Brunel.*

2.3.2 The cortical microcircuit model

The cortical microcircuit model used in this dissertation is the same one proposed by Potjans and Diesmann (PD model) (Potjans & Diesmann, 2012). In this model the network is divided in four layers, each one containing a cortical population segregated into excitatory and inhibitory neurons. The layers are: $L23$e, $L23$i, $L4$e, $L4$i, $L5$e, $L5$i, $L6$e, and $L6$i, where the letter L stands for layer followed by its number, and e/i stands for excitatory/inhibitory respectively. In Figure 2.9 we show a schematic representation of the model.

The population of neurons in each layer is given in Table 2.8. Each neuron receives N_{syn} connections from each layer, drawn randomly, with N_{syn} given by Equation 2.5.

$$N_{\text{syn}} = \frac{\log(1 - C_{\text{a}})}{\log(1 - 1/(N_{\text{pre}} N_{\text{post}}))}, \tag{2.5}$$

where C_{a} is the probability of connection between two layers (see Table 2.4), N_{pre} the number of neurons in the presynaptic population, and N_{post} the number of neurons in the postsynaptic population.

The network is composed of LIF neurons (see Section 2.2.1). In the PD model, the initial value for the membrane potential ($V(0)$) of each neuron is drawn from a normal distribution $\mathcal{N}(\mu = -58.0, \sigma = 10)$ mV. All parameters used to model neurons are presented in Table 2.5.

The synaptic input (I_{sin}) coming from the presynaptic neuron i is modeled

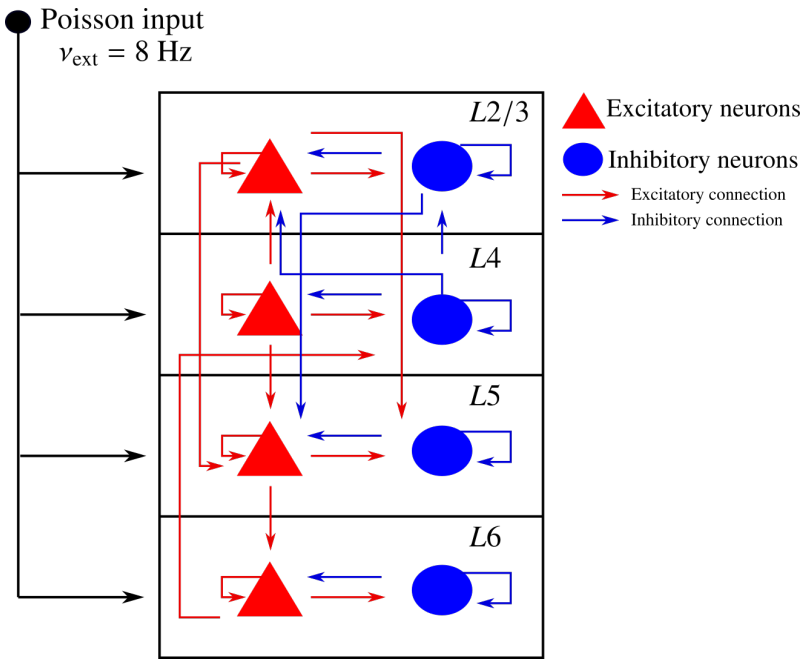

Figure 2.9: *Schematic representations of the Potjans and Diesmann cortical microcircuit model. The model consists of four cortical layers: L23e, ,L4e, L4i, L5e, L5i, L6e, and L6i. Excitatory neurons are represented by red triangles, and inhibitory neurons by blue circles. Excitatory connections are indicated by red arrows and inhibitory connections are indicated by blue arrows. Poissonian inputs arrive in each layer (indicated by black arrows) with frequency* 8 *Hz. The number of Poisson inputs per layer is given in Table 2.7.*

		From							
		L23e	L23i	L4e	L4i	L5e	L5i	L6e	L6i
	L23e	0.101	0.169	0.044	0.082	0.032	0.0	0.008	0.0
	L23i	0.135	0.137	0.032	0.052	0.075	0.0	0.004	0.0
	L4e	0.008	0.006	0.050	0.135	0.007	0.0003	0.045	0.0
To	L4i	0.069	0.003	0.079	0.160	0.003	0.0	0.106	0.0
	L5e	0.100	0.062	0.051	0.006	0.083	0.373	0.020	0.0
	L5i	0.055	0.027	0.026	0.002	0.060	0.316	0.009	0.0
	L6e	0.016	0.007	0.021	0.017	0.057	0.020	0.040	0.225
	L6i	0.036	0.001	0.003	0.001	0.028	0.008	0.066	0.144

Table 2.4: *Layer-specif connection probabilities. In this table we show the probability that a neuron from layer* ***A*** *(rows) makes a connection to a neuron in layer* ***B*** *(columns).*

V_{r} [mV]	V_{reset} [mV]	V_{th} [mV]	C_{m} [pF]	τ_{m} [ms]	τ_{ref} [ms]
-65	-65	-50	250	10	2

Table 2.5: *Parameters used in the LIF model of the PD model. Note that in this model there is a capacitance term C_{m} that is used to convert the input current to mV (by taking the ratio of the input current and C_m).*

by Equation 2.6.

$$\frac{dI_{\mathrm{i,sin}}}{dt} = -\frac{I_{\mathrm{i,sin}}(t)}{\tau_{\mathrm{sin}}} + \sum_j J_{ij} \sum_k \delta(t - t_j^{f,k} - d), \tag{2.6}$$

where τ_{sin} is the synaptic time constant, the parameters J_{ij}, $t_j^{f,k}$, and D have the same meaning as in the random model discussed in Section 2.3.1. Here, the delay has two different values depending on the presynaptic neuron: D_e for synapses coming from excitatory neurons, and D_i for synapses coming from inhibitory neurons respectively. Note that, differently from the random network, the synaptic current for the PD model has an exponential decay and is incremented every time a spike arrives.

To set the network parameters, the delays and synaptic weights are drawn from normal distributions. For the delays (excitatory and inhibitory): $\mathcal{N}(\mu = d_{\mathrm{e/i}}, \sigma = \sigma_{d_{\mathrm{e/i}}})$. For the excitatory synaptic weights: $\mathcal{N}(\mu = J, \sigma = \sigma_{\mathrm{J}})$; for the inhibitory synapses these numbers are multiplied by $-g$. In Table 2.6, we show all the parameters for the synapses in the model.

J	$\mathcal{N}(\mu = 87.8, \sigma = 8.8)$ pA
g	4.0
d_{e}	$\mathcal{N}(\mu = 1.5, \sigma = 0.75)$ ms
d_{i}	$\mathcal{N}(\mu = 0.8, \sigma = 0.4)$ ms

Table 2.6: *Values for the synaptic weight (J), the excitatory (d_{e}) and inhibitory d_{i} delays, and the relative excitatory and inhibitory strength (g). Note that J, d_{e}, and d_{i} values are drawn from normal distribution with mean μ, and standard deviation σ.*

Finally, neurons in each layer receive external inputs given by independent Poisson processes with frequency ν_{ext}, which represent stimuli coming from other

brain region not explicitly modeled. In Table 2.7 we give the number of Poisson inputs that each neuron receives, as well as the frequency of the Poisson generator.

L23e	L23i	L4e	L4i	L5e	L5i	L6e	L6i
1600	1500	2100	1900	2000	1900	2900	2100
ν_{ext}				8 Hz			

Table 2.7: *Number of Poisson generators in each layer (second row), and their frequency (ν_{ext}).*

$L23$e	$L23$i	$L4$e	$L4$i	$L5$e	$L5$i	$L6$e	$L6$i
20683	5834	21915	5479	4850	1065	14395	2948

Table 2.8: *Size of the neuronal population in each layer of the model.*

2.4 Numerical integration and computational platform

All codes used in this dissertation were written in Python 3.6.6 (except the one to compute the computational performance of the stochastic model that was written in C#). The implementation of neuron and network models were using the neurosimulator Brian 2 (version 2.2.2.1) (Goodman & Brette, 2009). For numerical and scientific computation we used the standard numpy (version 1.16.2) and scipy (version 1.2.1) modules. To data visualization the matplotlib (version 3.0.3) and seaborn (version 0.9.0) modules.

Chapter 3

General methods

To avoid definitions to be spread along the text, and to make it more convenient for the reader to consult them, in this chapter we present the most commonly used measures in this dissertation.

3.1 Measures

3.1.1 Spike trains

The spike train $x(t)$, defined by Equation 3.1, is a discrete representation of action potentials in a given time series $V(t)$ of the membrane potential. To build $x(t)$ we divide $V(t)$ in N bins, where N is the ratio between the length of the simulation T_{sim} and the its time step Δt.

$$x(t) = \sum_{[t^f]} \delta(t - t^f). \tag{3.1}$$

In Equation 3.1, t^f is the time array containing all the times where spikes occurred, and δ is the Dirac's function. Note that when there is a spike $x(t) = 1/\Delta t$, otherwise it will be $x(t) = 0$. Figure 3.1 shows the discretization of a times series recorded from a CA1 pyramidal neuron into a spike train.

3.1.2 Firing rate

The firing rate f of a given neuron is defined as the ratio between the number of spikes N_{spikes} within a time window T, which can be directly obtained from

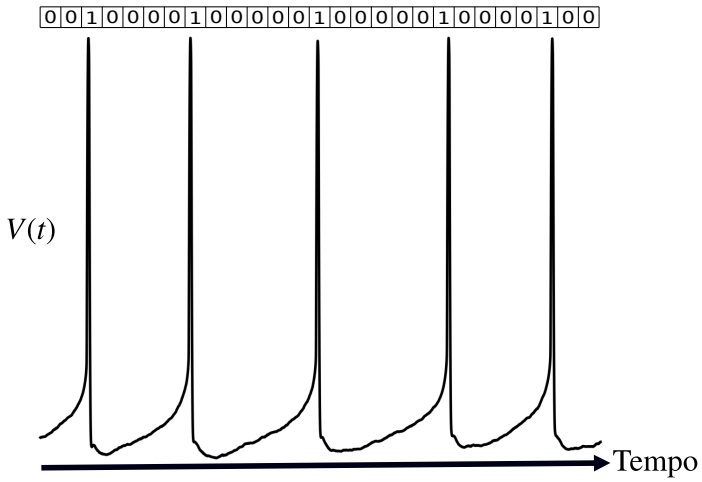

Figure 3.1: *Electrophysiological recordings in vitro from a pyramidal cell from rat's hippocampus, stimulated by a constant current ($I = 260$) pA applied to the cell body (soma), showing part of the APs emitted by the cell. Above voltage trace there is a binary sequence (zeros and ones) illustrating the spike train.*

Equation 3.1,

$$f = \frac{1}{T}\int_T x(t)dt = \frac{N_{\text{spikes}}}{T}. \tag{3.2}$$

For the case where we have a network composed of N neurons, the average firing rate can be obtained by using Equation 3.3,

$$\langle f \rangle_N = \frac{1}{T}\sum_{i=1}^{N}\int_T x_i(t)dt = \frac{\langle N_{\text{spikes}} \rangle}{T}, \tag{3.3}$$

where $\langle . \rangle_{\text{N}}$ indicates an average over all neurons in the network, and i indicates the index of a given neuron. Equation 3.3, can also be used to estimate the average firing rate of a neuron submitted to the same input protocol several times.

3.1.3 Input frequency curve (IF)

The firing rate can be used to characterize neuron's response. This characterization is done by applying several step current inputs with distinct amplitudes I into the neuron, for each amplitude we measure its firing rate, and

then plot it against I as in Figure 3.2, where it is shown the IF curve of a LIF neuron.

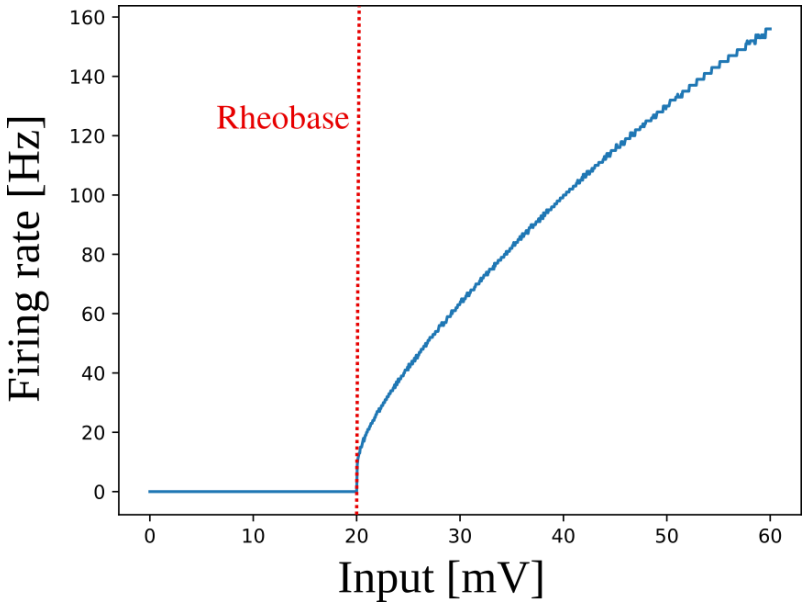

Figure 3.2: *Input-frequency curve for a LIF neuron model, note that after the rheobase current (indicated by the vertical dashed red line) the neuron starts firing at a non-zero frequency.*

The use of an IF curve can be useful to characterize some properties of the neuronal response, as its rheobase defined as the minimum current injection that is necessary to make the neuron fire.

3.1.4 Inter spike interval (ISI)

The inter spike interval (ISI) is defined as the time gap between two consecutive spikes, and can be defined by Equation 3.4:

$$ISI_i = t^f_{i+1} - t^f_i, \tag{3.4}$$

for a given spike train, the average ISI, is given by:

$$\langle ISI \rangle = \frac{1}{N_{\text{spikes}} - 1} \sum_{i=1}^{N_{\text{spikes}}} ISI_i. \tag{3.5}$$

The variance $\sigma^2_{\langle \text{ISI} \rangle}$ of $\langle ISI \rangle$ is given by Equation 3.6:

$$\sigma^2_{\langle \text{ISI} \rangle} = \frac{1}{N_{\text{spikes}} - 2} \sum_{i=1}^{N_{\text{spikes}}-1} [ISI_i - \langle ISI \rangle]^2. \tag{3.6}$$

The standard deviation of the ISI, $\sigma_{\langle \text{ISI} \rangle}$, can be interpreted as a measure of regularity of the neuronal spiking activity, where great values of $\sigma_{\langle \text{ISI} \rangle}$ indicate irregularity, whereas $\sigma_{\langle \text{ISI} \rangle} = 0$ indicate periodic firing.

3.1.5 Coefficient of variation (CV)

Although the standard deviation of the ISI can be thought as a measure of regularity on the neuronal firing, usually its normalized version, called CV is used. The CV is defined as the ratio by the standard deviation of a feature and its mean. For the ISI it is given by Equation 3.7.

$$CV = \frac{\sigma_{\langle \text{ISI} \rangle}}{\langle ISI \rangle}. \tag{3.7}$$

The neuron is considered to fire irregularly if $CV \to 1$, and regularly if $CV \to 0$. For a network of neurons we measure the mean value of the CV distribution given by Equation 3.8.

$$\langle CV \rangle_{\text{N}} = \frac{1}{N} \sum_{i=1}^{N} CV_i. \tag{3.8}$$

3.1.6 Raster plot

The raster plot is used to visualize spike trains and could be used to represent (i) the spike trains of the same neuron for different repetitions of an experimental protocol, or (ii) to represent spike trains of different neurons in a network.

The y-axis in the raster plot represents the neuron ID (or the trial number if an experimental protocol is being repeated) and the x-axis the time. In each instant t^f in which a spike is emitted by neuron i a dot is marked in time t^f for y-axis equals i. Figure 3.3 illustrates the raster plot of a network.

Using the raster plot it is possible to extract several measures such as the peristimulus time histogram (for a single neuron) or the activity of a network.

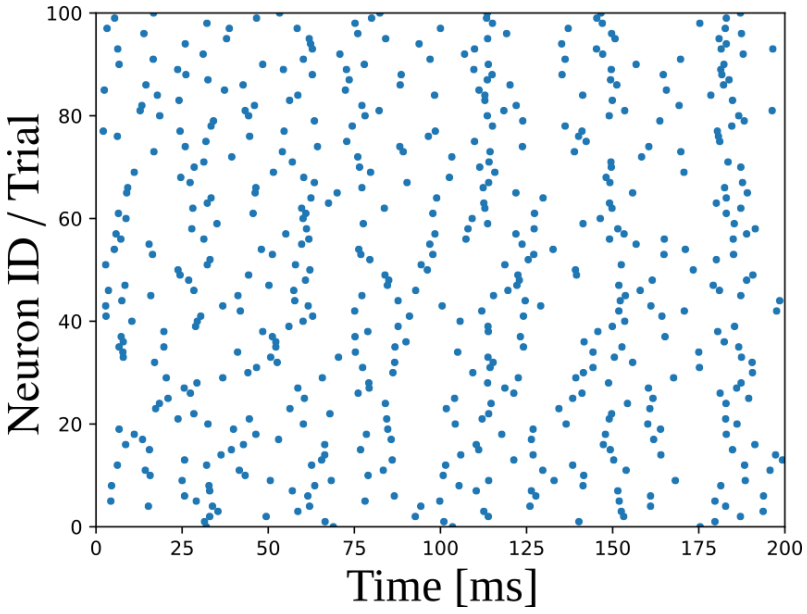

Figure 3.3: *Example of a raster plot where for each time in which the neuron fires (x-axis) a dot is marked for neuron i (y-axis). Note that for a network the y-axis indicates the ID of this neuron in the network; if the same experiment is repeated for one neuron the y-axis indicates the trial number.*

3.1.7 Peristimulus time histogram and activity

In neurophysiology, the peristimulus time histogram (PSTH) is a histogram of the spike times of a single neuron for the repetition of the same stimulus, and it is used to visualize the firing pattern of this neuron for different stimuli.

It can be built from a raster plot (see Section 3.1.6), following the algorithm:

1. Use a given stimuli $S(t)$ to stimulate the neuron n times and for each repetition determine the spike train using Equation 3.1;
2. Once determined, use the spike trains to build the raster plot as explained in Section 3.1.6;
3. Choose a time bin length Δt, to discretize the raster plot in k windows;
4. For each window calculate the firing rate using $f_{\text{bin}} = N_{\text{spikes}}^{\text{bin}}/(k\Delta t)$, where $N_{\text{spikes}}^{\text{bin}}$ is the number of spikes in a given bin;
5. With the frequency for each bin determined, the PSTH can be built as a bar graph.

Figure 3.4, illustrates the procedure to determine the PSTH.

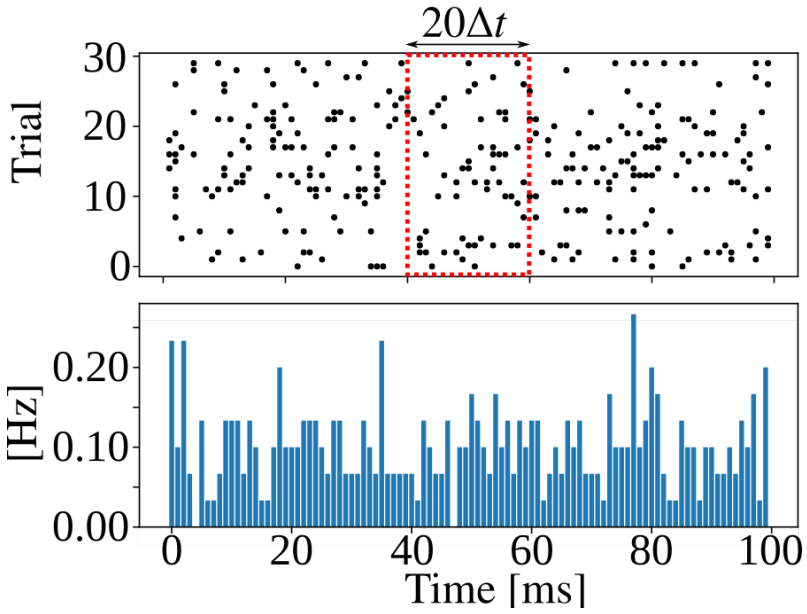

Figure 3.4: *Peristimulus time histogram for a sample raster plot (top), we used* $\Delta t = 1$ *(the dashed rectangle shows the size of* $20\Delta t$*). The bottom graph shows the PSTH constructed for this raster plot.*

The procedure to calculate the network activity ($r(t)$) follows the same steps above. Therefore the main difference between the PSTH and activity is that the first is used as a single neuron measure and the latter is a populational measure.

3.1.8 Synchrony

Synchrony is a populational measure that indicates rhythmic adjust between two or more oscillatory phenomena, such as neuronal firing, due to weak interactions among the oscillators (Pikovsky, Rosenblum, & Kurths, 2001). To quantify the degree of synchrony among neurons in a network, we use the phase locking value (PLV) which is a standard measure to evaluate phase synchronization (Lachaux, Rodriguez, Martinerie, & Varela, 1999; Celka, 2007; Rosenblum et al., 2001; Aydore, Pantazis, & Leahy, 2013; Lowet, Roberts, Bonizzi, Karel, & De Weerd, 2016). We define the PLV as the average over K neuron pairs and T sample time points:

$$PLV = \frac{1}{K} \sum_{\{ij\}}^{K} \left| \sum_{t}^{T} e^{i\Delta\Phi_{xy}(t)} \right|, \tag{3.9}$$

where $\Delta\Phi_{xy}(t)$ are the phase differences $\Phi_x(t) - \Phi_y(t)$ from two randomly chosen spike-trains $(x(t), y(t))$ that are obtained using the Hilbert transform. First we express the signal $x(t)$ in the complex plane as:

$$z(t) = z_r(t) + jz_i(t) = x(t) + j\mathcal{H}[x(t)], \tag{3.10}$$

where $z_r(t)$ is the real component, $z_i(t))$ is the imaginary component, j is the imaginary unit, and $\mathcal{H}$ the the Hilbert transform. Then we compute the instantaneous phase of the signal using:

$$\phi_x = \arctan\left[\frac{z_i(t)}{z_r(t)}\right] = \arctan\left[\frac{\mathcal{H}[x(t)]}{x(t)}\right]. \tag{3.11}$$

The PLV is bounded between 0 (asynchronous) and 1 (synchronous). It is also useful to plot the distributions of $\Delta\Phi_{xy}(t)$ to see in which phase the signals are locked for instance. For $PLV \to 0$, the distribution will have no clear peak. As PLV goes towards 1 the distribution will narrow around the phase in which the two signals are synchronized. To illustrate, we show the $\Delta\Phi_{xy}(t)$ distributions along the PLV values in Figure 3.5 of two coupled Rossler oscillator (Rössler, 1976) for three different coupling (ϵ) values.

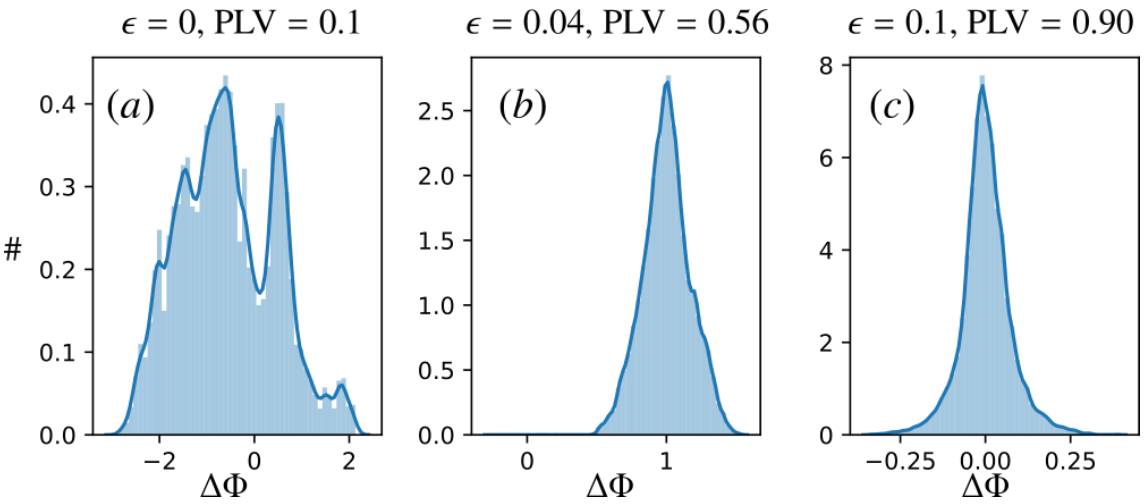

Figure 3.5: *Distribution of phase differences $\Delta\Phi$ for two coupled Rossler oscillators (where ϵ is the coupling strength). We show the distributions for three ϵ values: (a) $\epsilon = 0$, (b) $\epsilon = 0.04$, and (c) $\epsilon = 0.1$, the PLVs are shown atop each distribution.*

3.1.9 Mean squared error (Q)

The least mean square (Q) is given by Equation 3.12, and quantifies the distance between two experimental discrete curves, each one having N points: $X = \{x_1, x_2, ..., x_N\}$ e $Y = \{y_1, y_2, ..., y_N\}$.

$$Q = \frac{1}{N}\sum_{i=0}^{N}(X_i - Y_i)^2 = \sum_{i=0}^{N}\Delta_i^2, \tag{3.12}$$

with $X_i = x_i$ e $Y_i = y_i$. Figure 3.6 illustrates the procedure for the extraction of Q between X and Y.

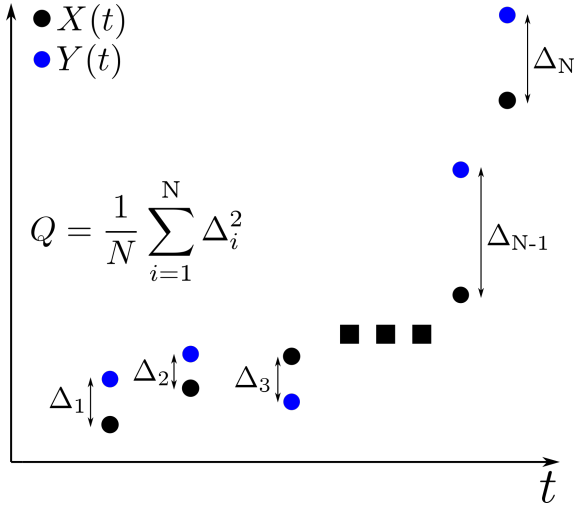

Figure 3.6: *Illustration of the procedure to compute the mean squared error. For each point i from dataset $X(t)$, and point j from dataset $Y(t)$ we measure the distance $\Delta_{i,j}$ between them. The mean squared error is given by the averaged distance between each pair of points in those datasets with Equation 3.12.*

3.1.10 Spectral analysis

To do spectral analysis we measure the power spectrum density (PSD), which tells us the frequency content of a signal. The PSD of a given time-dependent signal $x_j(t)$ is defined as:

$$S_{xx,j}(f) = \frac{\langle \tilde{x}_j(f)\tilde{x}_j^*(f)\rangle}{T}, \tag{3.13}$$

where T is the simulation time and $\tilde{x}_j(f)$ is the Fourier transform of the jth spike-train given by $\tilde{x}_j(f) = \int_0^T dt e^{2\pi i f t} x_j(t)$ and $\tilde{x}_j^*(f)$ is its complex conjugate.

In general we consider the averaged spike-train power spectrum over a number K of neurons

$$\bar{S}_{xx}(f) = \frac{1}{K} \sum_{j \in K} S_{xx,j}(f). \tag{3.14}$$

The PSD can also be computed to continuous signals such as the network's rate $r(t)$, using Equation 3.13. To illustrate, we show the PSD for two sinusoidal signals, $X(t)$ and $Y(t)$, In Figure 3.7. The first with frequency 1.0 kHz, and the second with two frequency components, 1.5 kHz, and 2.0 kHz. Both signals are contaminated with a Gaussian noise.

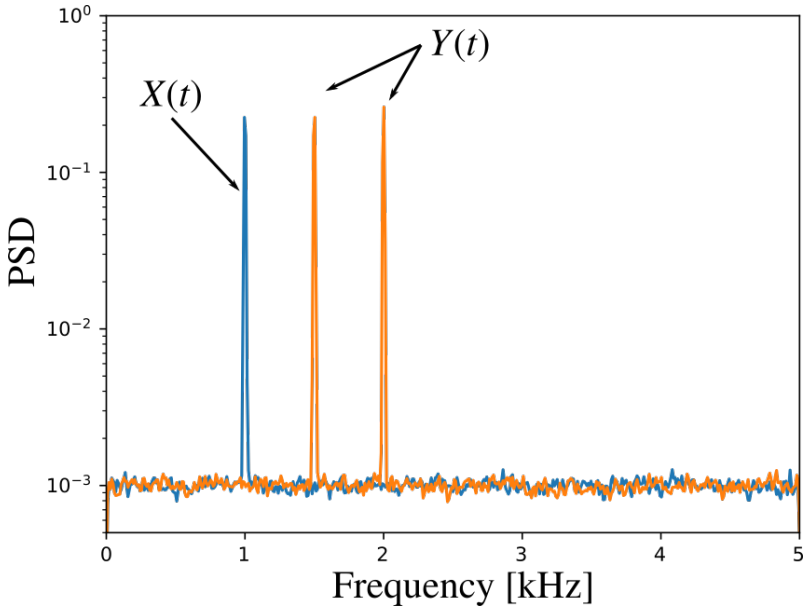

Figure 3.7: *Power spectrum for two sinusoidal signals (the first with frequency* 1.0 *kHz, and the second with* 1.5*, and* 2.0 *kHz), both signals where contaminated with Gaussian noise with average power* ≈ 5 *Hz. The power spectrum of signal* $X(t)$ *(in blue) exhibits a peak in* 1.0 *kHz, and* $Y(t)$ *(in orange) exhibits a peak in* 1.5*, and* 2.0 *kHz as expected.*

3.1.11 Correlation measurements

To quantify how much one random variable is related to another, one has to use a correlation measure. One of the most used coefficients to measure how much two random variables X, and Y are linearly correlated is the Pearson correlation coefficient given by Equation 3.15.

$$\rho_{X,Y} = \mathrm{corr}(\mathrm{X}, \mathrm{Y}) = \frac{\mathrm{cov}(\mathrm{X}, \mathrm{Y})}{\sigma_{\mathrm{X}} \sigma_{\mathrm{Y}}} = \frac{\mathrm{E}[(\mathrm{X} - \mu_{\mathrm{X}})(\mathrm{Y} - \mu_{\mathrm{Y}})]}{\sigma_{\mathrm{X}} \sigma_{\mathrm{Y}}}, \tag{3.15}$$

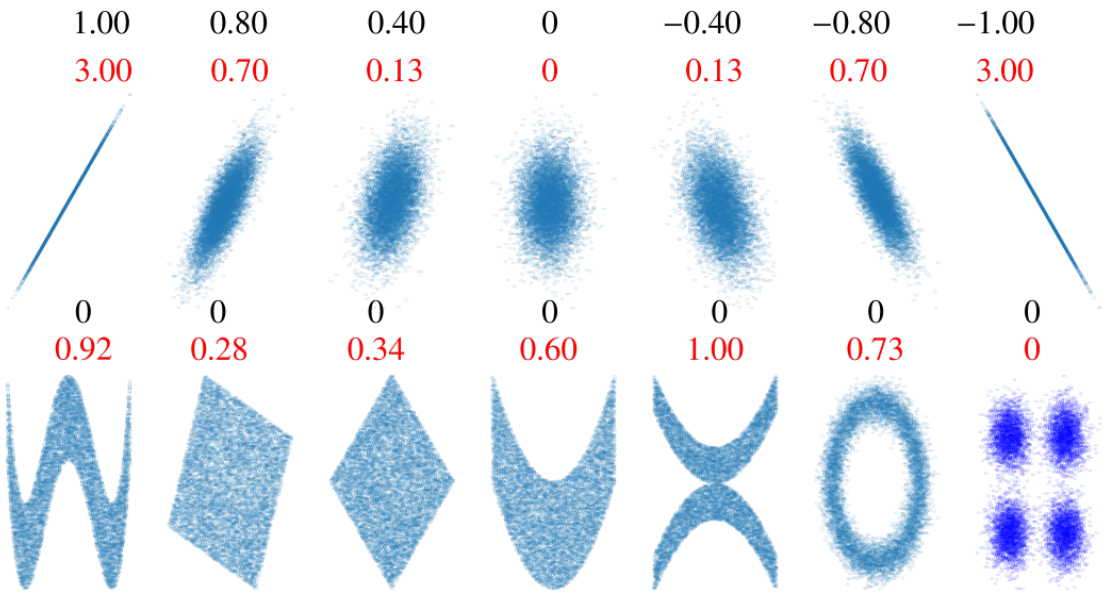

Figure 3.8: *Scatter plots for two random variables X and Y. In the top row all relations were linear, while in the bottom row non-linearities were introduced. Atop each scatter plot the Person's coefficient (in black) and mutual information (in red) are shown. The correlation coefficient can efficiently detect linear relations between the two variables, but not non-linearities. The mutual information, as a generalization of correlation, can detect both linear, and non-linear correlations (for more details see Section 3.1.12.2).*

where corr(X, Y) is the correlation, cov(X, Y) the covariance, σ are the standard deviations, and μ the average values. The Pearson coefficient goes from -1 to 1. The coefficient will be 1 if X, and Y are perfectly directly correlated ($Y = X$), -1 if they are perfectly inversely correlated ($Y = -X$), and 0 if they are uncorrelated. If x (y) are values drawn from X (Y), $\rho_{X,Y}$ can be calculated using Equation 3.16.

$$\rho_{X,Y} = \frac{\sum(x - \tilde{\mu}_X)(y - \tilde{\mu}_Y)}{\sqrt{\sum(x - \tilde{\mu}_X)^2(y - \tilde{\mu}_Y)^2}} \tag{3.16}$$

where $\tilde{\mu}$ are the population averages of the variables. In Figure 3.8 (Python replication of Fig. 2 from (Ince et al., 2017)) we show scatter plots depicting the relation between two random variables X and Y. In the top row X and Y are linearly related, while in the bottom row there are non-linearities. We show, atop each scatter plot the value of the Pearson's coefficient (in black), and the mutual information (in red, for details on the mutual information see Section 3.1.12), we see that the Pearson's coefficient can capture linear correlation (top row) effectively

but not non-linear correlation (bottom row).

It is also possible to measure how a signal correlates with itself and other signals temporally, by means of the auto- and cross-correlation functions, respectively. For the average across K spike-trains we compute the auto-correlation function with Equation 3.17. In summary, the auto- and cross-correlations can be thought as a measure of similarity between two series as a function of the shift of one in respect to the other

$$c_{xx}(\tau) = \frac{1}{K}\sum_{j\in K}\left(\langle x_j(t)x_j(t+\tau)\rangle - \langle x_j(t)\rangle\langle x_j(t+\tau)\rangle\right), \tag{3.17}$$

where τ is the delay applied between the two signals. Note that the correlation functions will depend on τ, to compute the cross-correlation $c_{xy}(\tau)$ we use Equation 3.17 between two distinct signals x, and y. In Figure 3.9, we show an example of the cross-correlation between a square and a triangular signal. We also show their auto-correlation.

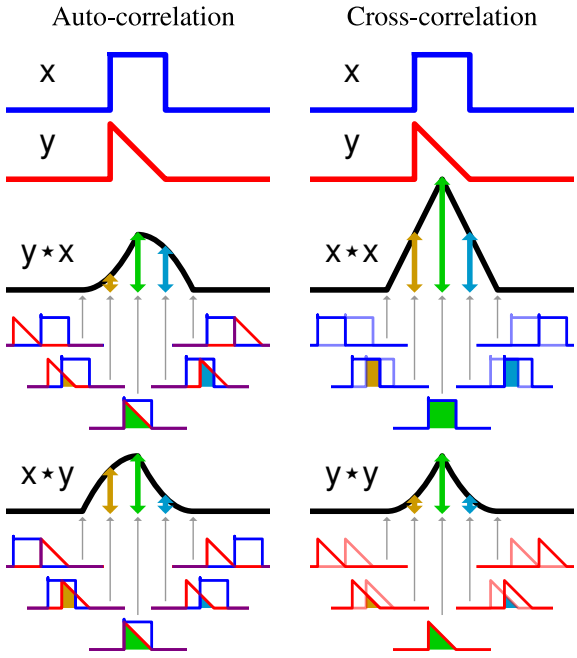

Figure 3.9: *Illustration of the auto- and cross-correlation operations for a square and triangular signal. The correlations are calculated by sliding one signal in relation to another, which can be thought as the convolution between the signals, i.e., $y * x$ (or with the signal itself, $x * x$). Notice that the auto- and cross-correlations are maximal when the intersection between the square and triangles areas are maximal. commons.wikimedia.org/wiki/File:Comparison_convolution_correlation_de.svg*

3.1.12 Information theory measurements

Information theory (IT) was created by Claude Shannon to create a mathematical formalism on how to quantify the information content of random variables, and what is the information capacity of a channel (Shannon, 1948; Stone, 2015). IT has been widely used in neuroscience (Borst & Theunissen, 1999; Cordeiro, Pena, Ceballos, Shimoura, & Roque, 2019) for (i) compute the information content of the spike-trains (Bialek et al., 1991; Rieke & Warland, 1999), and (ii) to determine the structural (Orlandi, Stetter, Soriano, Geisel, & Battaglia, 2014; Neymotin, Jacobs, Fenton, & Lytton, 2011), and functional (Wibral et al., 2011; Liao et al., 2011) connectivity of networks.

Next, we will briefly define the most fundamental IT quantities: the entropy, and the mutual information.

3.1.12.1 Entropy (H)

Given a random variable X and one of its possible outcomes x_k with $0 < k < m$, with probability of occurrence $p_k = P(X = x_k)$. We define the information content I_k of x_k as:

$$I_k = \log_2 \left(\frac{1}{p_k} \right), \tag{3.18}$$

the information content is a measure of how informative a single outcome of X is. It will go toward zero for events with high occurrence probability (Figure 3.10(a)). Intuitively, it is expected to gain no information from high probability events given that they are expected to happen, in other words, there is no *surprise* in observing them.

The entropy (H) is defined as the average information content of the underlying probability distribution of X, and is given by Equation 3.19.

$$H = -\sum_{k=0}^{m} p_k \log_2(p_k), \tag{3.19}$$

both I_k, and H are measured in bits if base 2 logarithm is used.

In Figure 3.10(b) we show the entropy for a random variable with two possible outcomes, as a function of the probabilities p (and $q = 1 - p$). In this scenario the

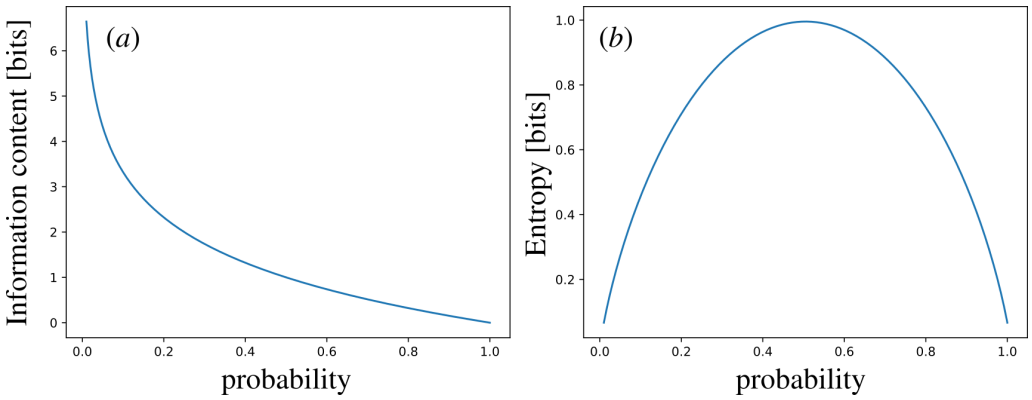

Figure 3.10: *We show (a) the information content of a single outcome of a random variable as a function of its probability, and (b) the entropy of a random variable with two outcomes (with probabilities p and $q = 1 - p$, respectively) as a function of the probability p. Notice that the entropy is maximum when $p = q = 0.5$.*

entropy will be maximum when $p = q = 0.5$. For a random variable with N outcomes it is possible to prove that H will be maximum when all outcomes have probability $p = 1/N$. Based on that, the entropy can also be thought as an uncertainty measure, that is maximum when all outcomes occur with the same probability, and minimum when one outcome has probability equal to one. In Figure 3.11 we show some discrete probability distributions and their entropy.

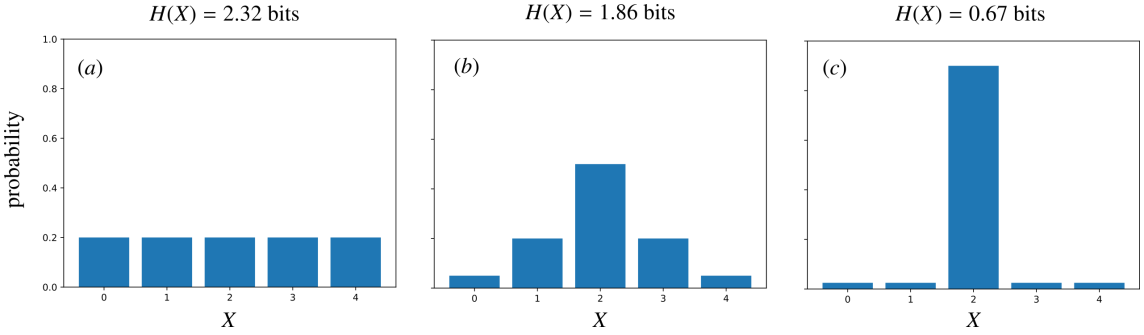

Figure 3.11: *Histograms for a random variable X with 5 possible outcomes and different probability distributions. The respective entropy values are shown above each graph. Notice that when the outcomes are equiprobable the entropy is maximum, as a the probability of a single outcome goes towards 1 the entropy tends to zero.*

3.1.12.2 Mutual Information (MI)

As already discussed the entropy is the average information content of a random variable X (or the uncertainty about the occurrence of a given outcome of

X). But, if X has some degree of correlation with another random variable Y, how can observing Y influence our knowledge about an outcome of X?

The reduction of uncertainty about the outcome of X given prior knowledge of the outcome in Y is defined as the mutual information (MI) between those two variables, and is given by Equation 3.20.

$$MI(X,Y) = \sum_k \sum_w p(x_k, y_w) \log_2 \left(\frac{p(x_k, y_w)}{p(x_k)p(y_w)} \right). \tag{3.20}$$

The mutual information can also be expressed as a sum of entropies:

$$MI(X,Y) = H(X) - H(X|Y) = H(X) + H(Y) - H(X,Y), \tag{3.21}$$

where $H(X|Y)$ is the conditional entropy, and can be interpret as the amount of uncertainty remaining about the outcome of X after observing Y. The term $H(X,Y)$ is called joint entropy and can thought as a container for all other entropy quantities, as shown in Figure 3.12 where the relation between each entropy is depicted.

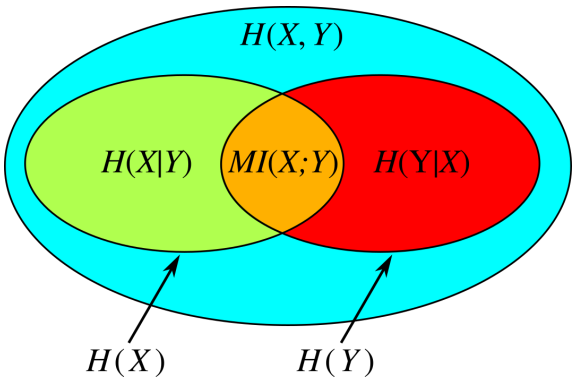

Figure 3.12: *Relation between all the entropies, as discussed in the text.*

The mutual information is also a generalization of the correlation between two variables, but different from the Pearson correlation discussed in section 3.1.11 the MI can capture even non-linear correlations (bottom row of Figure 3.8, MI values are shown in red) between two random variables.

Finally, MI information is a model-free measurement, however it is possible to obtain an analytical expression for some random distributions. For two Gaussian

variables the mutual information can be expressed as in Equation 3.22.

$$MI(X, Y) = \frac{1}{2}[(2\pi e)^2|\Sigma|], \tag{3.22}$$

where Σ is the covariance matrix between X and Y.

In this dissertation we use the Gauss-copula estimator (Ince et al., 2017) to compute the mutual information between variables. This method consists of projecting non-Gaussian variables into a space where their distributions is normal, via a copula function, and estimate MI using Equation 3.22.

Chapter 4

Method for estimating the voltage-dependent firing probability curve

In this chapter we will discuss the method used to determine the voltage-dependent probability of spiking function for the stochastic model. After presenting the method, we will apply it to the electrophysiological data, and discuss the results.

The algorithm developed to determine the voltage-dependent spike probability curves ($\phi(V)$, see Section 2.2.2), uses long time series. The electrophysiological data used in this project recorded 10 minutes of spontaneous activity of a CA1 pyramidal neuron[1], making it suitable for our goals[2]. In Figure 4.1 we show different segments of the recorded data.

Once the membrane potential time series ($V(t)$) is in hands the next step is to determine the values of V in which an action potential was initiated, i.e. the threshold value. In *in vitro* studies, in which neurons are stimulated with step currents with variable intensity applied to the soma, the threshold is obtained from the cell's rheobase (i.e. the minimum current amplitude necessary to cause an action potential). However in *in vivo* studies the rheobase is not defined and usually the threshold is considered as the value of membrane potential V_{th} in which an action

[1] The data (Borges et al., 2018) was collected by Guilherme Higa in the laboratory of Dr. Roberto de Pasquale at ICB-USP

[2] Other time series were used during the development of the method, for all time series used the results were similar with the voltage-dependent firing probability curve having zero probability of firing for low voltage values and saturating at one for high voltage values.

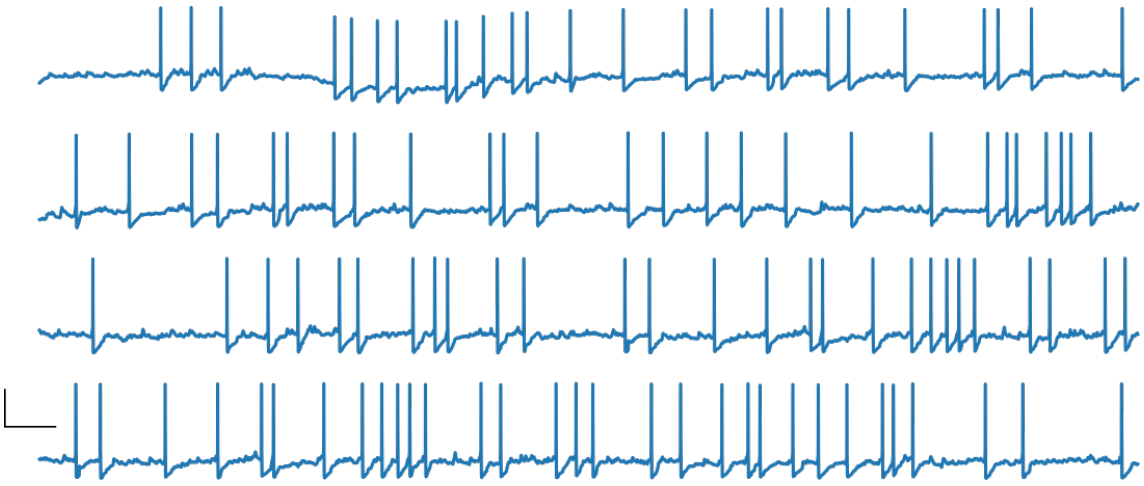

Figure 4.1: *Intracellular recordings of spontaneous activity pattern. The figure shows different segments of the data (see text). In the bottom panel, horizontal black bar denotes* 0.25 *s and vertical black bar denotes* 25 *mV. Data kindly provided to the author by the laboratory of Dr. Roberto de Pasquale at ICB-USP*

potential happened (Platkiewicz & Brette, 2010). Given that the value V_{th} where the spike is initiated is variable, there is more then one definition for this quantity. The definition adopted here is the one considered to be the more accurate in (Sekerli et al., 2004). In this definition the detection of AP's thresholds involves the computation of the maximum curvature (K_{p}) of the time series $V(t)$ in the moments preceding the emission of an action potential.

The maximum curvature of a given function can be computed according to Eq. 4.1.

$$K_{\text{p}} = \ddot{V}[1 + \dot{V}^2]^{-\frac{3}{2}}, \tag{4.1}$$

where $\dot{V}$ and $\ddot{V}$ indicates the first and second derivative of the time series $V(t)$, respectively.

Then we define the threshold as:

$$V_{\text{th}} = \underset{V}{\text{argmax}}\, K_{\text{p}} \tag{4.2}$$

To determine the points of maximum curvature of the action potentials, first we isolate all the spikes of the time series. To do so we find all the peaks above $V(t) = -10$ mV in $V(t)$, this will return an array of indexes $t_{\text{spike}} = \{t^1_{\text{spike}}, t^2_{\text{spike}}, \ldots, t^{N_{\text{spike}}}_{\text{spike}}\}$,

with each one corresponding to the time of occurrence of a given peak, where N_{spike} is the total number of spikes in the time series. Then, for each peak i, we create a time window from $t^i_{\text{disp}} - \Delta t$ to t^i_{spike}. After that we isolate the ascending half of the action potential in a window of length Δt. With the values within the interval $[V(t^i_{\text{spike}} - \Delta t), V(t^i_{\text{spike}})]$ of the time series we compute the maximum curvature using Eq. 4.1, this equation is applied for each window $i = 1, \ldots, N_{\text{spike}}$, and with the K_{p} values determined the threshold is estimated with Eq. 4.2. At the end we will have an array $V_{\text{thr}} = \{V^1_{\text{thr}}, V^2_{\text{thr}}, ..., V^{N_{\text{spike}}}_{\text{thr}}\}$ containing all thresholds for the time series analyzed. In Figure 4.2(a) we illustrate the procedure described above.

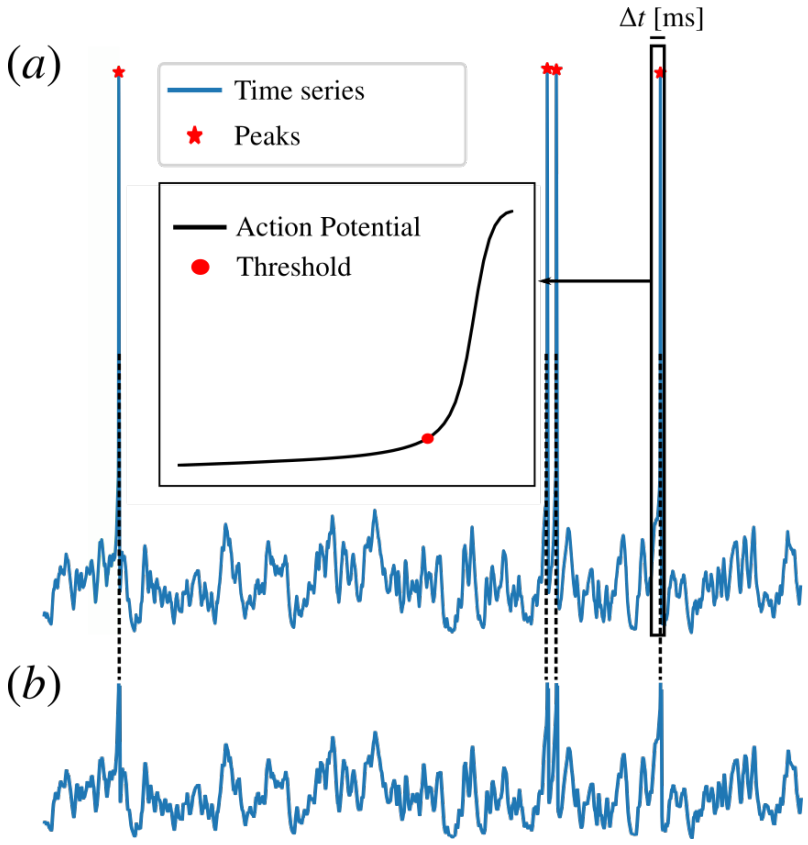

Figure 4.2: *Schematic representation of the method to detect the threshold values (a) Application of the method to a given time series, where the peaks are detected and around each peak is placed a time window of length Δt. For each window the V_{th} will be determined using Equation 4.1 (see inset). (b) Resulting time series after the removal of membrane potential values greater than its respective threshold.*

After determining all V_{thr} values, the action potential will be removed from the original time series. Hence, for the i^{th} action potential all values of $V \geq V^i_{\text{thr}}$

will be erased from the time series in the interval $[t^i_{\text{disp}} - \Delta t, t^i_{\text{disp}}]$. This results in a second time series $V^{'}(t)$ as illustrated in Figure 4.2(b).

Finally, two histograms are built: one for the series $V^{'}(t)$, and another for the values V_{th}. Both histograms will be superposed as in Fig. 12 of Azous and Gray (1999) (Azouz & Gray, 1999). Lastly, $\phi(V)$ can be estimated as the binwise ratio of these two histograms. For the j^{th} bin, $\phi(V)$ is given by Equation 4.3.

$$\phi(V^j) = \frac{\#V^j_{\text{th}}}{\#V'^j}. \tag{4.3}$$

The discrete probability function can be obtained by doing this ratio for all N bins, and is given by Equation 4.4.

$$\phi(V) = \{\frac{\#V^1_{\text{th}}}{\#V'^1}, \frac{\#V^2_{\text{th}}}{\#V'^2}, .., \frac{\#V^N_{\text{th}}}{\#V'^N}\} = \{\phi(V^1), \phi(V^2), ..., \phi(V^N)\}. \tag{4.4}$$

Then $\phi(V)$ can fitted by an appropriate function.

A similar method to the one presented here is found elsewhere (Jolivet, Rauch, Lüscher, & Gerstner, 2006), however instead of finding the threshold values using some criteria, such as the maximum curvature for instance, they set an approximate threshold v, and then plot the histograms of $V^{'}(t)$, and $v - V^{'}(t)$ to determine the firing probability (see Fig. 5B in Jolivet et. al., (2006)), following the formalism of the escape rate model (Plesser & Gerstner, 2000b; Gerstner et al., 2014).

Next, we show the results obtained by applying the method to estimate $\phi(V)$ in our experimental data. In Figure 4.3 we randomly selected action potentials from the time series, the time window used to crop APs as described in Figure 4.2 is $\Delta t = 1.5$ ms, the threshold values found with Equations 4.1 and 4.2 are shown as red dots.

After detecting threshold values we plot the histograms for $V^{'}$ and V_{th} (Figure 4.4(a)). By taking the ratio of those two histograms as in Equation 4.4 we have obtained the experimental discrete $\phi(V)$ shown in Figure 4.4(b) (red dots).

We fitted the experimental $\phi(V)$ obtained with the function given by

Equation 4.5.

$$\phi(V) = \frac{1}{b} \exp\left[\frac{V - V_{1/2}}{a}\right], \tag{4.5}$$

where $V_{1/2}$ is the voltage in which $\phi(V) = 0.5$, b is the average time to spike emission when in near $V_{1/2}$, and a the width of the zone where spikes can be emitted (i.e., the interval of $V(t)$ values where the neuron has probability non-zero of firing) (Jolivet et al., 2006). Note that we can control the neuron stochasticity level by adjusting a. In Table 4.1 we show the parameters a, b, and $V_{1/2}$ obtained via the exponential fitting.

a [mV^{-1}]	b	$V_{1/2}$ [mV]
1.19	27.0	−51.3

Table 4.1: *Parameters of Equation 4.5 obtained via exponential fitting.*

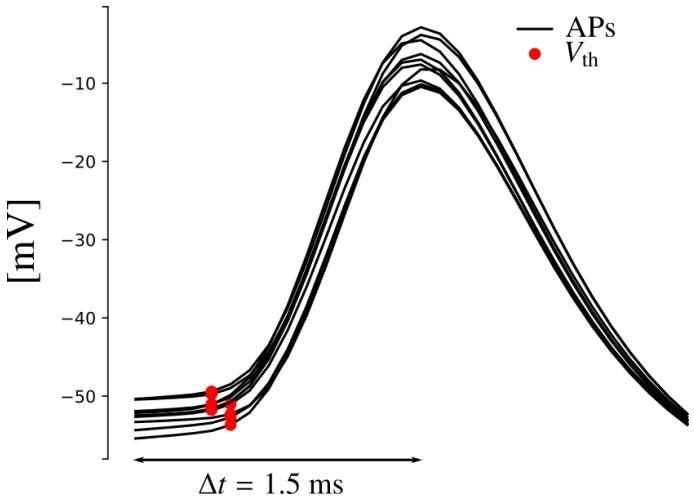

Figure 4.3: *Randomly selected action potentials from the data time series, the threshold detected using the method discussed in the text for each AP is indicated by the red dots.*

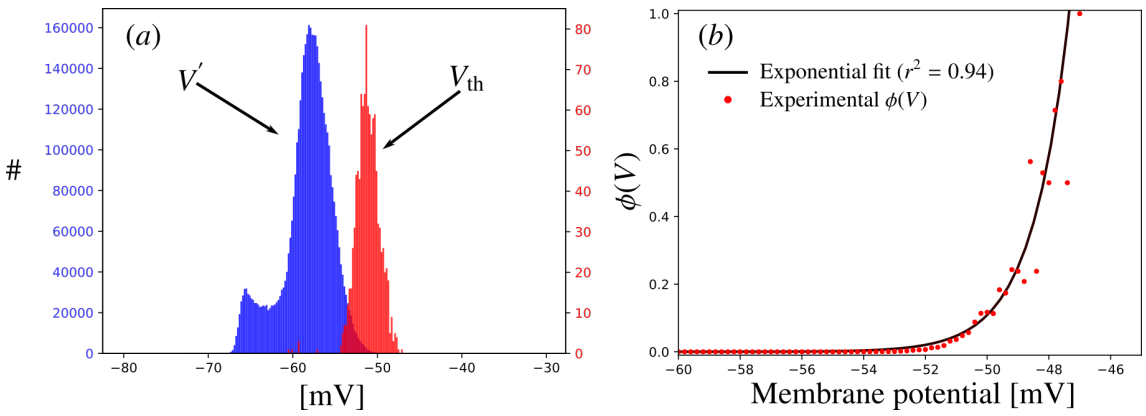

Figure 4.4: *Estimating the voltage-dependent probability curve. In (a) we show the histograms of $V^{'}(t)$ (in blue), and $V_{\text{th}}(t)$ (in red), (b) the estimated discrete $\phi(V)$ (red) dots were fitted by an exponential function (black curve) with $r^2 = 0.94$.*

Chapter 5

Single neuron studies

In this chapter we will focus in single neuron analysis of the stochastic model, primarily aiming to see if the model can be used to reproduce well known phenomena. Particularly, we reproduced the phenomena of spiking time reliability, and stochastic resonance due to intrinsic noise.

5.1 Stochastic threshold and spiking time reliability

As discussed in Section 2.1, experimentally it was shown that adding a fluctuating input to a DC stimulation increases the spiking time reliability of a neuron across trials (Mainen & Sejnowski, 1995). Here we reproduced this phenomenon using the stochastic model.

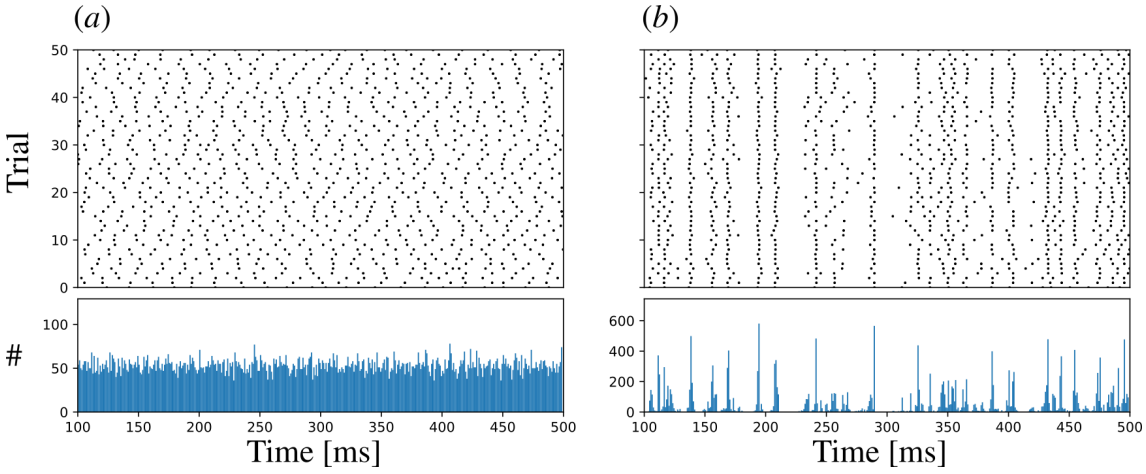

Figure 5.1: *Raster plots (top panels) and PSTH (bottom panels).* 10000 *trials were simulated, in the raster plots* 50 *are shown for (a) neurons receiving a constant DC input of* 400 *pA, and (b) with a fluctuating input with* $\eta = 7$ *mV summed to the DC current.*

The parameters of the membrane potential equation for the stochastic model are the ones in Table 2.5. For $\phi(V)$ we have used the parameters obtained via the exponential fitting in the experimental probability curve in Chapter 4, and given in Table 4.1. To integrate the model we used the standard Euler's method with integration time step $\Delta t = 0.1$ ms.

In Figure 5.1, we show the raster plot for 50 (out of 10000) trials. In Figure 5.1(a) the neuron received a constant DC input of $I_{\mathrm{DC}} = 400$ pA. The raster plot (top panel) shows that the spiking times across trials are highly variable, and the PSTH (bottom panel; done with $\Delta t = 1$ ms, see Section 3.1.7) becomes "flat" after a transient of approximately 80 ms, indicating that the spiking times are not reliably reproduced over trials.

Next we added a fluctuating Gaussian current with standard deviation η. In Figure 5.1(b) (top panel) we show the raster plot for $\eta = 7$ mV. The PSTH in Figure 5.1(b) (bottom panel) shows several peaks indicating that the spiking times tend to be more repeatable across trials. To measure reliability (R) we adopted a procedure similar to the one in Mainen et. al., (1995): first we constructed the spike counting histogram (similar to the PSTH but without taking the ratio of the count by the bin's length), then we defined the reliability in a given bin as:

$$R_i = \frac{c_i}{N_{\mathrm{trials}}}, \tag{5.1}$$

where R_i is the reliability of the spiking times in the i^{th} bin with width $\Delta t = 0.1$ ms, c_i is the spike counting in that bin, and N_{trials} the total number of trials. Then, R is defined as the average of R_i for all bins that are above a certain threshold, here we only average bins that have $c_i > 0.7 c_{\max}$, where $c_{\max}$ is the maximum counting (for a maximum of one spike per bin $c_{\max} = N_{\mathrm{trials}}$). Therefore, $R = 1$ if the neuron emits the maximum number of spikes in every bin that is considered in the calculation of R.

In Figure 5.2(a) we show the reliability as a function of η (similar to Fig. 2C in (Mainen & Sejnowski, 1995)). Notice that R grows continuously towards 1 as η increases, replicating, at least qualitatively, the behavior of the reliability shown in (Mainen & Sejnowski, 1995). This is different from the deterministic LIF model (red dashed line in Figure 5.2(a)), where $R = 1$ if η is sufficiently strong and $R = 0$

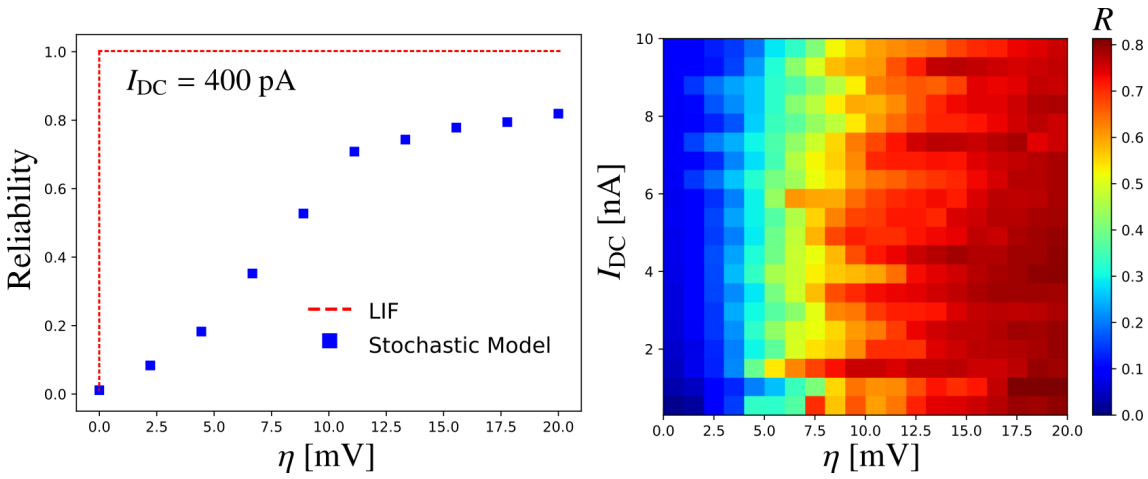

Figure 5.2: *Reliability plots. In (a) we show the reliability for a neuron receiving a constant DC input of* 400 *pA as a function of* η*, and in (b) we show the map with reliability values when both the DC current amplitude (*I_{DC}*) and the noise standard deviation (*η*) are varying.*

otherwise. Since for our example η is greater than the rheobase value $R = 1 \ \forall \ \eta$, for the LIF model in Figure 5.2(a).

One might argue that reliability can be obtained by increasing I_{DC} forcing the neuron to saturate (i.e. force it to fire every time step). In Figure 5.2(b), we show the reliability as a function of I_{DC} and η, it is possible to see that reliability, as we defined, only increases with η for the range of DC currents analyzed. But how can I_{DC} not increases R? This is due the stochastic threshold of our model, where if I_{DC} is less than a saturation current I_{sat} it is not guaranteed that the neuron will emit spikes every time step, while in the LIF model if the current is strong enough the neuron will always emit the same spike train for every trial. In Figure 5.3 we show the relation between the reliability and the spiking frequency for the stochastic model to determine I_{sat}, that is of about 50000 pA.

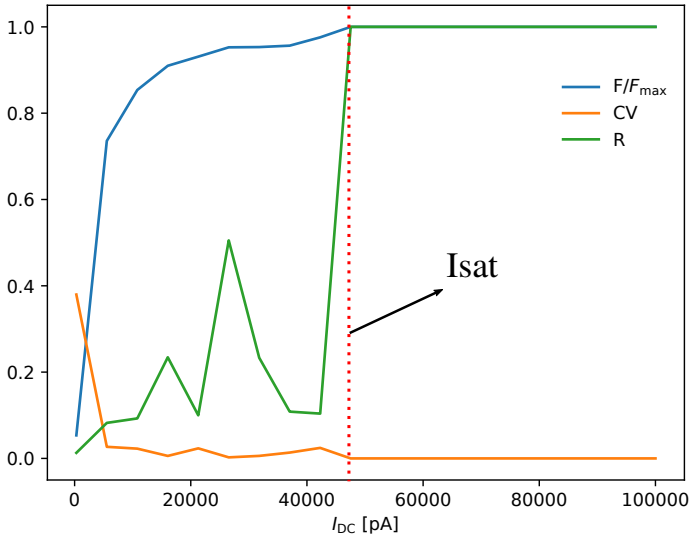

Figure 5.3: *Plot showing the neurons' average frequency divided by the maximum frequency achievable for this model, the CV and the reliability. For our parameters the reliability is low for the stochastic model for* $I \leq 50000$ *pA, when the system saturates, i.e.* $F = F_{\max}$*, and* $CV = 0$*.*

5.2 Stochastic resonance due channel noise in the stochastic model

In this section we will study the phenomenon of stochastic resonance (SR). As discussed in Section 2.1, SR is a phenomenon in which the detection of oscillatory subthreshold signals in non-linear system is enhanced by the presence of an optimal level of noise. Usually, SR is detected by plotting the signal-to-noise ratio (SNR) of a signal as a function of the noise level. Systems that exhibit SR will show a maximum in the SNR for a noise level greater than zero (McDonnell & Abbott, 2009).

Here we are interested in testing whether the intrinsic noise of the stochastic model is capable of manifesting SR. Other experimental (Bezrukov & Vodyanoy, 1995), and computational (Schmerl & McDonnell, 2013) works showed that channel noise is capable of generating SR. To do so, we will vary the parameter a, which controls the firing probability of the stochastic model, by adjusting the inclination of $\phi(V)$ in Equation 4.5. To measure the resonance instead of the SNR we will compute the mutual information (MI, see Section 3.1.12.2) between the neuron's spike train (with bin size $\Delta t = 1$ ms) for each trial and a sinusoidal subthreshold

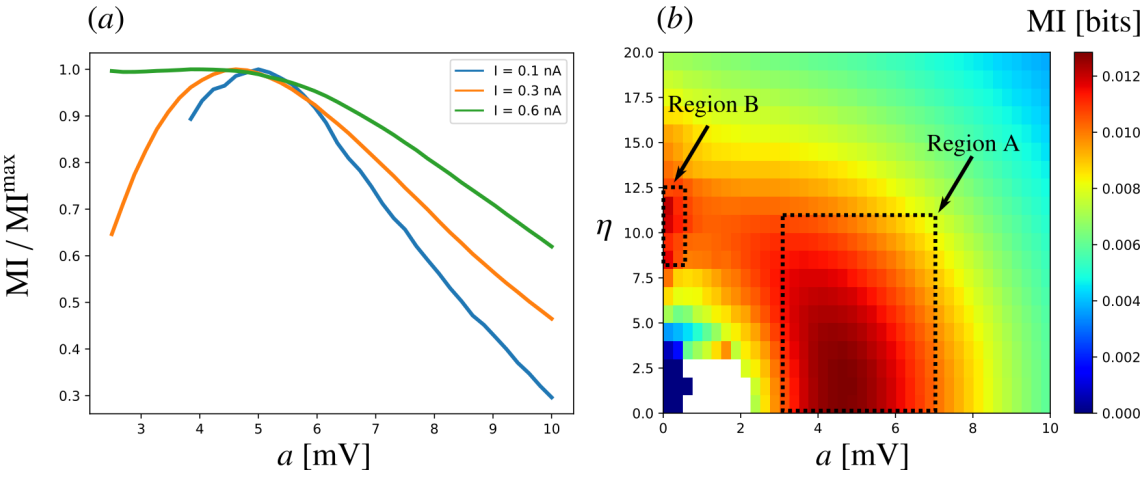

Figure 5.4: *Mutual information between the spike trains and the sinusoidal input to which the neuron was submitted as a function of the stochasticity level (a) of the stochastic model. In (a) we show the mutual information (normalized by its maximum) for three DC currents* 0.1 *(in blue),* 0.3 *(in orange), and* 0.6 *nA (in green), where the latter is a supra-threshold stimulus and the two first sub-threshold; in (b) we show a map of the mutual information as a function of a and the standard deviation of a fluctuating input η added to the sinusoidal signal. The dashed rectangles indicate regions A, and B (see text).*

input, with frequency of 10 Hz and amplitude $I_{\mathrm{a}} = 300$ pA, to which the neuron was submitted (the MI is also used in works related to SR (Stocks & Mannella, 2001)), as a function of a. The other parameters, for the membrane equation, and $\phi(V)$, are the same used in the past section.

In Figure 5.4(a), we show the MI (normalized by its maximum) as a function of a, for three different values of I_{a}, and without the presence of a fluctuating external signal ($\eta = 0$). For subthreshold I_{a} (100, and 300 pA) the neuronal response showed SR, visualized as a maximum in the MI for $a \approx 5$ mV. For suprathreshold currents (600 pA) the resonance peak vanishes as expected. Since the detection of the signal is guaranteed in this scenario the inclusion of noise will not act as an agent to facilitate its detection.

Further, we wanted to compare the effects of obtaining SR via a fluctuating signal (similar to synaptic noise, as the one used in the last section) added to the sinusoidal input, and via the intrinsic noise in the voltage threshold. In Figure 5.4(b) we show the mutual information as a function of the fluctuating input's standard deviation (η), and the level of intrinsic stochasticity (a). For a deterministic threshold ($a \approx 0$), we see that the maximum of MI is between $10 \leq \eta \leq 12$. We

refer to this region as B in Figure 5.4(b). Interestingly, for a stochastic threshold ($a > 0$) the region where η causes SR is amplified. This is identified as Region A in Figure 5.4(b), and it is limited approximately by $3.0 \leq a \leq 7.0$ and $0 \leq \eta \leq 11$). This results suggests that the joint effect of the intrinsic and extrinsic stochasticity seem to create a larger region where the neuronal response can exhibit the SR effect.

Finally, we try to explain why the mutual information is maximized when an optimal value of intrinsic stochasticity (a_{res}) is reached. In Figure 5.5(a1,b1,c1) we show the raster plots for three different values of a: $a < a_{\text{res}}$, $a \approx a_{\text{res}}$, and $a > a_{\text{res}}$. For $a < a_{\text{res}}$, we observe periodic firing interleaved by silent moments. As we come close to a_{res}, the periodicity is maintained but higher frequencies are observed in the active periods and a few spikes are found in the silent periods. For $a > a_{\text{res}}$, the moments of high activity are still visually distinguishable, however the silent moments are replaced by low-frequency firing periods (frequency ≈ 40 Hz).

Moreover, in Figure 5.5(a2,b2,c2) we show the PSTH (top panel), and the membrane voltage of a randomly selected neuron (bottom panel). The sinusoidal input is shown in dashed red line in both panels. For $a < a_{\text{res}}$ the activity is above zero when the sinusoidal current is near its maximum amplitude (300 pA), the subthreshold membrane potential oscillates following the sinusoidal input, and spikes are emitted only when the input is close to its peak with a frequency of approximately 0.6 spikes per cycle within the window of high amplitudes. Near the resonance, the activity follows the input's shape more reliably, the spiking emission still happens mostly when the stimuli is at higher amplitudes, but with higher frequency of approximately 2.6 spikes per cycle within the window of high amplitudes. When the stochasticity level is above resonance, the activity does not reflect entirely the input (for instance, even when the input is near zero or negative we observe high activity). This can be seen in the membrane potential by the spikes emitted when the sinusoidal input is between -300, and 0 pA. In summary, for $a < a_{\text{res}}$ the activity gives us information about the period of the input, but not about its shape; for $a \approx a_{\text{res}}$ the activity gives information on both the period and the shape of the signal; and for $a > a_{\text{res}}$ the activity is not very informative about any of those features.

Finally, we analyze both the amplitude and phase in which the spikes are

being emitted. In Figures 5.5(d1,d2,d3) we show the polar scatter plots, in which each dot is placed as a function of the sinusoidal input amplitude $I(t)$, and the relative phase ($\Delta\Phi$) between the PSTH and the input signal at the spike times. For $a < a_{\text{res}}$ (Figure 5.5(d1)), most spikes occur for $I(t) > 100$ pA. However, $\Delta\Phi$ values are mostly scattered in a wide range between 0° and 90° (a few between $\approx$ 340°, and 0°). Near the resonance, most spikes are concentrated in the region $I(t) > 100$ pA between 0° and 45°; spikes that happen at lower amplitudes ($I(t) < 0$ pA) are mostly locked at approximately 45°; and a band with low concentration of dots, for spikes happening at all $I(t)$ values is found scattered in the range $270° < \Delta\Phi < 0°$. This distribution of scattered dots for $a \approx a_{\text{res}}$ gives to the plot a "pinch-like" shape. When $a > a_{\text{res}}$, the spikes are homogeneously scattered between 270°, and 90° for all $I(t)$, forming an approximately circular shape.

We suggest that at the resonance the emission of spikes happen mostly when the oscillatory input signal is near its maximum amplitude in a small range of phase differences ($0° < \Delta\Phi < 45°$), and spikes emitted when the oscillatory signal is at lower amplitudes happen mostly locked at a specific phase difference (in our study $\Delta\Phi \approx 45°$). However, spikes emitted at low amplitudes are found in small numbers scattered in a wide range of phase differences ($270° < \Delta\Phi < 0°$).

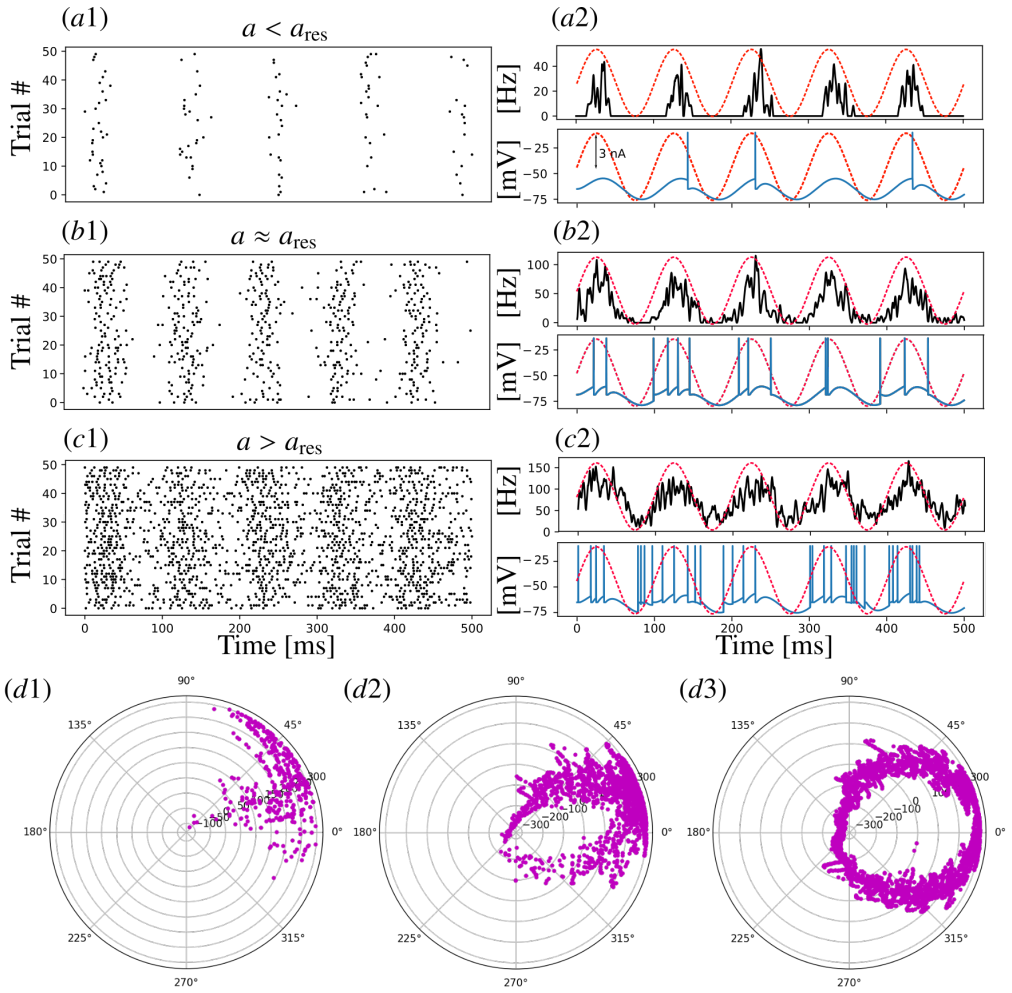

Figure 5.5: *In graphs (a1, b1 and c1) we show the raster plots for three values of a: $a < a_{res}$, $a \approx a_{res}$, and $a > a_{res}$; in (a2, b2, and c2) we show the PSTH (top panels) and the membrane potential of a randomly selected neuron (bottom panel) the red dashed line is the sinusoidal input; in (d1, d2, d3) we show the polar scatter plots in which each dot is placed as a function of the sinusoidal input amplitude $I(t)$, and the relative phase $(\Delta\Phi)$ between the PSTH and the input signal at the spike times, for $a < a_{res}$ $a \approx a_{res}$, and $a > a_{res}$, respectively.*

Chapter 6

Random network

In this chapter we will focus on studying the random network proposed by Brunel (2000) using as its building block the stochastic model (see Section 2.2.2). To do so first we reproduce the original model using LIF neurons. Then, we will compare the original (deterministic) network model and the one composed of stochastic neurons by means of first- and second-order statistics in each type of activity state produced by the network (see Section 2.3.1). The analysis for each network state is done to study how the network dynamics interact with, and potentially can be modified by, intrinsic properties of the stochasticity neurons.

6.1 Deterministic network model

We start by constructing the original Brunel network as described in Section 2.3.1. In Figure 6.1 we show the raster plot (top), and the activity (bottom, the red dashed line in each activity panel shows the average firing rate) for the four major activity states displayed by this model: (i) synchronous and regular (SR, Figure 6.1(a)); (ii) asynchronous and irregular (AI, Figure 6.1(b)); (iii) slow synchronous and irregular (SI slow, Figure 6.1(c)); and (iv) fast synchronous and irregular (SI fast, Figure 6.1(d)). The description of each state is presented in Section 2.3.1.

Next, we varied the parameters g and ν_{ext} (see Section 2.3.1) to reconstruct the diagram in Fig.2A of Brunel's original paper. Our goal is to check if using the PLV (see Section 3.1.8) as a synchrony criterion between two spike trains, and the

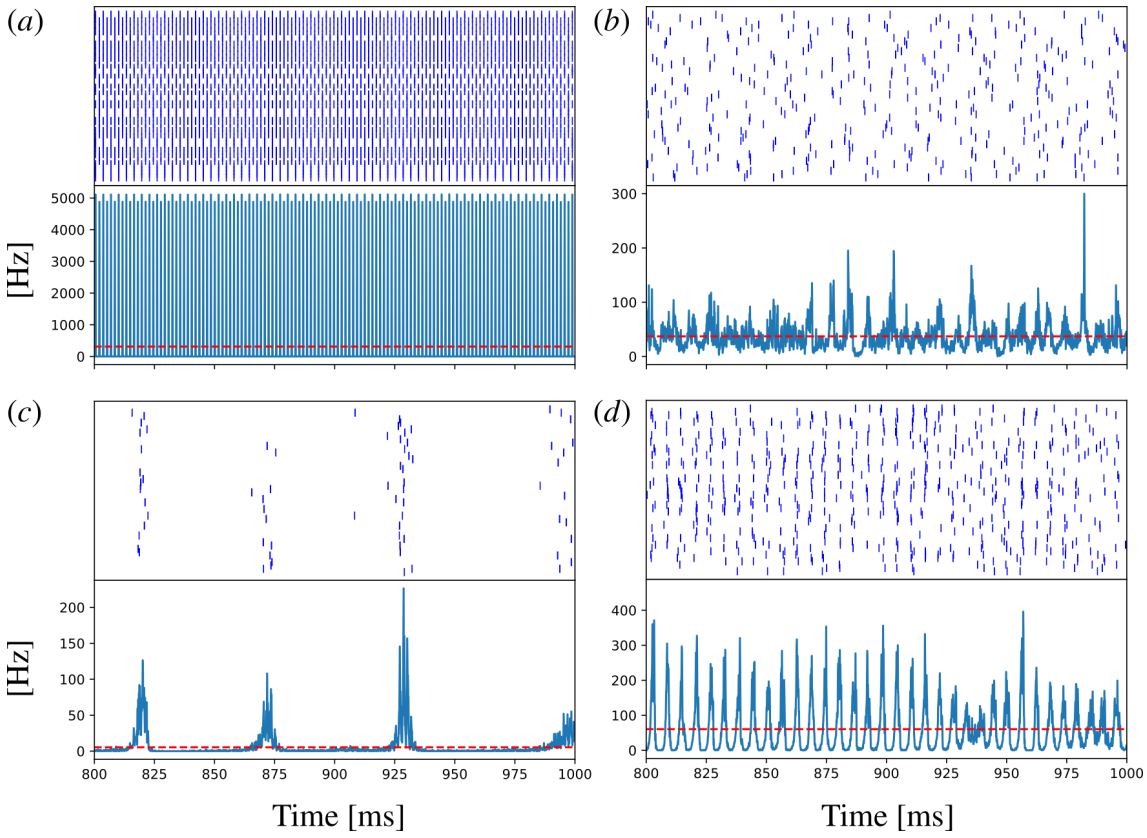

Figure 6.1: *Raster plots (top panels), and network activity (bottom panels, the red dashed line indicates its average value) for the original Brunel model. We show the four major states displayed by the model: (a) synchronous and regular (SR); (b) asynchronous and irregular (AI); (c) slow synchronous and irregular (SI slow); and (d) fast synchronous and irregular (SI fast).*

CV (see Section 3.1.5) as a regularity criterion for one spike train we will be able obtain the same regions in the $\nu_{\text{ext}} - g$ diagram as obtained by Brunel.

To do so, we used ν_{ext} ranging from 2.5 Hz to 40 Hz, and g from 0 (no inhibition) to 7 (strong inhibition). First, in Figure 6.2, we computed the CV map (Figure 6.2(a)) and the PLV map (Figure 6.2(b)). Then we define thresholds for CV (not a normalized) and PLV (ranges from 0 to 1) to determine the state of the network for each pair (ν_{ext}, g) in Table 6.1.

In Figure 6.3 we show the diagram obtained. Qualitatively it is similar to Brunel's diagram, with four different regions: (i) contained in $0 \leq g < 7$ and $0 \leq \nu_{\text{ext}} \lessapprox 7.5$ (black region); (ii) in $0 \leq g \lessapprox 3$ and $7.5 \lessapprox \nu_{\text{ext}} \leq 40$ (dark grey region); (iii) in $3 \lessapprox g \leq 7$ and $7.5 \lessapprox \nu_{\text{ext}} \leq 40$ (light grey region); and (iv) two sub-regions within region (iii) located in the upper and lower right corners (white

State	Threshold
SR	PLV $>$ 0.3 and CV $\leq$ 0.7
AR	PLV $\leq$ 0.3 and CV $\leq$ 0.7
AI	PLV $\leq$ 0.3 and CV $>$ 0.7
SI	PLV $>$ 0.3 and CV $>$ 0.7

Table 6.1: *Thresholds used to set the activity state of the network in each point (ν_{ext}, g) in Figure 6.3.*

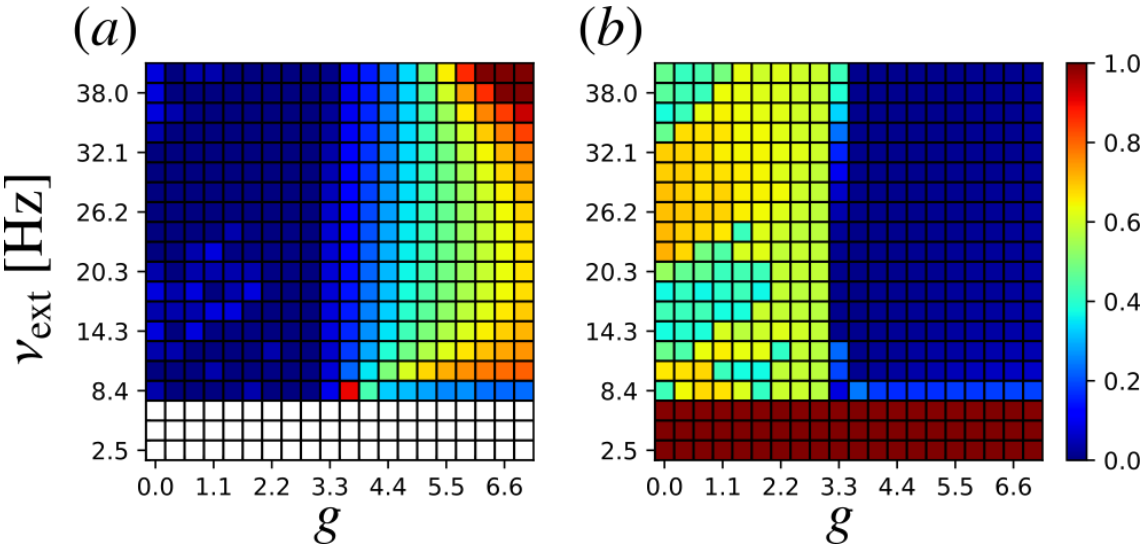

Figure 6.2: *Value maps of (a) CV and (b) PLV for the deterministic Brunel network in the $\nu_{\text{ext}} - g$ diagram.*

region). The state obtained for each region are the following: (ii) SR, (iii) AR, and (iv) AI. Note that in region (i) the network neurons do not fire, therefore CV is not defined, consequently a state is not assign to the network for those parameter ranges. In Brunel's diagram, region (ii) is also SR, however region (iii) in Brunel's paper is AI, and region (iv) SI, where he defines the upper region as fast SI, and the lower as slow SI. Herein, we will name the regions according to our diagram in Figure 6.3.

Note that, to produce our diagram we have used a low threshold for the PLV (0.3) to be able to reproduce the shape of Brunel's diagram as close as possible. This indicates that what Brunel defines as synchrony may not be accurate, and we were

only able to find a region with the SI state in our diagram when the PLV threshold was low < 0.20 (data not shown).

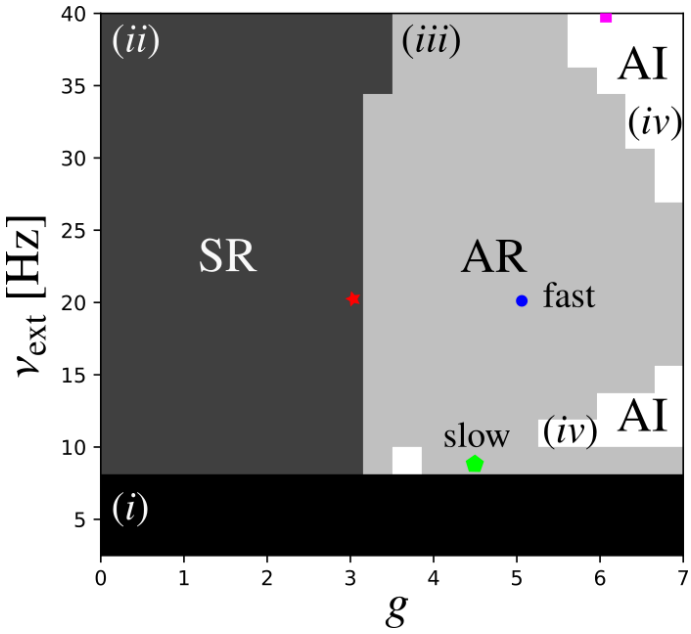

Figure 6.3: *Regions corresponding to different activity states in the $\nu_{\text{ext}} - g$ diagram. The marks indicate points used to produce Figure 6.1: SR (red star), AR fast (blue circle), AR slow (green pentagon), and AI (magenta rectangle).*

Finally, note that the network dynamics within a given region in not uniform. For instance, in Figure 6.2(a), in the region correspondent to AR state the values of CV vary depending on the pair (g, ν_{ext}). This is also noticeable via the raster plots. Both rasters in Figures 6.1(b,c) are in an AR region but have distinct activity dynamics. Thus, we will define the first as fast AR, and the second as slow AR, similarly as Brunel did for the SI state. Also we demarcate the points given in Table 2.3 and used to produce the raster plots (Figures 6.1) in Figure 6.3 as: SR (red star), AR fast (blue circle), AR slow (green pentagon), and AI (magenta rectangle).

Here we aimed to reproduced the original (deterministic) Brunel model. In the next session we will study this network after introducing the stochastic neuron model. We consider that our replication was successful. In the next session we will use our definition of activity states based on Figure 6.3.

6.2 Stochastic network model

In Figure 6.4 we show the same as in Figure 6.1 but using the stochastic model (using the parameters found in Section 4 for $\phi(V)$) as the basic element of the network. The comparison between the raster plots and activities for the deterministic (Figure 6.1) and stochastic (Figure 6.4) model, already show qualitative differences, mostly for the states SR, and AR slow.

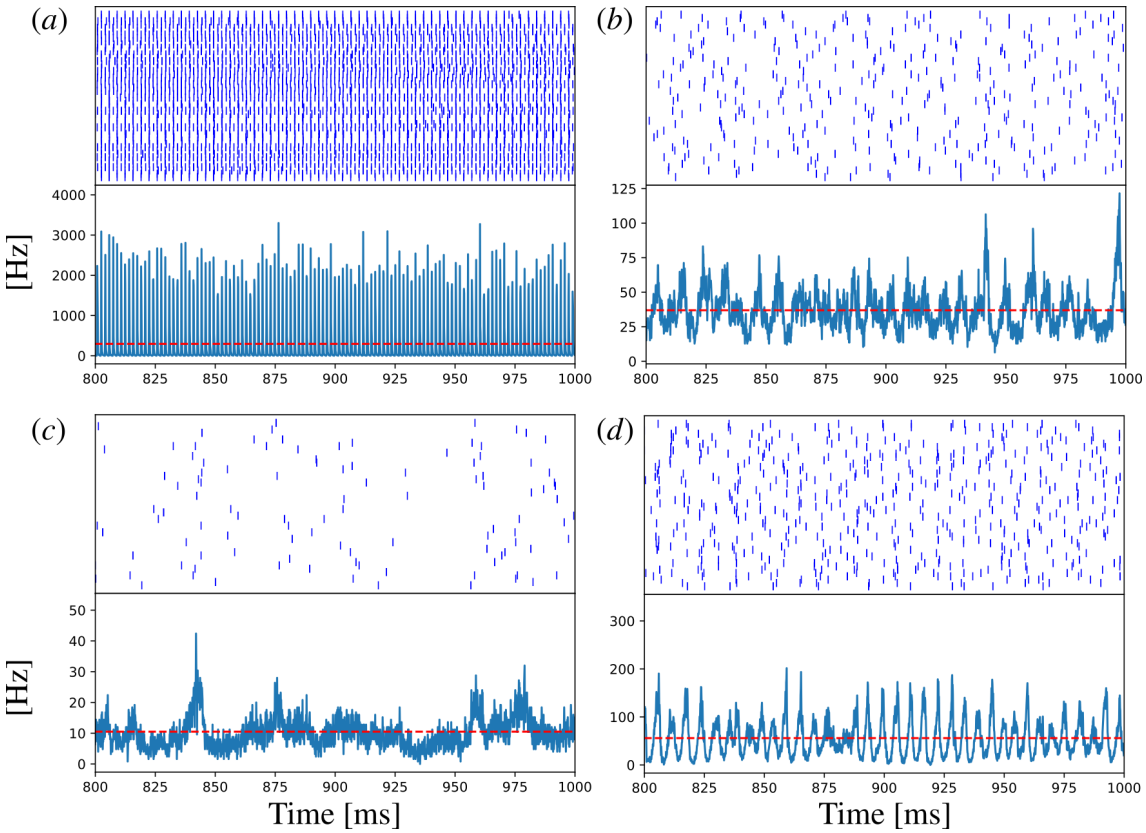

Figure 6.4: *Raster plots (top panels), and network activity (bottom panels, the red dashed line indicates its average value) for the stochastic Brunel model. We show the four states reproduced by the model: (a) synchronous and regular (SR); (b) fast asynchronous and regular (AR fast); (c) slow asynchronous and regular (AR slow) (AI); and (d) asynchronous and irregular (AI).*

For the SR state (Figure 6.4(a)), irregularities in the spike times are observed. These irregularities are noticeable in the fluctuations of the network activity, however the periodicity in the activity is still preserved. In the fast AR state (Figure 6.4(b)) both the raster plot, and the network activity show no apparent differences in comparison to the deterministic network, except for the absence of high frequency

peaks (as the one of ≈ 300 Hz in Figure 6.1(b) in the deterministic model). In the slow AR (Figure 6.4(c)) state the spikes in the raster plot for the stochastic model are more scattered than in the original model, resulting in an activity fluctuating around ≈ 10 Hz with peaks between 20 and 40 Hz. In the deterministic network the average frequency is close to 4 Hz and the high frequency peaks reach between 100 and 200 Hz. Finally, in the AI (Figure 6.4(d)) state the deterministic and stochastic models are also very similar. The major difference between the two models is in the network firing rate peaks, which are higher for the deterministic model.

		Frequency [Hz]	CV	PLV
SR	Deterministic	312.37 ± 0.02	0.005 ± 0.001	0.602 ± 0.003
	Stochastic	296.80 ± 0.02	0.045 ± 0.001	0.087 ± 0.001
AR (fast)	Deterministic	37.21 ± 0.01	0.403 ± 0.001	0.027 ± 0.001
	Stochastic	37.07 ± 0.01	0.430 ± 0.001	0.026 ± 0.001
AR (slow)	Deterministic	4.96 ± 0.01	0.718 ± 0.001	0.075 ± 0.001
	Stochastic	10.36 ± 0.01	0.669 ± 0.001	0.051 ± 0.001
AI	Deterministic	59.63 ± 0.03	0.922 ± 0.001	0.023 ± 0.001
	Stochastic	55.63 ± 0.02	0.548 ± 0.001	0.022 ± 0.001

Table 6.2: *Average frequency, coefficient of variation, and phase locking value of each network state (SR, AR, AI, and SI) for the deterministic and stochastic neuron models.*

In Table 6.2 we show the network average firing frequency, the CV and the PLV for the deterministic and stochastic models for each network state. To test for significant difference between the deterministic and stochastic cases we used the non-parametric Kolmogorov-Smirnov (K-S) statistical test. If the K-S statistic (ks) is small (high p-value), then we cannot reject the null hypothesis that the distributions of the two samples are the same. We will use as criterion to reject the null hypothesis the threshold ks > 0.6. In Table 6.2 quantities that have ks ≤ 0.6 have their cells colored in light grey, which means that cells in white correspond to significant differences.

The analysis of the values in Table 6.2 shows that: (i) for the SR state, the

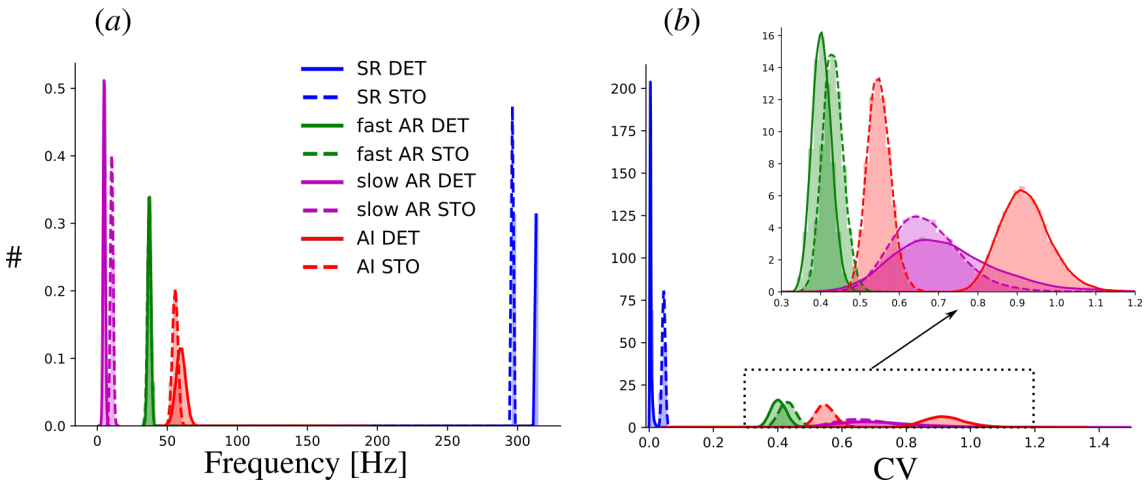

Figure 6.5: *Distributions of single neurons average firing frequency (a), and coefficient of variation (b) for the deterministic (solid lines), and stochastic (dashed lines) versions of the Brunel network. SR (blue), AR (green), AI (magenta), and SI (red).*

network average firing rate slightly decreases and the CV strongly increases (the analysis of PLV will be done below) when changing from the deterministic to the stochastic network; (ii) for the fast AR state, the average firing frequency remains unchanged with the introduction of stochastic neurons, however the CV slightly increases; (iii) in the slow AR state the average firing frequency strongly increases and the CV slightly decreases; (iv) finally, for the AI state, the average firing rate slightly decreases and the CV gets considerably smaller.

We also show the distributions (Figure 6.5) of the firing rates and CVs of individual neurons in Table 6.2. Note that depending on the network activity state the introduction of stochasticity can not only change (increase or decrease) the average value of those quantities but also the shape of their distributions. This suggests that the effect caused by the intrinsic stochasticity in the network will also depend on the activity state of the network, i.e. there is an interplay between the parameters ν_{ext} and g, which determine the activity state, and the parameters that control the level of stochasticity of single neurons Section 2.3.1.

Next, we analyzed how introducing the stochastic neuron model changes the overall synchrony of the network in each activity state. In Table 6.2 we show the PLV (see Section 3.1.8) for the four activity states in the deterministic and stochastic cases. The PLV value was calculated taking averages over 20,000 neurons pairs, for each case. In Figure 6.6 we show the distributions of the PLVs for the 20,000 neuron

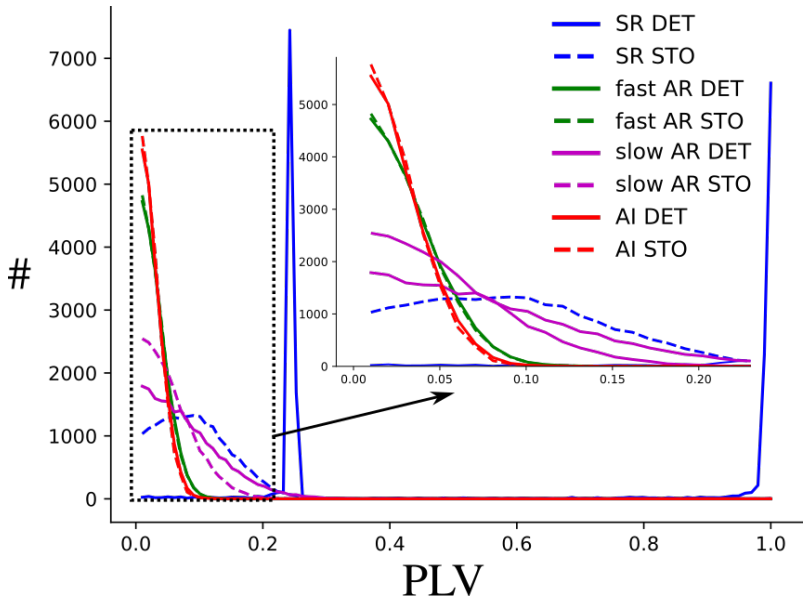

Figure 6.6: *Distributions of the phase locking values (PLV) of 20,000 neuron pairs for each network activity state: SR (blue), AR (green), AI (magenta), and SI (red).*

pairs for the four activity states in the deterministic and stochastic networks. From Table 6.2, we see that synchrony in the network is reduced in the stochastic situation in comparison to the deterministic one for the SR and slow AR states, and remains unchanged for the fast AR and AI states.

In Figure 6.6 we see that, for the deterministic SR state, there are two peaks in the distribution of PLV values: one around PLV$\approx$ 1.0 for neurons spiking at the same time and the other at PLV$\approx$ 0.23 for neurons spiking out of phase (see the raster plot in Figure 6.1). For the stochastic model, the PLV distribution changes completely, being unimodal and spreading over an interval between 0 and 0.20. So, the introduction of stochasticity breaks down the high level of synchrony in the network. The strong relative increase in spiking irregularity introduced by stochasticity (average CV goes from 0.005 to 0.045, see Table 6.2), though only slightly changing the average network firing frequency (see Table 6.2), may be considered as the possible cause of this decrease in synchrony.

In the slow AR state, which is a state already of low synchrony in the deterministic case, with a distribution of PLVs below 0.2, the introduction of stochasticity reduces even more the global network synchrony by enhancing the fraction of neuron pairs with PLVs below 0.1 (see Figure 6.6). In spite of this,

average firing rate increases because in the stochastic case neurons can emit spikes even if their voltages are not close to threshold (as discussed above). For the fast AR and AI states, the global synchrony and the corresponding distributions of PLVs remained unchanged.

The analysis of first-order statistics such as the average firing frequency and CV, together with the synchrony already gave us a glimpse on how the intrinsic stochasticity of the elements composing the network changes network behavior depending on the activity state of the network. However, frequency and CV may not capture all differences caused by the introduction of stochasticity in the model (due to non-linearities in the system, for instance). Thus, next we will also analyze the power spectrum density (PSD) and the auto- ($C_{\mathrm{xx}}(\tau)$) and and cross-correlations ($C_{\mathrm{xy}}(\tau)$) of the neurons.

In Figure 6.7 we show the PSD for each network state, for the deterministic (colored lines) and stochastic model (black lines). In the SR (Figure 6.7(a)) state, the introduction of stochastic neurons reduces the peak close to 300 Hz, indicating a "weakening" of the oscillatory activity close to this frequency. The loss of power concentrated at this point seems to be redistributed to other frequency values, increasing low and high frequency oscillations in the network. Besides that, the peak close to $300Hz$ is slightly shifted to the left due to the reduction of the network average firing frequency, as we already discussed above.

For the fast AR (Figure 6.7(b)) state, the PSD seems unchanged. The only noticeable difference is the reduction in the fluctuations between 150 Hz and 200 Hz (the PSD becomes more flat in this region). In the slow AR (Figure 6.7(c)) state we also observed a smoother PSD for the stochastic model, and an increase in power for all the frequencies due to the increase in the average network activity to ≈ 10 Hz. Finally, for the AI (Figure 6.7(d)) state we also observed a reduction in the peak close to 200 Hz, with implications similar to what we have discussed for the SR state. We also observe a general "flattening" of the spectrum for frequencies above < 100 Hz and a strong reduction of power for frequencies below this point.

In Figure 6.8 we show the comparison between the deterministic and stochastic models of the average auto-correlations ($C_{\mathrm{xx}}(\tau)$) of spike trains, and in Figure 6.9 we show similar graphs for the average cross-correlations ($C_{\mathrm{xy}}(\tau)$).

The auto-correlation does not change from the deterministic to the stochastic model, except for the AI state (Figure 6.8(c)). We suggest that the main cause of the enhancement in auto-correlation for the AI state is the approximately two-fold increase in the average firing frequency in this state when stochasticity is introduced. However, notice that even with this increase of auto-correlation in the slow AR state, the auto-correlation magnitudes are still smaller than the auto-correlation magnitudes for the other states.

For the cross-correlations, differences are observed for all states, even though for the fast AR (Figure 6.9(b)) they are negligible. In the SR state (Figure 6.9(a)), the cross-correlation peaks decrease, indicating that patterns in the spike trains are less repetitive than in the deterministic model (or oscillations are weakened). For the slow AR state (Figure 6.9(c)), the cross-correlation increases in magnitude (for the same reason as the increase in the auto-correlation for this state) and becomes more uniform. For the AI state (Figure 6.9(d)), the central peak decreases and the magnitude for greater delays (absolute values between 2 and 4 ms) slightly increases, i.e. the shape becomes more uniform as in the slow AR case. This indicates that for the stochastic AI and slow AR states there is an increase of long-range temporal

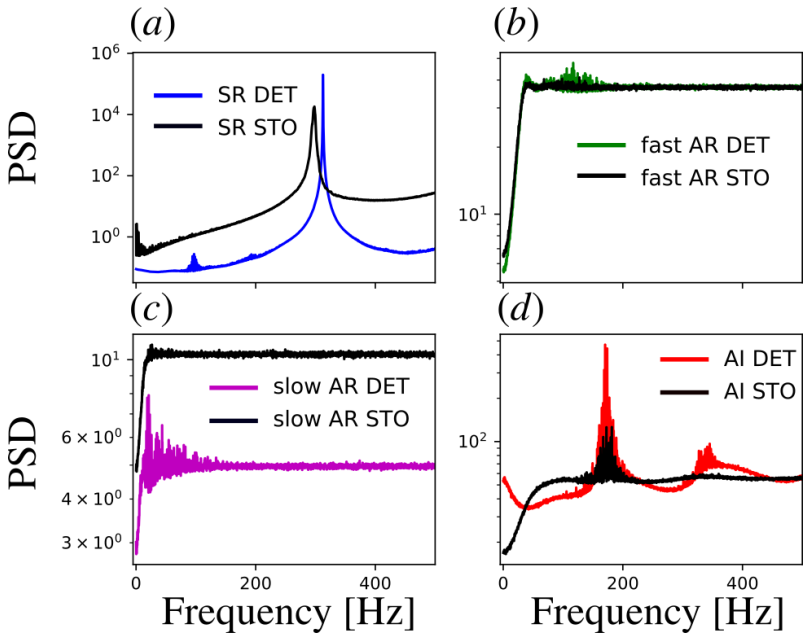

Figure 6.7: *Power spectrum density (PSD) for each network state (a) SR, (b) fast AR, (c) slow AR, and (d) AI. For the deterministic (colored solid lines) and stochastic models (black solid lines).*

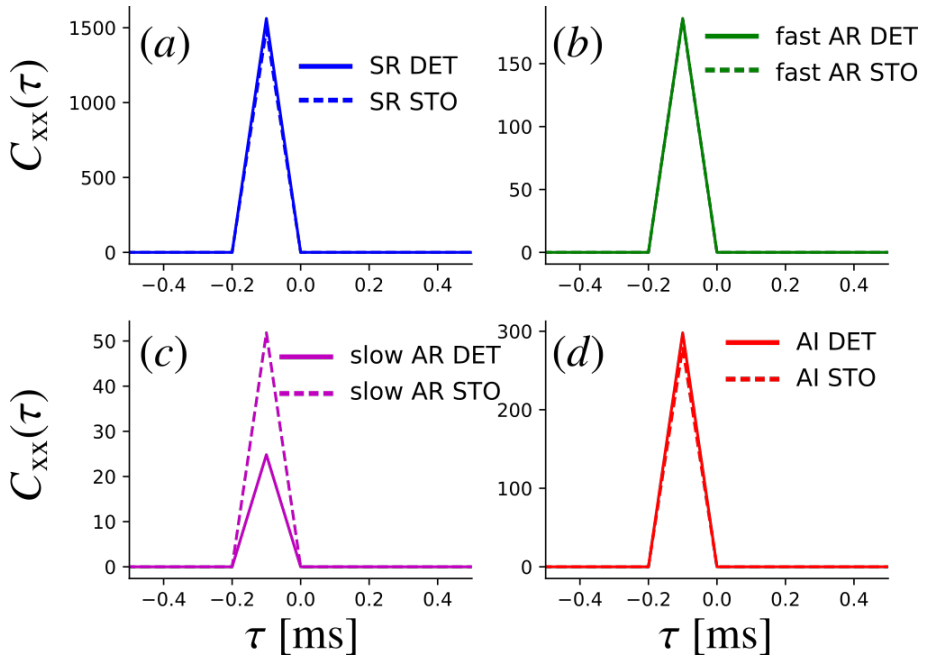

Figure 6.8: *Auto-correlation ($C_{xx}(\tau)$) for each network state (a) SR, (b) fast AR, (c) slow AR, and (d) AI. For the deterministic (solid lines) and stochastic models (dashed lines).*

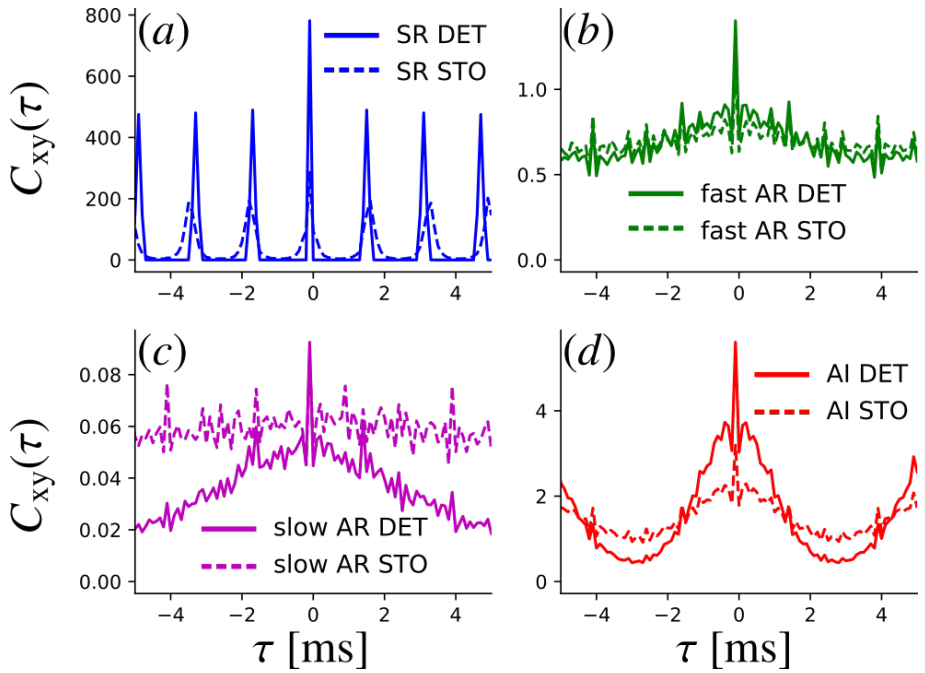

Figure 6.9: *Cross-correlation ($C_{xy}(\tau)$) for each network state (a) SR, (b) fast AR, (c) slow AR, and (d) AI. For the deterministic (solid lines) and stochastic models (dashed lines)*

correlations between spike trains.

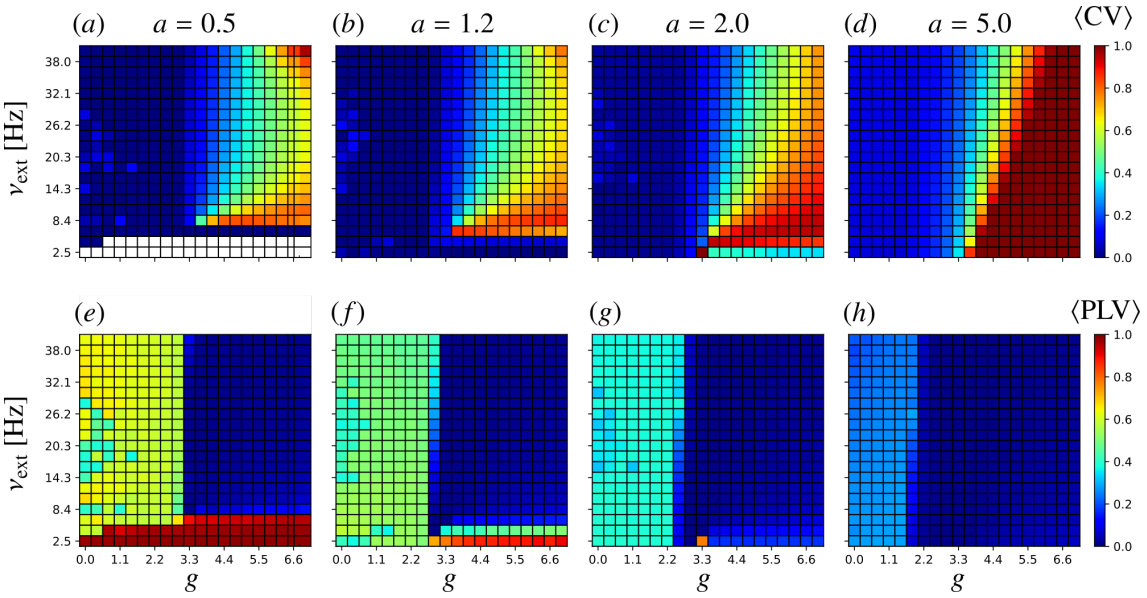

Figure 6.10: *Maps of CV (first row) and PLV (second row) values in the $\nu_{ext} - g$ diagram for the stochastic Brunel network for four different stochasticity a levels. First column: $a = 0.5$; second column: $a = 1.2$; third column: $a = 2.0$; fourth column: $a = 5.0$.*

In the previous paragraphs we have analyzed several first-order and second-order statistics for the deterministic and stochastic versions of the Brunel network model. We have concluded that the effect of the introduction of stochasticity at neuronal level changes these statistics differently depending on the network state. This suggesting a joint effect of network dynamics and single neuron intrinsic noise in determining the statistical features of the network.

Finally, we would like to study how stochasticity affects the regions corresponding to the four activity states in the $\nu_{ext} - g$ diagram (see Figure 6.3). To do so, we first plot the values of CV and PLV in the $\nu_{ext} - g$ diagram for four different stochasticity levels a (see Section 4): 0.5, 1.2, 2.0, and 5.0. These diagrams are shown in Figure 6.10. Using the thresholds in Table 6.1 we then construct the diagrams showing the regions corresponding to the four states for the four stochasticity levels a (Figure 6.11).

In Figure 6.11 we show the diagrams for each stochasticity value. For $a = 0.5$ (deterministic limit) the map (Figure 6.11(a)) is similar to the one for the deterministic model in Figure 6.3. As we increase a, the region (i) in the map vanishes turning into SR (region (ii)). This happens because the intrinsic neuronal

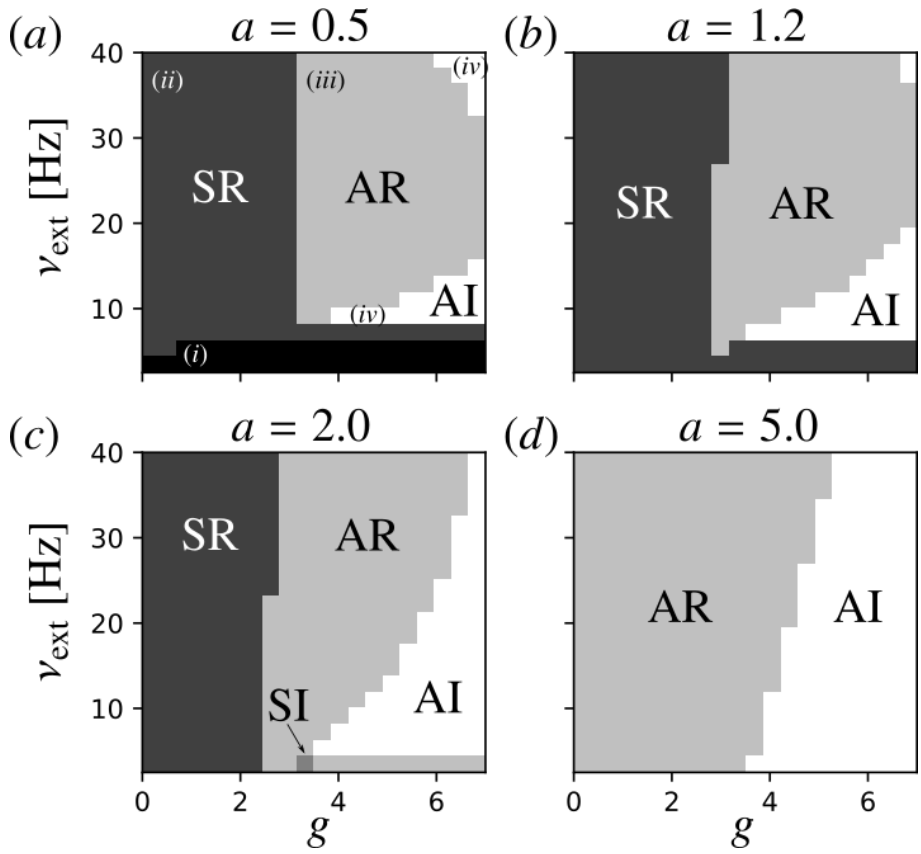

Figure 6.11: *Activity states in the $\nu_{\text{ext}} - g$ diagram for the stochastic Brunel network. Each diagram corresponds to a stochasticity a level (shown atop): (a) $a = 0.5$, (b) $a = 1.2$, (c) $a = 2.0$, and (d) $a = 5.0$.*

stochasticity makes neurons fire even for small ν_{ext}. As a increases the region (ii) gets smaller and the AI region (region (iv)) gets bigger. Note that for $a = 2$ a single point in the map , given by $g = 3.3$ and $\nu_{\text{ext}} = 2.5$ Hz, displays SI behavior. As we approach high stochasticity the SR region vanishes and the map has only one AR and one AI region, with most of the display area (for $g < 4$) corresponding to AR.

In Appendix B we study the effect of inserting the stochastic neuron in the cortical microcircuit network model (see Section B). Since the differences found between the deterministic and stochastic network statistics are not significant, we restricted the discussion of this network model to the appendix.

Chapter 7

Conclusion

During this dissertation, we focused on exploring the effects of introducing intrinsic stochasticity in a simplified neuron model. Particularly, this randomness was introduced by mean of a voltage-dependent spike probability function, generating a fluctuating voltage threshold for the emission of a spike.

To justify the use of our stochastic model, in Chapter 2, we start by discussing the main sources of noise in the brain: the synaptic and channel noise. We have related the stochasticity of our model to the latter due to the similar effects they both generate in the membrane voltage such as spike threshold, and trial-by-trial response variability.

We also discussed phenomena in which the presence of noise can be beneficial. This discussion also emphasizes the importance of studying neuron models that considers the presence of noise. In particular, we focus on two phenomena: spike time reliability, and stochastic resonance that we have studied using the stochastic neuron model in this dissertation.

In Chapter 4, our first results chapter, we derived the voltage-dependent spike probability function for the stochastic model. We did this by proposing a method to extract this function from electrophysiological data. The method consisted of finding the voltage thresholds for each action potential (AP) by estimating the maximum curvature at the moments just before the occurrence of an AP. Then, the discrete probability of firing was determined by the bin-wise ratio of the membrane voltage (with values greater than the threshold for each AP removed), and the thresholds histogram (Figure 4.4(a)).

We have obtained the spike probability function using data registered from

CA1 pyramidal neuron of the rat. The discrete function could be fitted by an exponential curve (Figure 4.4(b)), as previously observed in the literature (Jolivet et al., 2006). We also computed the computational cost of the stochastic model using the experimental probability of spike curve found in Appendix A, since the model requires the generation of a random number every time step it revealed itself as a computational costly (in respect to simulation time) model being only more advantageous than the Hodgkin-Huxley conductance based model.

After fitting the spike probability function, we used the stochastic model to study single neuron phenomena in Chapter 5. We started by reproducing the experiment by Mainen et. al., 1995, in which they measure the spike timing reliability as a function of the standard deviation of an input fluctuating noisy signal.

We showed that using the stochastic model the reliability of spiking times continuously increases towards one as the standard deviation of the fluctuating signal increases (Figure 5.2(a)). Although reliability is a general property of deterministic models, this experiment would not be reproducible by, for instance, a LIF neuron where the reliability is one if the input is sufficiently strong and zero otherwise (Figure 5.2(a), red dashed line).

We finish this analysis by showing that only increasing the DC input current is not enough to increase reliability as we measure, due to the fact that even high DC inputs do not ensure that the neuron will fire every time step (forcing the reliability towards one) due to the stochastic threshold of our model (Figure 5.2(b)). Also, increasing the DC input yields non-biological results such as high frequency and low irregularity in the spike train (Figure **??**).

Next, we studied the phenomenon of stochastic resonance generated by channel (or intrinsic) noise. We showed that the intrinsic noise of the stochastic neuron model is capable of generating SR by measuring the mutual information of the spike train and a sinusoidal subthreshold input as a function of the stochasticity level of the neuron model. The SR is detected by a peak in the MI for a given non-zero value of intrinsic stochasticity (Figure 5.4(a)).

To study the effects of introducing both intrinsic and the synaptic noise we used the same fluctuating input discussed above. In our model, the presence of

intrinsic noise combined with the synaptic noise seems to increase the region in which SR occurs (Figure 5.4(b)). Finally, we investigated how SR is generated by analyzing the phase of spike times in relation to the input sinusoidal signal. For an optimal intrinsic stochasticity level the number of spikes emitted during the excitation phase of the signal increases, and the PSTH gives information on both period and shape of the input signal (Figure 5.5).

We finish the results in this dissertation by studying the effect of introducing the stochastic neuron models on complex networks.

In Chapter 6 we introduced the stochastic neuron in the random network developed by Brunel (Brunel, 2000). We started by reproducing the original deterministic model, in particular, we used four dynamical states reproduced by the network: asynchronous and irregular (AI), synchronous and regular (SR) and synchronous irregular (fast and slow, SI). Those dynamical states are obtained by varying the frequency of the Poisson input each neuron receives and the inhibitory/excitatory relative synaptic force. Then, by using the CV as a measure of regularity in the spike train and the PLV as a measure of synchrony we estimated the map Brunel presented in Fig.2A of his paper (Brunel, 2000).

Using those measures, our map, shown in Figure 6.3, was qualitatively equivalent to the map Brunel proposed however, the dynamical states changed. In particular, his AI region for us is asynchronous and regular (AR), and the SI region is AI with no SI regions present. To reproduce this diagram as close as possible to the original, we had to use a low PLV threshold (0.3) indicating that the definition of synchrony used by Brunel may not match the one quantitatively measured.

After the analysis of the deterministic model, we introduced the stochastic neurons as the building blocks of the network. We compared the deterministic and stochastic networks by means of first- and second-order statics for each dynamical state: SR, AR (fast and slow), and AI. This analysis showed that introducing the stochasticity will affect those measurements differently (increasing, decreasing or maintaining their values) depending on the dynamical state of the network.

Since it was possible that introducing the stochastic elements in the network changed the disposition of regions in the map at Figure 6.3, and it could be the cause of differences observed in the statistics measured, we finished this chapter by

seeing how increasing the stochasticity level of neurons changed the map.

For low stochasticity (0.5) the map remains the same as the deterministic one, at the stochasticity level of 1.2 obtained via the data fitting in Chapter 4 we see a reduction of the AI area at the top right corner of the map. For stochasticity level 2.0 a single point exhibited SI behavior, but as we increased the stochasticity (5.0) the map remained only with two regions: AR and AI.

In Appendix B we performed a similar analysis to the one above, using a more complex topology based on a cortical microcolumn (Potjans & Diesmann, 2014b). However, we have not observed significant statistical differences between the deterministic and stochastic models. One interesting result though was presented in Figure B.4 were the introduction on stochastic elements in this network makes an oscillation peak around 370 Hz vanishes in the network power spectra, removing this peak of the PSD was an object of study elsewhere (Bos, Diesmann, & Helias, 2016). The vanishing of this peak due to the introduction of intrinsic stochasticity is an interesting result that deserves further investigation in future projects seeking enlightenment on how specifically the individual stochasticity interacts with the network dynamics resulting in the differences observed in this model.

Appendix A

Performance analysis of the stochastic model

In this section we will analyze the computational performance of the stochastic model using a similar approach found in (Izhikevich, 2004; Girardi-Schappo et al., 2017). In Figure 2.5 we show different single neuron models in a two-dimensional diagram having the number of biological features in the vertical axis and the number of FLOPS per time step used to run the model in the horizontal axis.

Here we consider the stochastic nature of the stochastic model as a biological feature, therefore the model has an extra feature when compared to the LIF model (which has a fixed threshold). We consider a lower-bound of 15 FLOPS per time step for the stochastic model, because it will depend on the method used to generate the random number during the simulation. To simulate the stochastic model, in each time step we draw a random number η from an uniform distribution to test whether the neuron will fire or not (if $\eta < \phi(V)$ the neuron fires).

Further, we also measured the CPU cycles per time step required by the stochastic model. A CPU cycles is the time required for the execution of one simple processor operation such as an addition (Hennessy & Patterson, 2012). Therefore, measuring it will give an idea of the model's execution time. In Table A.1 we show the cycles required per time step for six models (including the stochastic). The values were obtained in a computer with a processor Intel® core™i5-7th generation 7300 Hq, with 2.5 GHz, 16 Gb ram Windows 10 64 bits.

In both measurements, cycles and FLOPS per time step, the stochastic model

Model	Cycles per time step	FLOPS per time step
LIF	17 ± 4	5
Izhikevich	24 ± 5	13
Rulkov	22 ± 4	14
logistic KTz	40 ± 5	12
Stochastic model	76 ± 12	> 15
Hodgkin-Huxley	577 ± 30	119

Table A.1: *Table with performance measurement for several models including the stochastic model used in this dissertation. To compare the performances of different models we computed the cycles per times step and FLOPS per time step for each model. The models considered were (model parameters as in the references given): LIF (Potjans & Diesmann, 2014a), Izhikevich (Izhikevich, 2003b), Rulkov (Rulkov, 2002), logistic KTz (Girardi-Schappo et al., 2017), and a Hodgkin-Huxley like model (Shilnikov & Cymbalyuk, 2005).*

is only less expensive computationally than the Hodgkin-Huxley model.

Appendix B

Cortical microcircuit network model

In this section we discuss some results obtained by inserting the stochastic neuron fitted in Section 4 in the Potjans and Diesmann (see Section 2.3.2) network model (Potjans & Diesmann, 2014a). In Figure B.1(a) and Figure B.2(a) we show the raster plots for the deterministic and stochastic networks, respectively.

The raster plots for both models look very similar, despite the fact that for the stochastic model it seems more synchronous (notice the horizontal spike lines in Figure B.2(a)). For further comparison we have measured layer-specific statistics for both models, being them: (i) average frequency (Figure B.1(b) and Figure B.2(b)); (ii) CV (Figure B.1(c) and Figure B.2(c)); and (iii) synchrony (Figure B.1(d) and Figure B.2(d)). The synchrony measure used in this plot is the same one defined in (Potjans & Diesmann, 2014a).

The layer-specific average firing frequency between the two models and the CV look the same (ks < 0.6). Regarding the synchrony, some differences are observed. In the stochastic model the layer-specific synchrony is higher than in the deterministic model. Other difference is that while in the deterministic model layer L4e has the largest synchrony value, and L23e has the second largest synchrony value, in the stochastic model this order is reversed. However, the overall qualitative synchrony behavior is the same, and the increase in synchrony for the stochastic model does not seem to interfere in the network's average firing frequency and CV.

We also computed the activity of each layer for both models. They are shown in Figure B.1(e) for the deterministic model and in Figure B.2(e) for the stochastic

model. Qualitatively, the activity behavior of each layer is similar. There is a large synchrony value for the stochastic model, which can be noticed by the higher peaks in the activities.

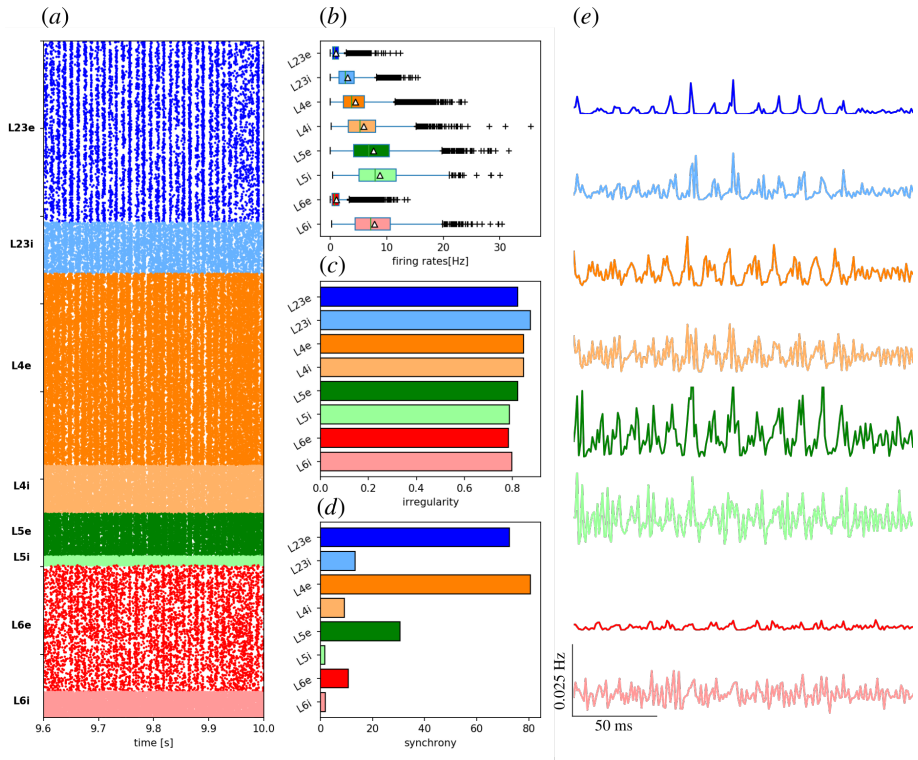

Figure B.1: *Potjans and Diesmann model for a cortical microcircuit using deterministic neurons. We show (a) the raster plot , (b) layer-specific average frequency, (c) CV, and (d) synchrony. In (e) we show the activity of each layer.*

In Figure B.3(a,d) we show the layer-specific and global average frequency, respectively (ks < 0.6); in Figure B.3(b,e) we show the layer-specific and global average CV (ks < 0.6). We also computed our standard synchrony measure, the PLV, in Figure B.3(c,f), which shows no observable differences in synchrony either (ks < 0.6).

We have not found any significant difference between the statistic measures above. One measure for which we found a difference is the global PSD. In Figure B.4 we show the spike trains power spectra for both networks. For the stochastic network the first peak (around ≈ 80 Hz) is more pronounced than for the deterministic model (peak around ≈ 100 Hz). Also, in the stochastic model frequencies between 100 Hz and 300 Hz are more uniformly distributed. Finally, we indicate by the black dashed

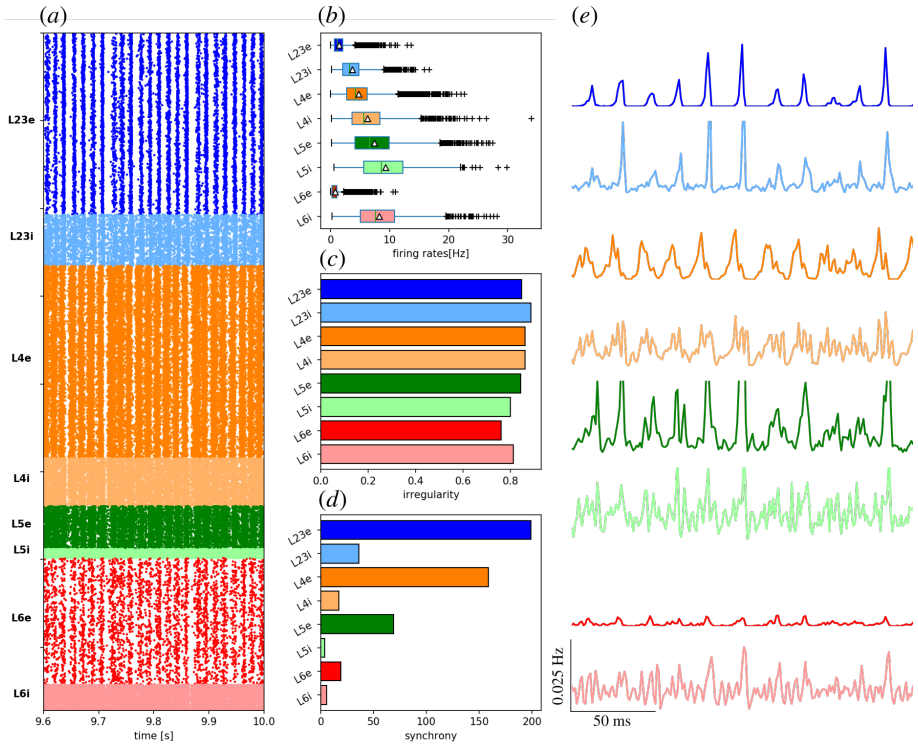

Figure B.2: *Potjans and Diesmann model for a cortical microcircuit using stochastic neurons. We show (a) the raster plot , (b) layer-specific average frequency, (c) CV, and (d) synchrony. In (e) we show the activity of each layer.*

circle that the peak around ≈ 370 Hz in the deterministic network vanishes for the stochastic model. This result is particularly interesting because there have been studies on what may cause this peak and how to remove it from the PSD (Bos et al., 2016). Apparently, the peak around ≈ 370 Hz disappears naturally by introducing intrinsic stochasticiy at the single neuron level.

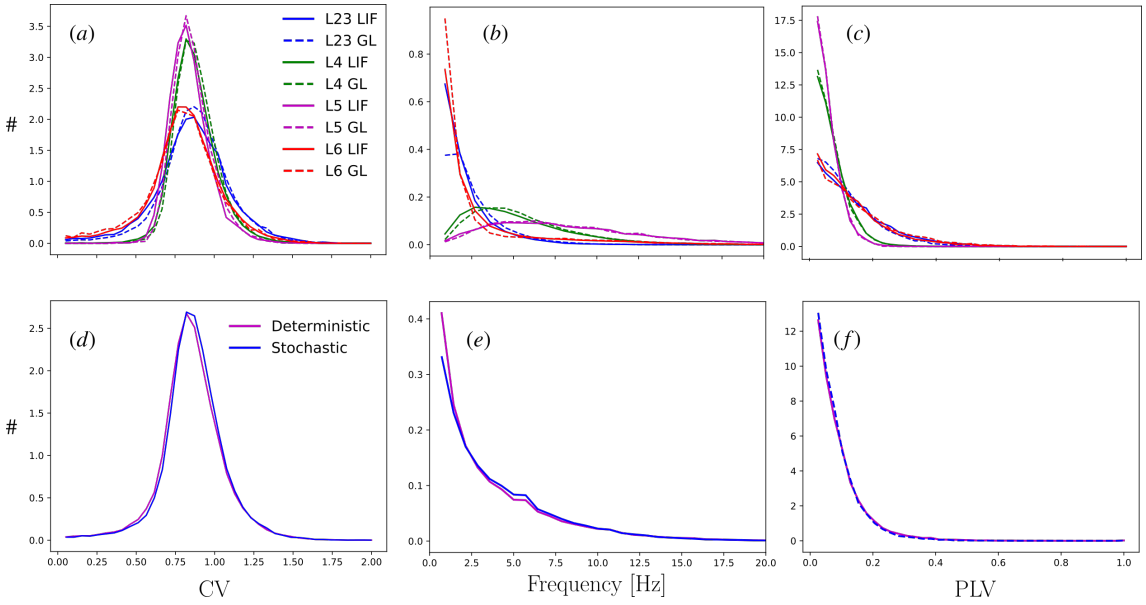

Figure B.3: *Layer-specif and whole-network (global) distribution for the (a,d) average frequency, (b,e) CV, and (c,f) PLV, respectively.*

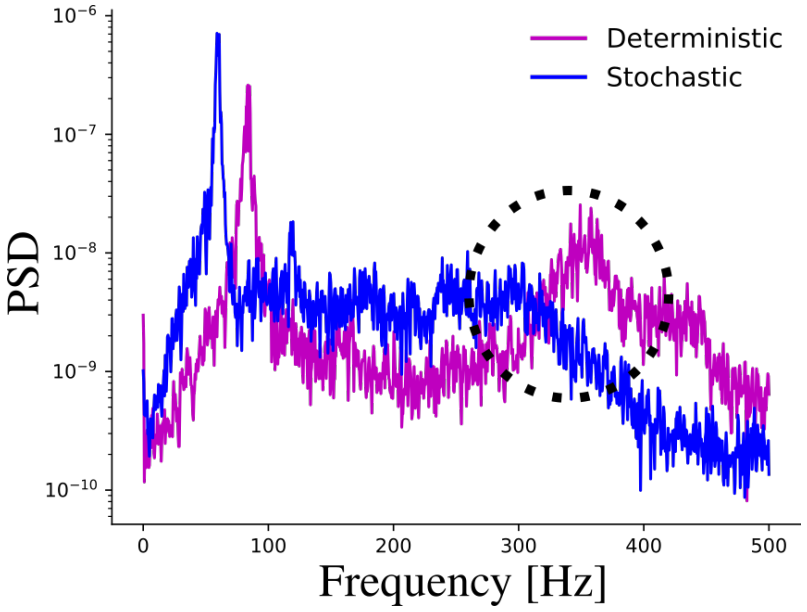

Figure B.4: *Global spike trains' power spectrum for the deterministic (blue), and stochastic (magenta) networks. The dashed black circle indicates the region between* 300 *Hz and* 400 *Hz.*

References

Abbott, L. F., Varela, J., Sen, K., & Nelson, S. (1997). Synaptic depression and cortical gain control. *Science*, *275*(5297), 221–224.

Adelman, T. L., Bialek, W., & Olberg, R. M. (2003). The information content of receptive fields. *Neuron*, *40*(4), 823–833.

Adrian, L. (1957). *The analysis of the nervous system.* SAGE Publications.

Attwell, D., & Laughlin, S. B. (2001). An energy budget for signaling in the grey matter of the brain. *Journal of Cerebral Blood Flow & Metabolism*, *21*(10), 1133–1145.

Aydore, S., Pantazis, D., & Leahy, R. M. (2013). A note on the phase locking value and its properties. *NeuroImage*, *74*, 231–244.

Azouz, R., & Gray, C. M. (1999). Cellular mechanisms contributing to response variability of cortical neurons in vivo. *Journal of Neuroscience*, *19*(6), 2209–2223.

Barna, J. S., Arezzo, J. C., & Vaughan Jr, H. G. (1981). A new multielectrode array for the simultaneous recording of field potentials and unit activity. *Electroencephalography and clinical neurophysiology*, *52*(5), 494–496.

Basser, P. J., Pajevic, S., Pierpaoli, C., Duda, J., & Aldroubi, A. (2000). In vivo fiber tractography using dt-mri data. *Magnetic resonance in medicine*, *44*(4), 625–632.

Bear, M. F., Connors, B. W., & Paradiso, M. A. (2007a). *Neuroscience* (Vol. 2). Lippincott Williams & Wilkins.

Bear, M. F., Connors, B. W., & Paradiso, M. A. (2007b). *Neuroscience* (Vol. 2). Lippincott Williams & Wilkins.

Bezrukov, S. M., & Vodyanoy, I. (1995). Noise-induced enhancement of signal transduction across voltage-dependent ion channels. *Nature*, *378*(6555), 362–364.

Bialek, W., Rieke, F., Van Steveninck, R. D. R., & Warland, D. (1991). Reading a neural code. *Science*, *252*(5014), 1854–1857.

Borges, F., Protachevicz, P., Pena, R., Lameu, E., Matias, F., Higa, G., ... others (2018). Self-sustained activity in balanced networks with low firing-rate. *arXiv preprint arXiv:1809.01020*.

Borst, A., & Theunissen, F. E. (1999). Information theory and neural coding. *Nature neuroscience*, *2*(11), 947.

Bos, H., Diesmann, M., & Helias, M. (2016). Identifying anatomical origins of

coexisting oscillations in the cortical microcircuit. *PLoS computational biology*, *12*(10), e1005132.

Braun, H. A., Schäfer, K., Voigt, K., Peters, R., Bretschneider, F., Pei, X., ... Moss, F. (1997). Low-dimensional dynamics in sensory biology 1: thermally sensitive electroreceptors of the catfish. *Journal of Computational Neuroscience*, *4*(4), 335–347.

Braun, H. A., Wissing, H., Schäfer, K., & Hirsch, M. C. (1994). Oscillation and noise determine signal transduction in shark multimodal sensory cells. *Nature*, *367*(6460), 270.

Brette, R. (2019). Is coding a relevant metaphor for the brain? *Behavioral and Brain Sciences*, 1–44.

Brette, R., & Gerstner, W. (2005). Adaptive exponential integrate-and-fire model as an effective description of neuronal activity. *J. Neurophysiol.*, *94*, 3637–3642.

Brette, R., & Guigon, E. (2003). Reliability of spike timing is a general property of spiking model neurons. *Neural Computation*, *15*(2), 279–308.

Brette, R., Rudolph, M., Carnevale, T., Hines, M., Beeman, D., Bower, J. M., ... others (2007). Simulation of networks of spiking neurons: a review of tools and strategies. *J. Comput. Neurosci.*, *23*(3), 349–398.

Brochini, L., de Andrade Costa, A., Abadi, M., Roque, A. C., Stolfi, J., & Kinouchi, O. (2016). Phase transitions and self-organized criticality in networks of stochastic spiking neurons. *Sci. Rep.*, *6*, 35831.

Brunel, N. (2000). Dynamics of sparsely connected networks of excitatory and inhibitory spiking neurons. *J. Comput. Neurosci.*, *8*, 183–208.

Buracas, G. T., Zador, A. M., DeWeese, M. R., & Albright, T. D. (1998). Efficient discrimination of temporal patterns by motion-sensitive neurons in primate visual cortex. *Neuron*, *20*(5), 959–969.

Burkitt, A. N. (2006). A review of the integrate-and-fire neuron model: I. homogeneous synaptic input. *Biological cybernetics*, *95*, 1–19.

Bzdok, D., & Yeo, B. T. (2017). Inference in the age of big data: Future perspectives on neuroscience. *Neuroimage*, *155*, 549–564.

Calvin, W. H., & Stevens, C. F. (1968). Synaptic noise and other sources of randomness in motoneuron interspike intervals. *Journal of neurophysiology*, *31*(4), 574–587.

Carr, C. E. (2004). Timing is everything: organization of timing circuits in auditory and electrical sensory systems. *The Journal of comparative neurology*, *472*(2), 131.

Celka, P. (2007). Statistical analysis of the phase-locking value. *IEEE Signal Proc. Let.*, *14*, 577–580.

Chow, C. C., & White, J. A. (1996). Spontaneous action potentials due to channel fluctuations. *Biophysical journal*, *71*(6), 3013–3021.

Cordeiro, V. L., Pena, R. F. d. O., Ceballos, C. A. C., Shimoura, R. O., & Roque, A. C. (2019). Information theory applications in neuroscience. *Revista Brasileira de Ensino de Física*, *41*(2).

Cordes, D., Haughton, V. M., Arfanakis, K., Wendt, G. J., Turski, P. A., Moritz,

C. H., ... Meyerand, M. E. (2000). Mapping functionally related regions of brain with functional connectivity mr imaging. *American Journal of Neuroradiology*, *21*(9), 1636–1644.

Costa, A., Brochini, L., & Kinouchi, O. (2017). Self-organized supercriticality and oscillations in networks of stochastic spiking neurons. *Entropy*, *19*(8), 399.

Dayan, P., & Abbott, L. F. (2001). *Theoretical neuroscience: computational and mathematical modeling of neural systems*. MIT press.

Debanne, D. (2004). Information processing in the axon. *Nature Reviews Neuroscience*, *5*(4), 304.

DeFelipe, J., & Fariñas, I. (1992). The pyramidal neuron of the cerebral cortex: morphological and chemical characteristics of the synaptic inputs. *Progress in neurobiology*, *39*(6), 563–607.

De Masi, G. A. L. E., A., & Presutti, E. (2015). Hydrodynamic limit for interacting neurons. *Journal of Statistical Physics*, *158*, 866–902.

De Pittà, M., Volman, V., Berry, H., Parpura, V., Volterra, A., & Ben-Jacob, E. (2012). Computational quest for understanding the role of astrocyte signaling in synaptic transmission and plasticity. *Frontiers in computational neuroscience*, *6*, 98.

Destexhe, A., Rudolph, M., Fellous, J.-M., & Sejnowski, T. J. (2001). Fluctuating synaptic conductances recreate in vivo-like activity in neocortical neurons. *Neuroscience*, *107*(1), 13–24.

Destexhe, A., & Sejnowski, T. J. (2009). The wilson–cowan model, 36 years later. *Biological cybernetics*, *101*(1), 1–2.

Dong, H. W. (2008). *The allen reference atlas: A digital color brain atlas of the c57bl/6j male mouse*. John Wiley & Sons Inc.

Dorval, A. D., & White, J. A. (2005). Channel noise is essential for perithreshold oscillations in entorhinal stellate neurons. *Journal of neuroscience*, *25*(43), 10025–10028.

Dotson, N. M., Hoffman, S. J., Goodell, B., & Gray, C. M. (2017). A large-scale semi-chronic microdrive recording system for non-human primates. *Neuron*, *96*(4), 769–782.

Douglas, R. J., & Martin, K. A. (2004). Neuronal circuits of the neocortex. *Annu. Rev. Neurosci.*, *27*, 419–451.

Duarte, A., & Ost, G. (2016). A model for neural activity in the absence of external stimuli. *Markov Processes and Related Fields*, *22*(1), 37–52.

Dykman, M., & McClintock, P. V. (1998). What can stochastic resonance do? *Nature*, *391*(6665), 344.

Eppler, J. M., Helias, M., Muller, E., Diesmann, M., & Gewaltig, M.-O. (2009). Pynest: a convenient interface to the nest simulator. *Frontiers in neuroinformatics*, *2*, 12.

Ermentrout, G. B., Galán, R. F., & Urban, N. N. (2008). Reliability, synchrony and noise. *Trends in neurosciences*, *31*(8), 428–434.

Evans, W. H., & Martin, P. E. (2002). Gap junctions: structure and function. *Molecular membrane biology*, *19*(2), 121–136.

Faisal, A. A., Selen, L. P., & Wolpert, D. M. (2008a). Noise in the nervous system. *Nature reviews neuroscience*, *9*(4), 292.

Faisal, A. A., Selen, L. P., & Wolpert, D. M. (2008b). Noise in the nervous system. *Nat. Rev. Neurosci.*, *9*, 292–303.

Fatt, P., & Katz, B. (1950). Some observations on biological noise. *Nature*, *166*(4223), 597.

Faure, P., Kaplan, D., & Korn, H. (2000). Synaptic efficacy and the transmission of complex firing patterns between neurons. *Journal of neurophysiology*, *84*(6), 3010–3025.

Fellous, J.-M., Rudolph, M., Destexhe, A., & Sejnowski, T. J. (2003). Synaptic background noise controls the input/output characteristics of single cells in an in vitro model of in vivo activity. *Neuroscience*, *122*(3), 811–829.

Franks, K. M., Stevens, C. F., & Sejnowski, T. J. (2003). Independent sources of quantal variability at single glutamatergic synapses. *Journal of Neuroscience*, *23*(8), 3186–3195.

Fries, P. (2015). Rhythms for cognition: communication through coherence. *Neuron*, *88*(1), 220–235.

Frigg, R., & Hartmann, S. (2006). Models in science.

Galán, R. F., Fourcaud-Trocmé, N., Ermentrout, G. B., & Urban, N. N. (2006). Correlation-induced synchronization of oscillations in olfactory bulb neurons. *Journal of Neuroscience*, *26*(14), 3646–3655.

Galves, A., & Löcherbach, E. (2013). Infinite systems of interacting chains with memory of variable length a stochastic model for biological neural nets. *Journal of Statistical Physics*, *151*(5), 896–921.

Gammaitoni, L., Hänggi, P., Jung, P., & Marchesoni, F. (1998). Stochastic resonance. *Reviews of modern physics*, *70*(1), 223.

Gao, L., Kostlan, K., Wang, Y., & Wang, X. (2016). Distinct subthreshold mechanisms underlying rate-coding principles in primate auditory cortex. *Neuron*, *91*(4), 905–919.

Gazzaley, A., Rissman, J., & D´ esposito, M. (2004). Functional connectivity during working memory maintenance. *Cognitive, Affective, & Behavioral Neuroscience*, *4*(4), 580–599.

Georgopoulos, A. P., Schwartz, A. B., & Kettner, R. E. (1986). Neuronal population coding of movement direction. *Science*, *233*(4771), 1416–1419.

Gerstner, W., & Brette, R. (2009). Adaptive exponential integrate-and-fire model. *Scholarpedia*, *4*(6), 8427.

Gerstner, W., Kistler, W. M., Naud, R., & Paninski, L. (2014). *Neuronal dynamics: From single neurons to networks and models of cognition.* Cambridge: Cambridge University Press.

Gerstner, W., Sprekeler, H., & Deco, G. (2012). Theory and simulation in neuroscience. *science*, *338*(6103), 60–65.

Girardi-Schappo, M., Bortolotto, G. S., Stenzinger, R. V., Gonsalves, J. J., & Tragtenberg, M. H. (2017). Phase diagrams and dynamics of a computationally efficient map-based neuron model. *PloS one*, *12*(3), e0174621.

Gleeson, P., Cantarelli, M., Marin, B., Quintana, A., Earnshaw, M., Sadeh, S., ... others (2019). Open source brain: A collaborative resource for visualizing, analyzing, simulating, and developing standardized models of neurons and circuits. *Neuron*.

Glowatzki, E., & Fuchs, P. A. (2002). Transmitter release at the hair cell ribbon synapse. *Nature neuroscience*, *5*(2), 147.

Gómez-Laberge, C., Smolyanskaya, A., Nassi, J. J., Kreiman, G., & Born, R. T. (2016). Bottom-up and top-down input augment the variability of cortical neurons. *Neuron*, *91*(3), 540–547.

Goodman, D. F., & Brette, R. (2009). The brian simulator. *Front. Neurosci.*, *3*, 192.

Gray, C. M., & McCormick, D. A. (1996). Chattering cells: superficial pyramidal neurons contributing to the generation of synchronous oscillations in the visual cortex. *Science*, *274*(5284), 109–113.

Griffiths, E. (2010). What is a model. *Sheffield University*, *4*, 1.

Haacke, E. M., Brown, R. W., Thompson, M. R., Venkatesan, R., et al. (1999). *Magnetic resonance imaging: physical principles and sequence design* (Vol. 82). Wiley-Liss New York:.

Hagmann, P., Cammoun, L., Gigandet, X., Meuli, R., Honey, C. J., Wedeen, V. J., & Sporns, O. (2008). Mapping the structural core of human cerebral cortex. *PLoS biology*, *6*(7), e159.

Hare, R. D., Smith, A. M., Forster, B. B., MacKay, A. L., Whittall, K. P., Kiehl, K. A., & Liddle, P. F. (1998). Functional magnetic resonance imaging: the basics of blood-oxygen-level dependent (bold) imaging. *Canadian Association of Radiologists Journal*, *49*(5), 320.

Hennessy, J. L., & Patterson, D. A. (2012). *Computer architecture: a quantitative approach. waltham, ma.* USA: Morgan Kaufmann.

Herculano-Houzel, S., Catania, K., Manger, P. R., & Kaas, J. H. (2015). Mammalian brains are made of these: a dataset of the numbers and densities of neuronal and nonneuronal cells in the brain of glires, primates, scandentia, eulipotyphlans, afrotherians and artiodactyls, and their relationship with body mass. *Brain, Behavior and Evolution*, *86*(3-4), 145–163.

Herreras, O. (2016). Local field potentials: myths and misunderstandings. *Frontiers in neural circuits*, *10*, 101.

Hessler, N. A., Shirke, A. M., & Malinow, R. (1993). The probability of transmitter release at a mammalian central synapse. *Nature*, *366*(6455), 569.

Hille, B. (2001). Ion channels of excitable membranes. sinauer associates. *Sunderland, MA*, *1375*.

Hines, M., Davison, A. P., & Muller, E. (2009). Neuron and python. *Frontiers in neuroinformatics*, *3*, 1.

Hines, M. L., & Carnevale, N. T. (1997). The neuron simulation environment. *Neural computation*, *9*(6), 1179–1209.

Hodgkin, A. L., & Huxley, A. F. (1952). A quantitative description of membrane current and its application to conduction and excitation in nerve. *J. Physiol.*,

117, 500–544.

Ince, R. A., Giordano, B. L., Kayser, C., Rousselet, G. A., Gross, J., & Schyns, P. G. (2017). A statistical framework for neuroimaging data analysis based on mutual information estimated via a gaussian copula. *Human brain mapping*, *38*(3), 1541–1573.

Izhikevich, E. M. (2000). Neural excitability, spiking and bursting. *Int. J. Bifurcat. Chaos*, *10*, 1171–1266.

Izhikevich, E. M. (2003a). Simple model of spiking neurons. *IEEE T. Neural Networ.*, *14*, 1569–1572.

Izhikevich, E. M. (2003b). Simple model of spiking neurons. *IEEE Transactions on Neural Networks*, *14*, 1569–1572.

Izhikevich, E. M. (2004). Which model to use for cortical spiking neurons? *IEEE T. Neural Networ.*, *15*(5), 1063–1070. doi: 10.1109/TNN.2004.832719

Izhikevich, E. M. (2007a). *Dynamical systems in neuroscience*. Cambridge, MA: MIT Press.

Izhikevich, E. M. (2007b). *Dynamical systems in neuroscience*. MIT press.

Izhikevich, E. M., & FitzHugh, R. (2006). Fitzhugh-nagumo model. *Scholarpedia*, *1*(9), 1349.

Jacobson, G. A., Diba, K., Yaron-Jakoubovitch, A., Oz, Y., Koch, C., Segev, I., & Yarom, Y. (2005). Subthreshold voltage noise of rat neocortical pyramidal neurones. *The Journal of physiology*, *564*(1), 145–160.

Johansson, R. S., & Birznieks, I. (2004). First spikes in ensembles of human tactile afferents code complex spatial fingertip events. *Nature neuroscience*, *7*(2), 170.

Jolivet, R., Rauch, A., Lüscher, H.-R., & Gerstner, W. (2006). Predicting spike timing of neocortical pyramidal neurons by simple threshold models. *Journal of computational neuroscience*, *21*(1), 35–49.

Kac, M. (1969). Some mathematical models in science. *Science*, *166*(3906), 695–699.

Kandel, E. R., Markram, H., Matthews, P. M., Yuste, R., & Koch, C. (2013). Neuroscience thinks big (and collaboratively). *Nature Reviews Neuroscience*, *14*(9), 659.

Katz, B. (1969). The release of neural transmitter substances. *Liverpool University Press*, 5–39.

Kavalali, E. T. (2015). The mechanisms and functions of spontaneous neurotransmitter release. *Nat. Rev. Neurosci.*, *16*, 5–16.

Kayser, C., Montemurro, M. A., Logothetis, N. K., & Panzeri, S. (2009). Spike-phase coding boosts and stabilizes information carried by spatial and temporal spike patterns. *Neuron*, *61*(4), 597–608.

Kirschstein, T., & Köhling, R. (2009). What is the source of the eeg? *Clinical EEG and neuroscience*, *40*(3), 146–149.

Kleppe, I. C., & Robinson, H. P. (2006). Correlation entropy of synaptic input-output dynamics. *Physical Review E*, *74*(4), 041909.

Knill, D. C., & Pouget, A. (2004). The bayesian brain: the role of uncertainty in neural coding and computation. *TRENDS in Neurosciences*, *27*(12), 712–719.

Koch, C., & Segev, I. (1998). *Methods in neuronal modeling: from ions to networks*. MIT press.

Krnjević, K. (1974). Chemical nature of synaptic transmission in vertebrates. *Physiological Reviews*, *54*(2), 418–540.

Kunkel, S., Schmidt, M., Eppler, J. M., Plesser, H. E., Masumoto, G., Igarashi, J., ... others (2014). Spiking network simulation code for petascale computers. *Frontiers in neuroinformatics*, *8*, 78.

Kurrer, C., & Schulten, K. (1995). Noise-induced synchronous neuronal oscillations. *Physical Review E*, *51*(6), 6213.

Lachaux, J.-P., Rodriguez, E., Martinerie, J., & Varela, F. J. (1999). Measuring phase synchrony in brain signals. *Hum. Brain Mapp.*, *8*, 194–208.

Landhuis, E. (2017). *Neuroscience: Big brain, big data*. Nature Publishing Group.

Lapicque, L. (1907). Recherches quantitatives sur l'excitation electrique des nerfs traitee comme une polarization. *Journal de Physiologie et de Pathologie Generalej*, *9*, 620–635.

Larkman, A. U. (1991). Dendritic morphology of pyramidal neurones of the visual cortex of the rat: Iii. spine distributions. *Journal of comparative neurology*, *306*(2), 332–343.

Laughlin, S. B., van Steveninck, R. R. d. R., & Anderson, J. C. (1998). The metabolic cost of neural information. *Nature neuroscience*, *1*(1), 36.

Lee, C., Rohrer, W. H., & Sparks, D. L. (1988). Population coding of saccadic eye movements by neurons in the superior colliculus. *Nature*, *332*(6162), 357.

Lent, R. (2004). Cem bilhões de neurônios: conceitos fundamentais de neurociência. In *Cem bilhões de neurônios: conceitos fundamentais de neurociência*.

Liao, W., Ding, J., Marinazzo, D., Xu, Q., Wang, Z., Yuan, C., ... Chen, H. (2011). Small-world directed networks in the human brain: multivariate granger causality analysis of resting-state fmri. *Neuroimage*, *54*(4), 2683–2694.

Lim, R., Alvarez, F. J., & Walmsley, B. (1999). Quantal size is correlated with receptor cluster area at glycinergic synapses in the rat brainstem. *The Journal of physiology*, *516*(2), 505–512.

Longtin, A. (2013). Neuronal noise. *Scholarpedia*, *8*, 1618.

Lopes da Silva, F., & Niedermeyer, E. (1998). Computer-assisted eeg diagnosis: pattern recognition and brain mapping. *Electroencephalography: Basic Principles, Clinical Applications and Related Fields, 4th edition*, 1164–1189.

Lowet, E., Roberts, M. J., Bonizzi, P., Karel, J., & De Weerd, P. (2016). Quantifying neural oscillatory synchronization: a comparison between spectral coherence and phase-locking value approaches. *PloS One*, *11*, e0146443.

Ma, W. J., Beck, J. M., Latham, P. E., & Pouget, A. (2006). Bayesian inference with probabilistic population codes. *Nature neuroscience*, *9*(11), 1432.

Mainen, Z. F., & Sejnowski, T. J. (1995). Reliability of spike timing in neocortical neurons. *Science*, *268*(5216), 1503–1506.

McClintock, P. (2002). Can noise actually boost brain power? *Physics World*, *15*(7), 20.

McDonnell, M. D., & Abbott, D. (2009). What is stochastic resonance? definitions, misconceptions, debates, and its relevance to biology. *PLoS computational biology*, *5*(5), e1000348.

McDonnell, M. D., Goldwyn, J. H., & Lindner, B. (2016). Neuronal stochastic variability: influences on spiking dynamics and network activity. *Frontiers in computational neuroscience*, *10*, 38.

McDonnell, M. D., & Ward, L. M. (2011). The benefits of noise in neural systems: bridging theory and experiment. *Nature Reviews Neuroscience*, *12*(7), 415.

Meunier, D., Lambiotte, R., & Bullmore, E. T. (2010). Modular and hierarchically modular organization of brain networks. *Frontiers in neuroscience*, *4*, 200.

Montemurro, M. A., Rasch, M. J., Murayama, Y., Logothetis, N. K., & Panzeri, S. (2008). Phase-of-firing coding of natural visual stimuli in primary visual cortex. *Current biology*, *18*(5), 375–380.

Mori, T., & Kai, S. (2002). Noise-induced entrainment and stochastic resonance in human brain waves. *Physical review letters*, *88*(21), 218101.

Moss, F., Douglass, J. K., Wilkens, L., Pierson, D., & Pantazelou, E. (1993). Stochastic resonance in an electronic fitzhugh-nagumo model. *Annals of the New York Academy of Sciences*, *706*(1), 26–41.

Mountcastle, V. B. (1997). The columnar organization of the neocortex. *Brain: a journal of neurology*, *120*(4), 701–722.

Movshon, J. A. (2000). Reliability of neuronal responses. *Neuron*, *27*(3), 412–414.

Neymotin, S. A., Jacobs, K. M., Fenton, A. A., & Lytton, W. W. (2011). Synaptic information transfer in computer models of neocortical columns. *Journal of computational neuroscience*, *30*(1), 69–84.

Nimchinsky, E. A., Yasuda, R., Oertner, T. G., & Svoboda, K. (2004). The number of glutamate receptors opened by synaptic stimulation in single hippocampal spines. *Journal of Neuroscience*, *24*(8), 2054–2064.

Nusser, Z., Cull-Candy, S., & Farrant, M. (1997). Differences in synaptic gabaa receptor number underlie variation in gaba mini amplitude. *Neuron*, *19*(3), 697–709.

Orlandi, J. G., Stetter, O., Soriano, J., Geisel, T., & Battaglia, D. (2014). Transfer entropy reconstruction and labeling of neuronal connections from simulated calcium imaging. *PloS one*, *9*(6), e98842.

Pecher, C. (1939). La fluctuation d'excitabilité de la fibre nerveuse. *Archives Internationales de Physiologie*, *49*(2), 129–152.

Pena, R. F., Zaks, M. A., & Roque, A. C. (2018). Dynamics of spontaneous activity in random networks with multiple neuron subtypes and synaptic noise. *Journal of computational neuroscience*, *45*(1), 1–28.

Pikovsky, A., Rosenblum, M., & Kurths, J. (2001). *Synchronization: A universal concept in nonlinear sciences*. U. K.: Cambridge Univ. Press.

Pinto, D. J., Brumberg, J. C., Simons, D. J., Ermentrout, G. B., & Traub, R. (1996). A quantitative population model of whisker barrels: re-examining

the wilson-cowan equations. *Journal of computational neuroscience*, *3*(3), 247–264.

Platkiewicz, J., & Brette, R. (2010). A threshold equation for action potential initiation. *PLoS computational biology*, *6*(7), e1000850.

Plesser, H. E., Eppler, J. M., Morrison, A., Diesmann, M., & Gewaltig, M.-O. (2007). Efficient parallel simulation of large-scale neuronal networks on clusters of multiprocessor computers. In *European conference on parallel processing* (pp. 672–681).

Plesser, H. E., & Gerstner, W. (2000a). Escape rate models for noisy integrate-and-fire neurons. *Neurocomp.*, *32/33*, 219.

Plesser, H. E., & Gerstner, W. (2000b). Noise in integrate-and-fire neurons: From stochastic input to escape rates. *Neural computation*, *12*(2), 367–384.

Poldrack, R. A., & Gorgolewski, K. J. (2014). Making big data open: data sharing in neuroimaging. *Nature neuroscience*, *17*(11), 1510.

Potjans, T. C., & Diesmann, M. (2012). The cell-type specific cortical microcircuit: relating structure and activity in a full-scale spiking network model. *Cerebral cortex*, *24*(3), 785–806.

Potjans, T. C., & Diesmann, M. (2014a). The cell-type specific cortical microcircuit: relating structure and activity in a full-scale spiking network model. *Cereb. Cortex*, *24*, 785–806.

Potjans, T. C., & Diesmann, M. (2014b). The cell-type specific cortical microcircuit: relating structure and activity in a full-scale spiking network model. *Cereb. Cortex*, *24*, 785–806.

Pulido, C., & Marty, A. (2017). Quantal fluctuations in central mammalian synapses: Functional role of vesicular docking sites. *Physiological reviews*, *97*(4), 1403–1430.

Purves, D., Augustine, G. J., Fitzpatrick, D., Hall, W., LaMantia, A.-S., & White, L. (2019). *Neurosciences*. De Boeck Supérieur.

Richmond, B. J., & Optican, L. M. (1990). Temporal encoding of two-dimensional patterns by single units in primate primary visual cortex. ii. information transmission. *Journal of Neurophysiology*, *64*(2), 370–380.

Rieke, F., & Warland, D. (1999). *Spikes: exploring the neural code*. MIT press.

Rosenblum, M., A., Kurths, J., Schäfer, C., & Tass, P. A. (2001). Phase synchronization: from theory to data analysis. In *Handbook of biological physics* (Vol. 4, pp. 279–321). North-Holland: Elsevier.

Rössler, O. E. (1976). An equation for continuous chaos. *Phys. Lett. A*, *57*, 397–398.

Roy, A. K., Shehzad, Z., Margulies, D. S., Kelly, A. C., Uddin, L. Q., Gotimer, K., ... Milham, M. P. (2009). Functional connectivity of the human amygdala using resting state fmri. *Neuroimage*, *45*(2), 614–626.

Rulkov, N. F. (2002). Modeling of spiking-bursting neural behavior using two-dimensional map. *Physical Review E*, *65*(4), 041922.

Salazar, R., Dotson, N., Bressler, S., & Gray, C. (2012). Content-specific fronto-parietal synchronization during visual working memory. *Science*, *338*(6110), 1097–1100.

Schmerl, B. A., & McDonnell, M. D. (2013). Channel-noise-induced stochastic facilitation in an auditory brainstem neuron model. *Physical Review E*, *88*(5), 052722.

Schmidt, M., Bakker, R., Shen, K., Bezgin, G., Hilgetag, C.-C., Diesmann, M., & van Albada, S. J. (2015). Full-density multi-scale account of structure and dynamics of macaque visual cortex. *arXiv preprint arXiv:1511.09364*.

Schneidman, E., Freedman, B., & Segev, I. (1998). Ion channel stochasticity may be critical in determining the reliability and precision of spike timing. *Neural computation*, *10*(7), 1679–1703.

Schwartz, E. L. (1993). *Computational neuroscience*. Mit Press.

Sekerli, M., Del Negro, C. A., Lee, R. H., & Butera, R. J. (2004). Estimating action potential thresholds from neuronal time-series: new metrics and evaluation of methodologies. *IEEE Transactions on Biomedical Engineering*, *51*(9), 1665–1672.

Shannon, C. E. (1948). A mathematical theory of communication. *Bell system technical journal*, *27*(3), 379–423.

Shepherd, G. M., & Erulkar, S. D. (1997). Centenary of the synapse: from sherrington to the molecular biology of the synapse and beyond. *Trends in neurosciences*, *20*(9), 385–392.

Shilnikov, A., & Cymbalyuk, G. (2005). Transition between tonic spiking and bursting in a neuron model via the blue-sky catastrophe. *Physical Review Letters*, *94*(4), 048101.

Shimoura, R. O., Kamiji, N. L., de Oliveira Pena, R. F., Cordeiro, V. L., Ceballos, C. C., Romaro, C., & Roque, A. C. (2018). Reimplementation of the potjans-diesmann cortical microcircuit model: from nest to brian. *bioRxiv*, 248401.

Siegel, M., Warden, M. R., & Miller, E. K. (2009). Phase-dependent neuronal coding of objects in short-term memory. *Proceedings of the National Academy of Sciences*, *106*(50), 21341–21346.

Sigworth, F. (1980). The variance of sodium current fluctuations at the node of ranvier. *The Journal of physiology*, *307*(1), 97–129.

Sporns, O. (2010). *Networks of the brain*. MIT press.

Stacey, W. C., & Durand, D. M. (2001). Synaptic noise improves detection of subthreshold signals in hippocampal ca1 neurons. *Journal of Neurophysiology*, *86*(3), 1104–1112.

Stein, R. B. (1967). The information capacity of nerve cells using a frequency code. *Biophysical journal*, *7*(6), 797–826.

Stein, R. B., Gossen, E. R., & Jones, K. E. (2005). Neuronal variability: noise or part of the signal? *Nature Reviews Neuroscience*, *6*(5), 389.

Steinmetz, P. N., Manwani, A., Koch, C., London, M., & Segev, I. (2000). Subthreshold voltage noise due to channel fluctuations in active neuronal membranes. *Journal of computational neuroscience*, *9*(2), 133–148.

Stevens, C. F., & Zador, A. M. (1998). Input synchrony and the irregular firing of cortical neurons. *Nature neuroscience*, *1*(3), 210.

Stocks, N., & Mannella, R. (2001). Generic noise-enhanced coding in neuronal arrays. *Physical Review E*, *64*(3), 030902.

Stone, J. V. (2015). *Information theory: a tutorial introduction*. Sebtel Press.

Talbot, W. H., Darian-Smith, I., Kornhuber, H. H., & Mountcastle, V. B. (1968). The sense of flutter-vibration: comparison of the human capacity with response patterns of mechanoreceptive afferents from the monkey hand. *Journal of neurophysiology*, *31*(2), 301–334.

Tolhurst, D. J., Movshon, J. A., & Dean, A. F. (1983). The statistical reliability of signals in single neurons in cat and monkey visual cortex. *Vision research*, *23*(8), 775–785.

Tomko, G. J., & Crapper, D. R. (1974). Neuronal variability: non-stationary responses to identical visual stimuli. *Brain research*, *79*(3), 405–418.

Tovee, M. J., Rolls, E. T., Treves, A., & Bellis, R. P. (1993). Information encoding and the responses of single neurons in the primate temporal visual cortex. *Journal of Neurophysiology*, *70*(2), 640–654.

Traynelis, S. F., & Jaramillo, F. (1998). Getting the most out of noise in the central nervous system. *Trends in neurosciences*, *21*(4), 137–145.

Tuckwell, H. C. (1988). *Introduction to theoretical neurobiology*. Cambridge: Cambridge University Press.

van den Heuvel, M. P., & Yeo, B. T. (2017). A spotlight on bridging microscale and macroscale human brain architecture. *Neuron*, *93*(6), 1248–1251.

VanRullen, R., Guyonneau, R., & Thorpe, S. J. (2005). Spike times make sense. *Trends in neurosciences*, *28*(1), 1–4.

van Steveninck, R. R. d. R., Lewen, G. D., Strong, S. P., Koberle, R., & Bialek, W. (1997). Reproducibility and variability in neural spike trains. *Science*, *275*(5307), 1805–1808.

Verveen, A. (1960). On the fluctuation of threshold of the nerve fibre. *Structure and function of the cerebral cortex*, 282–288.

Vogt, N. (2018). Machine learning in neuroscience. *Nature Methods*, *15*(1), 33.

Ward, L. M., MacLean, S. E., & Kirschner, A. (2010). Stochastic resonance modulates neural synchronization within and between cortical sources. *PloS one*, *5*(12), e14371.

Wedeen, V. J., Wang, R., Schmahmann, J. D., Benner, T., Tseng, W.-Y. I., Dai, G., ... de Crespigny, A. J. (2008). Diffusion spectrum magnetic resonance imaging (dsi) tractography of crossing fibers. *Neuroimage*, *41*(4), 1267–1277.

White, J. A., Klink, R., Alonso, A., & Kay, A. R. (1998). Noise from voltage-gated ion channels may influence neuronal dynamics in the entorhinal cortex. *Journal of neurophysiology*, *80*(1), 262–269.

White, J. A., Rubinstein, J. T., & Kay, A. R. (2000). Channel noise in neurons. *Trends in neurosciences*, *23*(3), 131–137.

Wibral, M., Rahm, B., Rieder, M., Lindner, M., Vicente, R., & Kaiser, J. (2011). Transfer entropy in magnetoencephalographic data: quantifying information flow in cortical and cerebellar networks. *Progress in biophysics and molecular biology*, *105*(1-2), 80–97.

Wiesenfeld, K., & Moss, F. (1995). Stochastic resonance and the benefits of noise: from ice ages to crayfish and squids. *Nature*, *373*(6509), 33.

Wu, X.-S., Xue, L., Mohan, R., Paradiso, K., Gillis, K. D., & Wu, L.-G. (2007). The origin of quantal size variation: vesicular glutamate concentration plays a significant role. *Journal of Neuroscience*, *27*(11), 3046–3056.

y Cajal, S. R. (1888). *Estructura de los centros nerviosos de las aves.*

Yuste, R. (2015). From the neuron doctrine to neural networks. *Nature reviews neuroscience*, *16*(8), 487.

Zhang, Q., & Haydon, P. (2005). Roles for gliotransmission in the nervous system. *Journal of neural transmission*, *112*(1), 121–125.